2010-08-20

Mechanical Flow Restoration in Acute Ischemic Stroke: A Model System of Cerebrovascular Occlusion: A Dissertation

Juyu Chueh
University of Massachusetts Medical School

MECHANICAL FLOW RESTORATION IN ACUTE ISCHEMIC STROKE: A MODEL SYSTEM OF CEREBROVASCULAR OCCLUSION

A Dissertation Presented

By

JU-YU CHUEH

Submitted to the Faculty of the

University of Massachusetts Graduate School of Biomedical Sciences, Worcester

in partial fulfillment of the requirements for the degree of

DOCTOR OF PHILOSOPHY

AUGUST 24, 2010

BIOENGINEERING AND BIOTECHNOLOGY PROGRAM

MECHANICAL FLOW RESTORATION IN ACUTE ISCHEMIC STROKE: A MODEL SYSTEM OF CEREBROVASCULAR OCCLUSION

A Dissertation Presented

By

JU-YU CHUEH

The signatures of the Dissertation Defense Committee signifies completion and approval as to style and content of the Dissertation

Matthew J. Gounis, Ph.D., Thesis Advisor

Ajay K. Wakhloo, M.D. Ph.D. FAHA, Member of Committee

Michael A. King, Ph.D., Member of Committee

Jerald Silverman, D.V.M., Member of Committee

Alexander M. Norbash, M.D., Member of Committee

The signature of the Chair of the Committee signifies that the written dissertation meets the requirements of the Dissertation Committee

Gregory H. Hendricks, Ph.D., Chair of Committee

The signature of the Dean of the Graduate School of Biomedical Sciences signifies that the student has met all graduation requirements of the school.

Anthony Carruthers, Ph.D.,
Dean of the Graduate School of Biomedical Sciences

BIOENGINEERING AND BIOTECHNOLOGY PROGRAM
AUGUST 24, 2010

Dedication

With love, I dedicate this work to my grandparents and my parents.

Acknowledgements

This dissertation would not have been possible without the generous support of my mentor, Dr. Matthew Gounis. During the past four years, he has invested so much of his time and energy to guide my thesis work and sharpen my research skills. Most importantly, he has started me on the path of becoming an independent investigator. I am honored to be his first PhD student, and truly appreciate all his help.

I would like to express my gratitude to Dr. Ajay Wakhloo for his encouragement and inputs to my study. I am amazed by his enthusiasm and expertise in interventional neuroradiology which has improved this dissertation tremendously. I owe many thanks to Dr. Greg Hendricks for being an excellent chair of both my TRAC and DEC committee and for his thoughtful comments and insightful suggestions for this study. I have learnt a lot from him. I would also like to acknowledge my thesis committee members, Dr. Ajay Wakhloo, Dr. Greg Hendricks, Dr. Michael King, Dr. Jerald Silverman and Dr. Alexander Norbash, for their time to evaluate my work.

Special thanks go to Dr. John P. Weaver, Dr. Andres Schanzer and Dr. Mohammad H. Eslami, for providing atherosclerotic plaques for characterization. I also thank Eileen A. Duhamel, Dr. Neil Patel and Anna Thors, for their dedicated clinical assistance with this study. In addition, I would like to thank my lab mates, for their support which kept me moving forward when times got tough.

Finally, my deepest gratitude goes to my family for their unconditional love and support over these years.

Abstract

Stroke is the third most common cause of death and a leading cause of disability in the United States. The existing treatments of acute ischemic stroke (AIS) involve pharmaceutical thrombolytic therapy and/or mechanical thrombectomy. The Food and Drug Administration (FDA)-approved recombinant tissue plasminogen activator (tPA) administration for treatment of stroke is efficacious, but has a short treatment time window and is associated with a risk of symptomatic hemorrhage. Other than tPA, the Mechanical Embolus Removal in Cerebral Ischemia (MERCI) retriever system and the Penumbra Aspiration system are both approved by the FDA for retrieval of thromboemboli in AIS patients. However, the previous clinical studies have shown that the recanalization rate of the MERCI system and the clinical outcome of the Penumbra system are not optimal. To identify the variables which could affect the performance of the thrombectomy devices, much effort has been devoted to evaluate thrombectomy devices in model systems, both in vivo and in vitro, of vascular occlusion. The goal of this study is to establish a physiologically realistic, in vitro model system for the preclinical assessment of mechanical thrombectomy devices.

In this study, the model system of cerebrovascular occlusion was mainly composed of a human vascular replica, an embolus analogue (EA), and a simulated physiologic mock circulation system. The human vascular replica represents the geometry of the internal carotid artery (ICA)/middle cerebral artery (MCA) that is derived from image data in a population of patients. The features of the vasculature were

characterized in terms of average curvature (AC), diameter, and length, and were used to determine the representative model. A batch manufacturing was developed to prepare the silicone replica.

The EA is a much neglected component of model systems currently. To address this limitation, extensive mechanical characterization of commonly used EAs was performed. Importantly, the properties of the EAs were compared to specimens extracted from patients. In the preliminary tests of our model system, we selected a bovine EA with stiffness similar to the thrombi retrieved from the atherosclerotic plaques. This EA was used to create an occlusion in the aforesaid replica. The thrombectomy devices tested included the MERCI L5 Retriever, Penumbra system 054, Enterprise stent, and an ultrasound waveguide device. The primary efficacy endpoint was the amount of blood flow restored, and the primary safety endpoint was an analysis of clot fragments generated and their size distribution.

A physiologically realistic model system of cerebrovascular occlusion was successfully built and applied for preclinical evaluation of thrombectomy devices. The recanalization rate of the thrombectomy device was related to the ability of the device to capture the EA during the removal of the device and the geometry of the cerebrovasculature. The risk of the embolic shower was influenced by the mechanical properties of the EA and the design of the thrombectomy device.

Table of Contents

List of Tables

List of Figures

List of Third Party Copyrighted Material

Figure Number	Publisher	License Number
Figure 1-2	Common variations of the CoW	Permission requested (Order detail ID:44179985)
Figure 1-4	Nature Publishing Group	2496260679787
Figure 1-5	Elsevier	2496270340249
Figure 1-6	Wolters Kluwer Health	2496270573746
Figure 1-7	Elsevier	2496270738806
Figure 1-8	Nature Publishing Group	2497280054734
Figure 1-9	Copyright © [1995] Massachusetts Medical Society. All rights reserved. MMS Invoice Number: RY - 2011 - 1020	
Figure 1-11	Wolters Kluwer Health	2496280015749

List of Abbreviations

AIS: acute ischemic stroke

FDA: Food and Drug Administration

tPA: tissue plasminogen activator

MERCI: Mechanical Embolus Removal in Cerebral Ischemia

EA: embolus analogue

ICA: internal carotid artery

MCA: middle cerebral artery

AC: average curvature

VA: vertebral artery

BA: basilar artery

ACA: anterior cerebral artery

CoW: the circle of Willis

CBF: Cerebral blood flow

CPP: cerebral perfusion pressure

NINDS: National Institute of Neurological Disorders and Stroke

AF: atrial fibrillation

EC: endothelial cell

vWf: von Willebrand factor

ECM: extracellular matrix

ICAD: intracranial atherosclerotic disease

LDL: low density lipoprotein

SMC: smooth muscle cell

VSMC: vascular smooth muscle cell

TF: tissue factor

FVII: factor VII

IV-tPA: intravenous fibrinolytic therapy with tissue plasminogen activator

mRS: modified Rankin Scale

TIMI: Thrombolysis in Myocardial Infarction

NIHSS: National Institutes of Health Stroke Scale

MRA: magnetic resonance angiography

NIHU: National Institutes of Health unit

ACD: anticoagulant citrate dextrose

CEA: carotid endarterectomies

DMA: dynamic mechanical analyzer

E: secant modulus

MSB: Martius Scarlet Blue

H&E: Hematoxylin and Eosin

SEM: scanning electron microscopy

EDS: energy dispersive X-ray spectroscopy

Preface

Portions of this dissertation have appeared in:

Chueh JY, Wakhloo AK, Gounis MJ. Neurovascular modeling: small-batch manufacturing of silicone vascular replicas. AJNR Am J Neuroradiol 2009;30:1159-1164.

Chapter I: Introduction

Brief Review: Anatomy of the Circle of Willis and Cerebral Blood Circulation

Cerebral blood flow is provided by two main pairs of arteries: the vertebral arteries (VAs), and the internal carotid arteries (ICAs). The VAs arise from the subclavian arteries and unite to form the basilar artery (BA). The posterior cerebral arteries, which extend from the terminal bifurcation of the BA, connect to the ICA by posterior communicating arteries at P1/P2 junction, and supply blood to the posterior circulation of the brain (Figure 1-1).

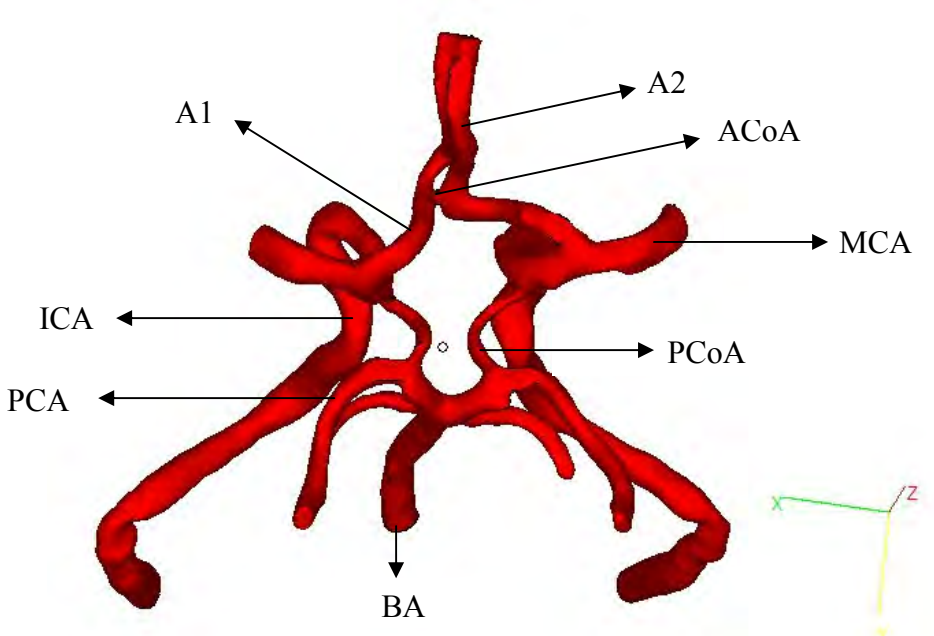

Figure 1-1 3D reconstruction of human intracranial arteries that form the circle of Willis (ACoA: anterior communicating artery, ICA: internal carotid artery, PCA: posterior cerebral artery, BA: basilar artery, PCoA: posterior communicating artery, MCA: middle cerebral artery, A1: A1 segment of the anterior cerebral artery, A2: A2 segment of the anterior cerebral artery).

About 70% of the common carotid blood flow is diverted into the ICA[1-3], and the ICA bifurcates into the middle cerebral artery (MCA) at the level of the olfactory trigone and anterior cerebral artery (ACA) opposite the olfactory trigone[4]. The left and right ACA are connected by the anterior communicating artery to form the anterior circulation. The arterial polygon which provides communication between the anterior and posterior circuits, shown in Figure 1-1, is known as the circle of Willis (CoW)[4-7]. The CoW represents a multiplexer and is regarded as the principal source of collateral flow in patients with ischemic cerebrovascular disease[8]. The ability of the CoW to redistribute blood flow is affected by the presence and diameter of the component vessels. Three-dimensional time-of-flight was used to determine the morphologic differences of the CoW among 150 healthy subjects, and the results show that only 42% of the subjects presented a complete CoW[9]. The most common variants include absence of the anterior communicating artery and one of the posterior communicating arteries. Typical variations are presented in Figure 1-2. Apart from the CoW, small pial vessels may also provide collateral flow in an acute ischemic event. A recent clinical study shows that stroke patients with higher pial collateral scores have improved clinical outcomes and smaller infarct volume as compared to those with lower pial collateral scores following intra-arterial tissue plasminogen activator (IA-tPA) treatment[10].

The brain requires continuous and sufficient blood perfusion that is approximately 15% of the cardiac output. The anterior circulation contributes 76-82% to the global cerebral blood flow[11, 12]. The capability of brain to store energy is low, as demonstrated by the finding that the adenosine triphosphate level quickly drops to zero in 7 minutes

after the termination of the oxygen supply[13]. The shortage of the oxygen stops cell growth; in addition, the deprivation of blood flow to the brain renders neurons unable to maintain the physiological ion gradient[14] that they need to function properly, and causes neuronal dysfunction and subsequent death. In a typical acute ischemic stroke that is caused by a large artery occlusion, 1.9 million neurons, 14 billion synapses and 7.5 miles of myelinated fibers are lost each minute[15] . Acute ischemic stroke is a major cause of neurological deficiencies.

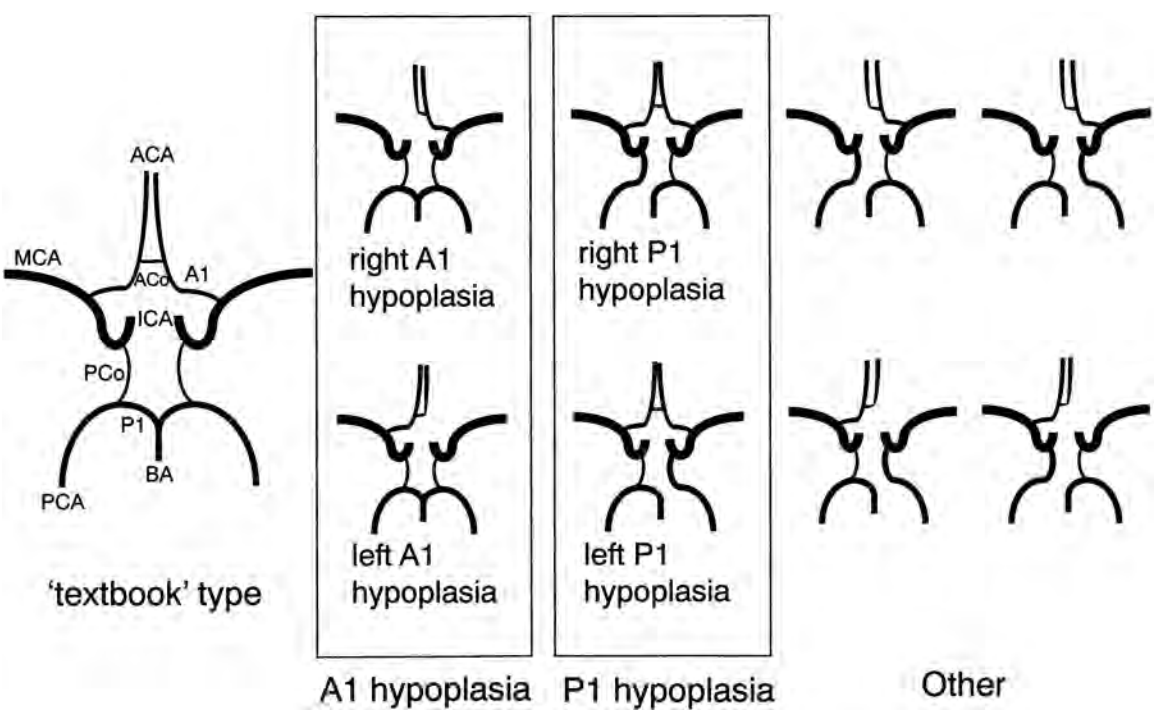

Figure 1-2 Common variations of the CoW[16].

Acute ischemic Stroke

Significance and Impact of AIS

Stroke is the second highest cause of mortality in the world[17] . In the United States, cardiovascular disease, principally heart disease and stroke, is the leading cause of death[18]. The 2010 Heart Disease and Stroke Statistical Update from American Heart Association[19] reports that about 795,000 people experience a new or recurrent stroke each year, and stroke accounted for about 1of every 18 deaths in the United States in 2006. On average, a stroke occurs every 40 seconds, and someone dies of a stroke every 4 minutes. The financial burden of stroke is high, with the estimated direct and indirect cost at 73.7 billion in 2010 (in US dollars).

According to the World Health Organization[20], stroke is defined as, "rapidly developing clinical signs of focal (at times global) disturbance of cerebral function, lasting more than 24 hours or leading to death with no apparent cause other than that of vascular origin." Some modifiable risk factors for stroke include diabetes, hypertension, elevated cholesterol, and smoking[21]. Nonmodifiable factors are age, race, gender and family history.

Cerebral blood flow (CBF) is determined by the ratio of cerebral perfusion pressure (CPP) and cerebrovascular resistance[22], and the CPP is generally described as the difference between mean arterial blood pressure and intracranial pressure[13]. The regional CBF of the normal brain tissue is about 50-60 ml/100g/min[23]. When the cerebral ischemia occurs, the cessation of blood flow results in varying gradients in hypoperfusion

over the affected region[24]. The central zone (CBF<12 ml/100g/min[25]) is termed "ischemic core" which is composed of the irreversibly and severely damaged tissue[26], and is surrounded by presumably viable tissue, namely the ischemic penumbra. The penumbra is a zone of tissue that receives insufficient blood flow (CBF:18-20 ml/100g/min[25]) to function properly and is at risk of irreversible damage should blood flow not be restored. The salvage of ischemic penumbra may be achieved when the reperfusion is established within 6 to 8 hours[27], and the penumbra is the target area to preserve for prevention of further neuronal deterioration. It is important to note that the evolution of the infarct and penumbral zone is dynamic and controlled by a number of factors including spontaneous fibrinolysis and systemic blood pressure. The oligemic tissue in the area between the unaffected brain and the ischemic penumbra is mildly hypoperfused and presents no functional or morphological impairment[23].

Frequent Locations of AIS and Clinical Symptoms

Of all strokes, 87% are ischemic and 13% are of hemorrhagic origin[19]. Five subtypes of the ischemic stroke are denoted according to data from the National Institute of Neurological Disorders and Stroke (NINDS) Stroke Data Bank. They are: 1. large-artery stenosis occlusion/atherosclerosis (8.9%), 2. embolism from a commonly accepted cardiac source (19.3%), 3. small-artery occlusion (lacune, 26.5%), 4. infarct with undetermined cause (39.9%), and 5. infarction with associated extracranial arterial pathology including embolism from a carotid source (5.4%)[28-30].

The origin of AIS can be attributed to local thrombosis, embolism from an upstream source or hemodynamics (hypoperfusion)[31, 32], with in situ thrombosis being the most common[33]. Thrombosis is a cascade of platelet-mediated events that result in blood coagulation with the presence of the dynamic shear stress, clotting factors, and other proteins and cells, whereas clotting generally refers to the polymerization of fibrinogen to fibrin in regions of stagnant blood flow[34]. Ischemia due to thrombosis is normally led by the excessive thrombus developed over the atherosclerotic plaque or an abnormality of blood clotting[31]. More frequently, thrombus forms at other locations, e.g. the common carotid artery bifurcation, and the thrombus may eventually break away from the plaque to form a cerebrovascular "embolus"-- meaning "plug" in Greek. The embolus is swept downstream by the circulating blood and lodges within a cerebral vessel, often at bifurcation sites, resulting in an artery-to-artery embolism. Aside from atherosclerotic plaques, other common sources of cerebral emboli are of cardiac origin associated with such diseases as atrial fibrillation (AF), infective endocarditis, mitral stenosis, myocardial infarction, patent foramen ovale and prosthetic mechanical valves[35-38]. Although it is difficult to estimate the origin of the embolus in stroke patients, cardioembolic stroke accounts for approximately 20% of all ischemic strokes, and about 15-20% of ischemic strokes occur in patients with AF[36, 39, 40]. Hemodynamically determined infarction happens when the proximal blood supply to the brain is unavailable (e.g., cardiac arrest, arterial dissection), and collateral compensatory blood flow is insufficient either due to global hypoperfusion[31] or normal anatomical variants.

Stroke related disability varies depending on the location and extent of the affected area. The most common site for large vessel occlusion is the MCA (Figure 1-3)[41-44]. Clinical symptoms such as acute hemiparesis, hemisensory loss, hemianopia, visuospatial neglect, and aphasia are attributed to infarction of the MCA territory[45, 46]. Due to the fact that the MCA is the most common site of AIS, a model system mimicking human MCA occlusion is developed in this study for thrombectomy device testing.

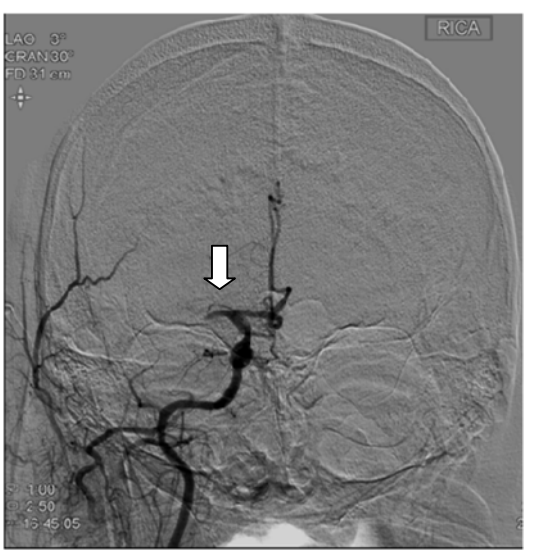

Figure 1-3 Angiogram of a typical stroke patient where the middle cerebral artery is occluded (arrow).

AF and AIS

Embolic stroke due to AF is a common observation; and patients with AF account for half of all patients with cardioembolic stroke[47, 48]. In AF, the disorganized electrical signals in the atria cause independent depolarization of atrial muscle fibers, and the atria quiver instead of beating effectively. The blood is not completely pumped out from the

atrium to the ventricleresulting in a consequent tendency of thrombogenesis (the pathogenesis of thrombus formation). The mechanism of thrombogenesis in AF may be understood according to the Virchow triad[49], in which three components including abnormal changes of blood flow, blood constituents, and vessel wall are proposed [50].

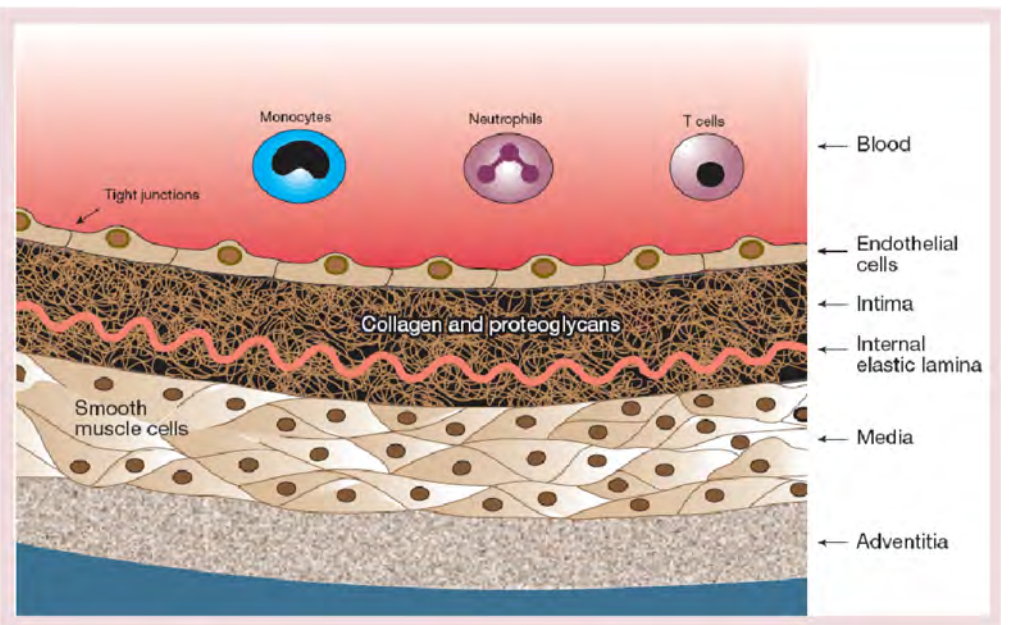

Figure 1-4 Structural features of the blood vessels[51].

The lining of the atrium, as with the entire circulatory system, is made of endothelial cells (ECs), which are directly exposed to the blood flow and supported by the internal elastic lamina (Figure 1-4). It has been noted that ECs do not act as a passive barrier; on the contrary, via shear stress from the circulating blood flow they adjust vascular tone by producing nitric oxide and play an important role in blood coagulation, fibrinolysis, angiogenesis (formation of new blood vessel), inflammation by expressing thrombomodulin, synthesizing von Willebrand factor (vWf), and releasing substances

such as tissue-type plasminogen activator, P-selectin and tissue factors[52, 53 54, 55]. In AF, blood stasis in the atrium, especially in the left atrial appendage (Figure 1-5), decreases the antithrombotic activity of ECs, and allows thrombin and fibrinogen to settle at the vessel wall, thereby facilitating thrombus formation[54].

Turnover of extracellular matrix (ECM), endothelial dysfunction and denudation occur as a consequence of AF (Figure 1-5). The abnormal changes in ECM induce fibrosis and infiltration of the endocardium, and further promote thrombogenesis. Damage of the ECs give rise to an elevated vWf level, which promotes platelet adhesion and activation of blood coagulation[56].

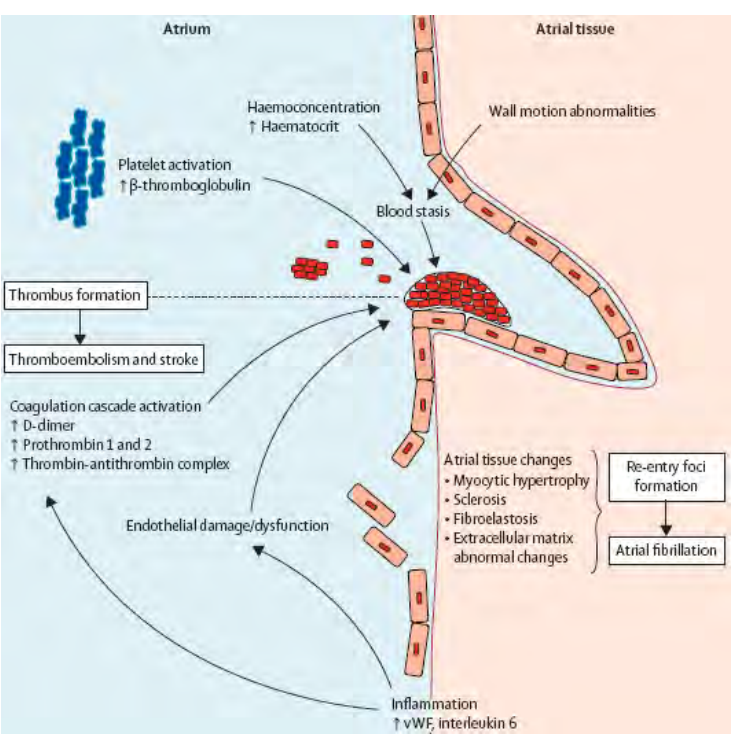

Figure 1-5 Thrombogenesis in atrial fibrillation: Virchow's triad revisited[50].

A hypercoagulable state in AF induced by abnormal changes in blood constituents such as fibrin D-dimer and platelets has been well-investigated[57-59]. It is found that patients with AF have increased amount of plasma D-dimer, a marker of the activation of the coagulation system[60], and β-thromboglobulin, a platelet-specific protein which is released during platelet aggregation and thrombus formation[50]. If the thrombus formed in the atrium is dislodged from the heart, an embolus can travel to an artery that supplies blood to the brain producing a cardioembolic stroke.

Atherosclerosis and AIS

The Northern Manhattan Stroke Study conducted between 1993 to1997 reveals that the prevalence of the intracranial atherosclerotic disease (ICAD)-related ischemic strokes is 3, 15, and 13 per 100,000 people for white, African American, and Hispanic subjects, respectively[61]. ICAD-related strokes account for 9, 17, and 15% of all ischemic strokes among white, African American, and Hispanic patients, respectively[62]. A higher incident rate of ICAD-related stroke (33 to 37% of all ischemic strokes) is observed in the Chinese population[63]. As mentioned earlier, expansion of the plaque and disruption of the unstable atherosclerotic plaque are two risk factors responsible for the occurrence of the AIS[64]. The plaque is morphologically characterized by a thin fibrous cap, a large atheromatous core, lipid-laden macrophages and reduced number of smooth muscle cells (Figure 1-6). There are two mechanisms by which intracranial plaques cause AIS, 1. Acute plaque rupture with distal embolus or 2. In situ thrombosis leading to occlusion of the vessel at the site of the plaque with or without plaque rupture.

Atherosclerosis is the thickening and hardening of the arteries due to the build-up of the fatty substances ("athero" means fatty, and "sclerosis" means scar). Risk factors for atherosclerosis include aging, diet, hypertension, smoking, and family history. The deposition, aggregation and oxidation of the low density lipoproteins (LDLs) are thought to trigger the progression of the atherosclerotic lesion[65, 66]. Oxidized LDL injures the endothelium and causes the endothelial cells to express endothelial leukocyte adhesion molecule-1[67], which attracts certain kinds of white blood cells such as monocytes and T-lymphocytes to the vessel wall[57]. With time, the monocytes transmigrate across the endothelial cells to form the foam cells (macrophages filled with cholesterol esters), and stimulate the growth of the smooth muscle cells (SMCs) from the media (Figure 1-6)[51, 68]. The development of the plaque can be classified into two different types: diffuse dilative atherosclerosis and focal stenotic atherosclerosis[69].

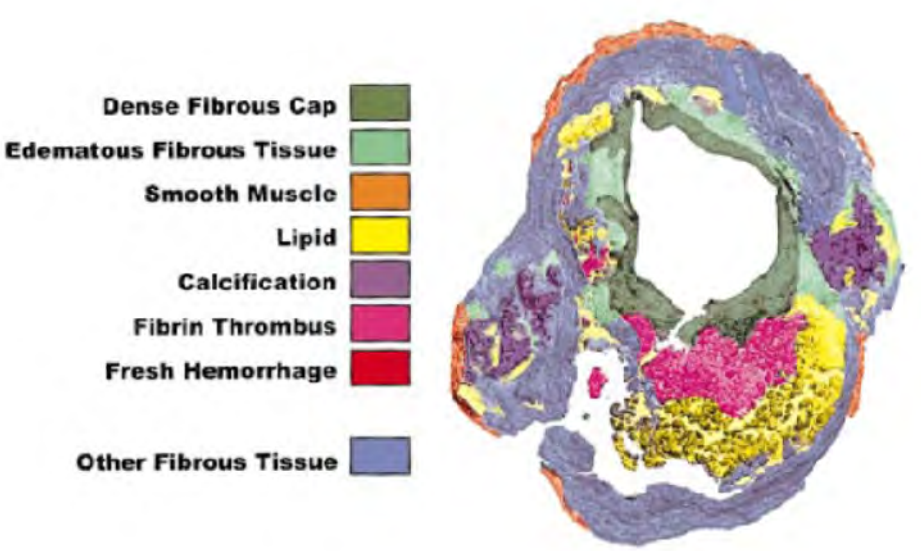

Figure 1-6 Various components of the atherosclerotic lesion of the human carotid endarterectomy specimen were identified by a color-coded image[70].

The diffuse dilative atherosclerosis is seen when smooth muscle cells and collagen fibers are accumulated in a slow and continuous manner. The presence of a large numbers of smooth muscle cells and collagen fibers increases the thickness of the fibrous cap, and strengthens the plaque structure, resulting in a stable fibroatheroma. A compensatory local dilation of the artery (vascular remodeling) is usually observed and assumed to be the final stage of this type of disease progression[71, 72].

The focal stenotic atherosclerosis is a rapid and unpredictable process. Compositional changes of the plaque could happen as a result of a multi-factorial process and make the plaque vulnerable. Vascular smooth muscle cells (VSMCs) synthesize collagen type I and III, and the balance between the collagen synthesis and degradation determines the stability of the fibrous cap[73, 74]. Previous studies have found that the cytokine interferon gamma, a product of activated T-cells, inhibit the collagen synthesis and induce VSMCs apoptosis[75, 76]. The inflammatory cells are found to be infiltrated and cluster in the shoulder region of the plaque, where disruption usually takes place. In addition, the foam cells die by necrosis or apoptosis, resulting in extracellular lipid deposition[77], and reduce the strength of the fibrous cap located between the lipid-rich atheromatous core and the endothelial layer [78-80]. The abovementioned determinants all make the plaque prone to rupture, and lead to excessive thrombus formation (thrombosis) over the ruptured plaque (Figure 1-7) [69, 81, 82].

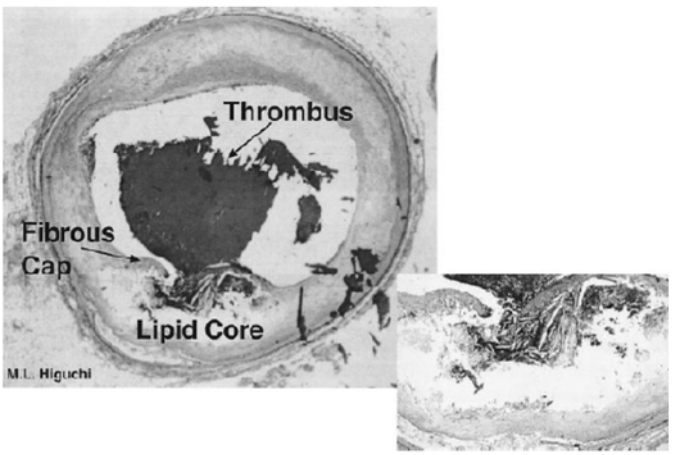

Figure 1-7 (Left) Thrombus is formed over a disrupted atherosclerotic plaque. [61] The close-up view of the lipid core, where cholesterol crystals are seen[82].

When the vessel wall is injured or the fibrous cap of the atherosclerotic plaque is ruptured, vWf binds to the exposed connective tissue, followed by the adhesion of platelet through the membrane-bound receptor glycoprotein Ib[83]. The injured endothelium exposes tissue factor (TF) to factor VII (FVII), and the resulting product, activated factor VII /TF complex is then able to enzymatically catalyze factor X, initiating the extrinsic coagulation pathway shown in Figure 1-8 [84-86]. Activated factor X combines with factor Va to form prothrombinase and further support thrombin generation. Thrombin, coupled with adenosine diphosphate and thromboxane A2 secreted by activated platelets, contribute to platelet aggregation and produce a stable fibrin thrombus[87].

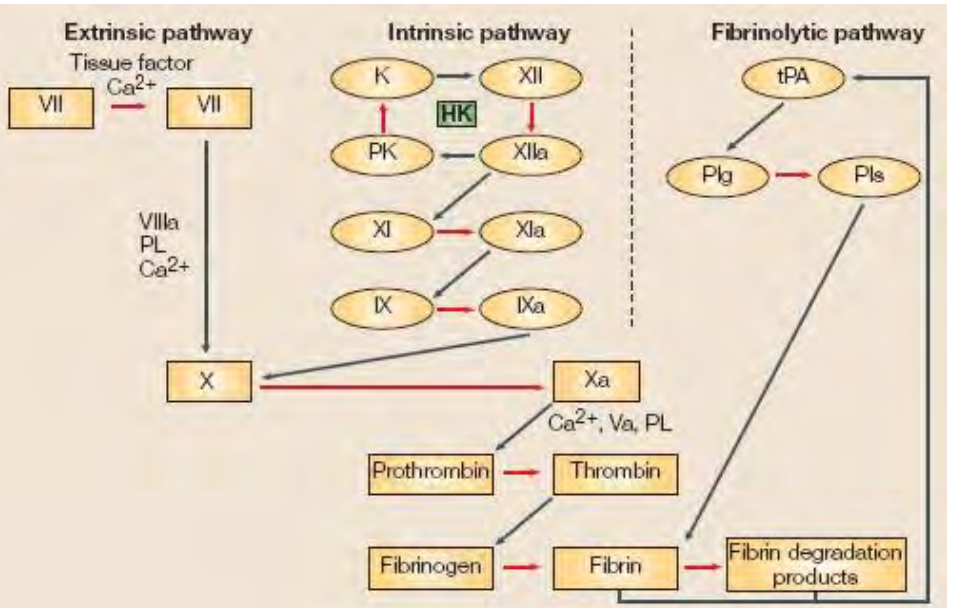

Figure 1-8 Mechanisms of clotting factor interactions[88].

FDA-Approved Pharmacological Treatment of AIS

Intravenous fibrinolytic therapy with tissue plasminogen activator (IV-tPA) is the only approved pharmacological treatment for acute ischemic stroke[89]. The product of the tPA-mediated plasminogen activation, plasmin, cleaves and degrades fibrin[90, 91]. The NINDS rt-PA Stroke trial, a randomized, double-blinded clinical trial, proved that a reperfusion strategy with IV-tPA dramatically improves patient outcome[92]. Figure 1-9 demonstrates that a greater proportion of patients left with minimal or no deficit 3 months after tPA therapy as indicated by mRS 3 or less. As compared with the placebo treatment, tPA therapy was not accompanied by an increase in severe disability and mortality. Mortality at three months was 17% in the t-PA group and 21% in the placebo group.

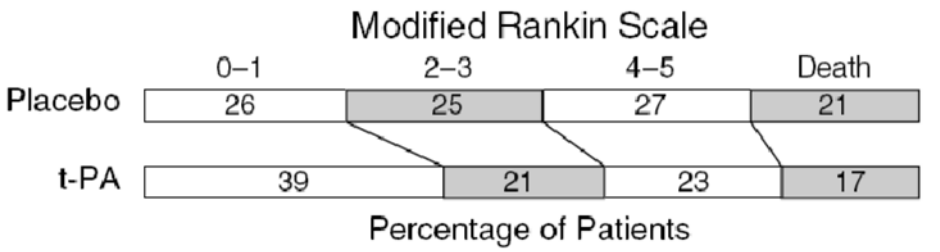

Figure 1-9 Clinical outcomes at 90 days by modified ranking scale (mRS) in the NINDS rt-PA Stroke Trial. The outcome measure favors the t-PA group[92].

However, this approach has severe limitations including short time window (within 3 hours of onset)[43], risk of symptomatic hemorrhage, and numerous contraindications[93]. Ultimately, this results in a low percentage of patients, 1-3%[94], eligible to receive this therapy. Note, the modified Rankin Scale (mRS) indicates the level of neurological disability on a 0-6 scale, where 0 is no neurological impairment and 6 is death. Importantly, a mRS score less than or equal to 2 signifies that the patient is capable of independent living and this is a commonly used threshold for therapeutic efficacy studies.

FDA-Approved Mechanical Thrombectomy Devices for AIS

There are two FDA-approved endovascular devices for the treatment for acute ischemic stroke, namely, the MERCI retriever system and the Penumbra System[94-96]. The MERCI retriever system (Concentric Medical Inc, Mountain View CA) is a flexible tapered nitinol wire with several helical loops that is deployed via a microcatheter and embedded within the thrombus for retrieval. An improvement in neurological outcome with the use of the X6 Merci Retriever (Figure 1-10 (a)) 8 hours after onset of ischemic symptoms (beyond the traditional 6-hour window) was reported[97]. The final results of the multi-MERCI trial published in 2008 shows an improvement in the recanalization rate by using new generation L5 MERCI (Figure 1-10 (b)) to treat patients with large vessel occlusion[98].

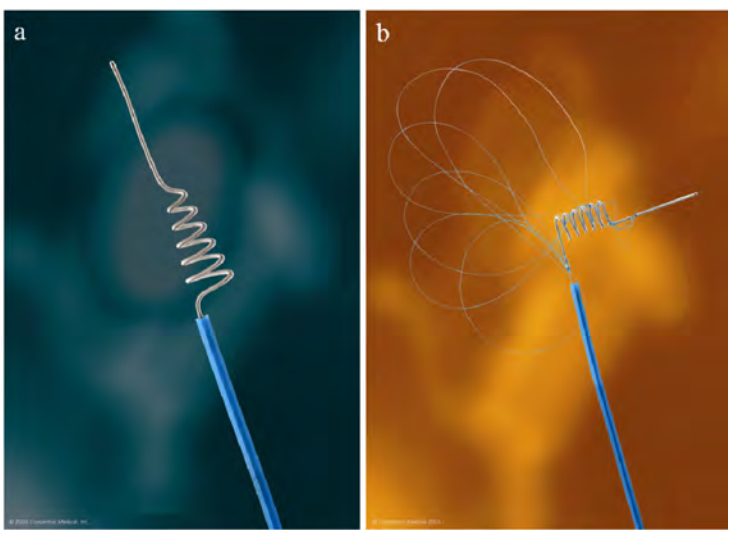

Figure 1-10 (a) The Merci non-filamented (X6) and (b) filamented retriever (L5) (Image source: Concentric Medical Inc, Mountain View CA)

The recanalization rates of the old (X5/X6) and new (L5) MERCI devices without adjunctive therapies are 46% and 57%, respectively. With adjunctive IA therapies (other mechanical interventions or administration of tPA or glycoprotein IIB/IIIA inhibitors), the recanalization rates of old (X5/X6) and new (L5) MERCI device are 64% and 70%, respectively. The mortality at 90 days is 34%, and symptomatic intracranial hemorrhages occurred in 10% of the patients. A final recanalization rate of 68% is reported, and overall, 36% of patients have a mRS score ≤ 2 after 90 days. Importantly, almost half of the patients (49%) in which recanalization is achieved have an independent lifestyle (mRS ≤ 2) after 90 days, as compared to only 9.6% in those patients in whom the intervention failed (Figure 1-11). More than half of the patients in whom revascularization was not achieved die within 90 days after the MERCI treatment. These data, which show an increase in independent living and a reduction in mortality when mechanical revascularization is achieved, have been consistent across all of the MERCI trials and provide a strong impetus for device mediated vessel recanalization.

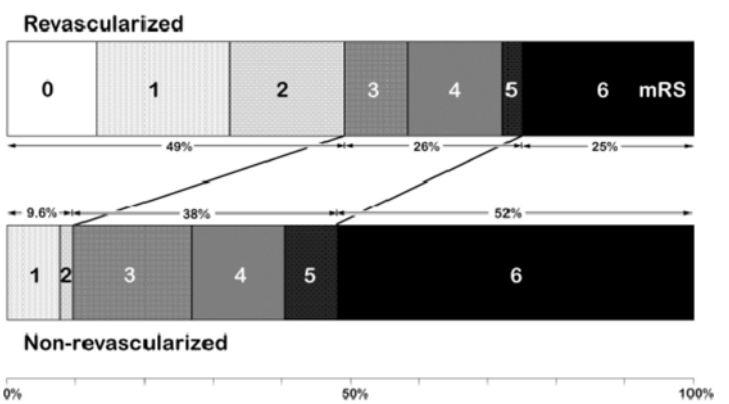

Figure 1-11 Clinical outcomes at 90 days by mRS show an increase in independent living and a reduction in mortality when mechanical revascularization is achieved[98].

Comparisons between the recanalization rate, functional status and mortality reported in the multi-MERCI trial and the PROACT II study are available[99]. In the PROACT II study, intra-arterial prourokinase recanalized 66% of the MCA occlusions, whereas the MERCI retriever restored the blood flow in 68% of the patients with the large vessel occlusions in the MCA, the carotid terminus or vertebrobasilar arteries. In the PROACT II study, an overall mortality is 25%, and 40% of the patients show favorable outcome (mRS≤ 2) at 3 month follow-up. Despite similar recanalization rates, the mortality presented in the multi-MERCI trials is higher than that reported in the PROACT II study, which could be due to the difference in the inclusion criteria as described above. Recently, Merci and Multi Merci investigators parsed their data for patients who would have been eligible for enrollment in PROACT II[99]. They were able to conclude that mortality was indeed explained by baseline stroke characteristics and trial design, and did not differ between the relevant patients in the MERCI trials and PROACT II control arm. Moreover, embolectomy produced similar functional outcome results in this subset of MERCI/multi-MERCI patients as compared to the PROACT II treatment arm. It is important to mention that adjusted comparisons were hampered by the failure to obtain access to the individual patient level data from PROACT II.

The second, more recently FDA-approved thrombectomy device is the Penumbra Aspiration System (Figure 1-12) consists of a reperfusion catheter, a separator, and a vacuum pump that removes the thrombus through 2 mechanisms: maceration and aspiration.

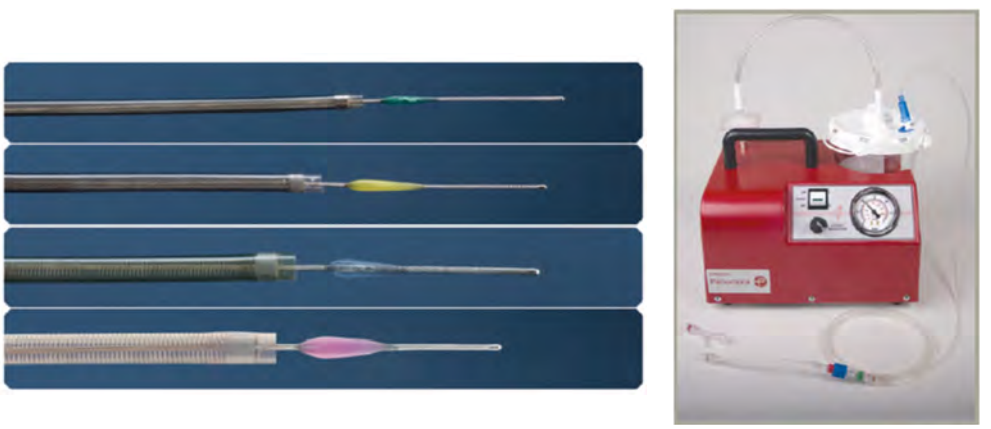

Figure 1-12 Reperfusion Catheter/Separator pairs are available in numerous sizes (left). The Penumbra reperfusion suction pump is connected to the Penumbra reperfusion catheter by an aspiration tubing and provides continuous suction when activated (right) (Courtesy of Penumbra, Inc., Alameda, CA)

In a recent clinical trial[100], the safety and effectiveness of the Penumbra system were tested in the treatment of 125 acute stroke patients. Before treatment, the average mRS of 125 patients was 4.5±0.8, and 96% had Thrombolysis in Myocardial Infarction (TIMI) 0 flow (no perfusion). The target vessel locations included ICA (18%), MCA (70%), vertebrobasilar (9%) and others (3%). The clinical outcome showed the Penumbra system was effective in revascularization, and resulted in 82% achievement of TIMI 2 (partial perfusion of the artery with incomplete or slow distal branch filling) or TIMI 3 (complete perfusion of the artery) flow. At 30-day follow-up, 42% of patients had a good clinical outcome, which was defined as a $\geq$ 4 points improvement in National Institutes of

Health Stroke Scale (NIHSS) score or mRS score ≤ 2. The mortality rate was 26% and the rate of symptomatic hemorrhage was 11%. Interestingly, in those patients in which the primary lesion was recanalized, only 29% had an mRS ≤ 2 after 90 days. That is nearly half the number of patients with an independent lifestyle than observed in the multi-MERCI trial following successful recanalization. It is reasonable to hypothesize that mitochondrial dysfunction triggered by the initial injury, inflammatory processes, initiation of apoptosis, and the distal emboli from maceration of the occlusive embolus may be potential explanation for this observation. Safety parameters, such as device related serious adverse events and rate of intracerebral hemorrhage were found to be comparable with historical controls.

Other Treatments for AIS

There are a variety of minimally-invasive treatments for acute ischemic events such as endovascular snares[101], balloon angioplasty[42, 102], intracranial stenting[103], and selective intra-arterial infusion of thrombolytic agents. During balloon angioplasty, the revascularization is achieved by inflating the balloon at the occlusion site to flatten or compress the plaque or thrombus. Improved clinical outcome after balloon angioplasty in patients who are resistant to intra-arterial thrombolysis has been documented[104]; however, the drawbacks of the balloon dilation such as risks of elastic recoil and dissection limit the applicability of this technique[105]. Favorable clinical outcomes (79% recanalization rate) with another endovascular treatment, balloon expandable stent, are also observed in previous studies[106, 107]. Balloon-assisted stenting provides higher radial force as compared

to balloon angioplasty, but the overexpansion of the stent may cause vessel damage[105]. In addition, the rigidity of the stent influences the deliverability in the tortuous intracranial circulation during the treatments of the intracranial diseases.

The recently available self-expanding stent combines the advantages of balloon angioplasty and balloon-assisted stenting, and is more suitable for the treatment of acute cerebrovascular occlusions[108]. The self-expanding stent is more flexible and applies less radial outward force against the vessel wall. In a first FDA-approved prospective trial of primary intracranial stenting for acute stroke[109], the safety of the Wingspan intracranial self-expanding stent system (Boston Scientific) was evaluated in 20 enrolled patients with AIS. A 100% recanalization rate was reported (12 patients had TIMI 3 and 8 patients had TIMI 2), and at 1-month follow-up, mRS $\leq$3 was achieved in 12 patients and mRS $\leq$1 was achieved in 9 patients. The promising results from this trial suggest the potential utility of the self-expanding stent in the treatment of AIS. The one drawback of the technique is the permanent implantation of a metallic endoprosthesis, which necessitates proper anti-platelet therapy. The administration of antiplatelet medications could complicate the risk of increased frequency or severity of intracranial bleeding. The concept of using the stent as a retriever was also documented in the previous studies. Wakhloo and Gounis first demonstrated the use of self-expanding stents for clot removal in the laboratory[110]. This technique has been applied clinically where the Solitaire FR (flow restoration) Revascularization Device (ev3, Irvine, California) successfully recanalized 90% of cases where the MERCI retriever had previously failed[111].

Ultrasound refers to sound waves with frequencies above 20 kHz, and is generated by a piezoelectric transducer. The transducer receives the electric input and vibrates when the frequency of the voltage reaches the resonance frequency of the piezoelectric material. The vibration is then transmitted as ultrasonic pressure waves. Two commonly used frequency ranges in medicine are assigned as low (20-400 kHz) and high (0.5-3 MHz) frequency[112]. Low frequency, high power ultrasound has better tissue penetration, and is utilized therapeutically. Currently, there are three different approaches to execute ultrasound thrombolysis: transcranial ultrasound thrombolysis[113], catheter-delivered transducer tipped ultrasound thrombolysis[114], and catheter-delivered external transducer ultrasound thrombolysis[115, 116]. One of the main mechanisms by which ultrasound thrombolysis occurs is called "cavitation". Cavitation happens when a fluid is violently agitated, and it involves creation, growth, oscillation, and collapse of bubbles in the medium. During negative phase of the ultrasound wave, the microbubbles form in the thrombus. These bubbles collapse and give rise to a series shock waves causing thrombus fragmentation[112]. Other forces produced from the bubble dynamics such as shear stress and liquid jets also contribute to the clot ablation[117].

Hong et al. employed a flexible titanium wire probe to disrupt the whole blood clot and cell-free fibrin clot in test tubes[118]. A continuous ultrasound wave was generated and delivered by an ultrasonic lithotripsy generator at a frequency of 20 kHz. It was observed that a 56 cm wire probe broke a 1.2 g whole blood clot in 45 seconds, and clot age had no effect on the time required for disruption. Debris as large as 80 μm was detected in the disrupted whole blood clot solution, while the size of the disrupted cell-

free fibrin clots was around 40 μm. Halkin et al. illustrated the ultrasound thrombolytic effect on cardiac vessel patency[112]. In coronary arteries, ultrasound wave decreased the degree of stenosis and increased the coronary blood flow. The safety and efficacy of the coronary ultrasound thrombolysis by using catheter-delivered external transducer ultrasound system were also documented in the previous animal data and clinical results. In this thesis work, the application of waveguide ultrasound technique is expanded to the ablation of the clot in cerebral arteries where the vessel geometry is more complex and tortuous. The waveguides are different than the EKOS ultrasound device (EKOS Corporation, Bothell, Washington, USA). The EKOS ultrasound device is delivery concurrently with infusion of a thrombolytic agent through the microcatheter. The acoustic pressure gradient generated by the ultrasound moves the drug into the clot and accelerates its dissolution. On the other hand, the waveguide ultrasound technique disrupts the clot by cavitation with a waveguide due to its mechanical motion (vibration) induced by the ultrasound energy. The success of this design may provide another option for physicians to treat patients with acute ischemic stroke.

Specific Aims

There is an incomplete understanding of the anatomy and physiology leading to stroke. Therefore, I hypothesize that AN ANATOMICALLY AND PHYSIOLOGICALLY REPRESENTATIVE MODEL SYSTEM OF CEREBROVASCULAR OCCLUSION IS REQUIRED AND CAN BE BUILT FOR

EVALUATION OF MECHANICAL THROMBECTOMY DEVICES IN-VITRO. To test this hypothesis, I propose the following specific aims:

Specific Aim I: To create a representative in-vitro model of human focal, vascular occlusion

a. To build realistic models of human intracranial vasculature and a flow loop to simulate human cerebral circulation. Brain magnetic resonance angiography (MRA) data sets from normal patients are collected for the geometric analysis, and the results from the vessel characterization are used to determine the best matching vasculature to build replicas with representative anatomical features by using a novel batch manufacturing process. A transparent replica with uniform wall thickness is connected to a flow loop which consists of a computer-controlled cardiac pulse duplicator, flow probes, pressure transducers, and data acquisition system to simulate and monitor human intracranial hemodynamics for testing of the thrombectomy devices.

b. To prepare and characterize EAs. EAs will be created to occlude the silicone replica mimicking the acute arterial occlusion in human. Impacts of species, thrombin and barium sulfate concentration on the mechanical properties of the EAs will be investigated. Moreover, the structural and mechanical characteristics of the EAs will be compared with those of the human sources of emboli.

Specific Aim II: To evaluate the efficacy of the mechanical thrombectomy device in the abovementioned model

The MERCI retrieval system, the Penumbra aspiration system, a self-expanding stent, and an ultrasonic endovascular system comprising an ultrasonic energy source, transducer and ultra thin wire are activated to mechanically interact with the embolus analogues in the flow loop. The flow restoration and particulate size analysis are critical indicators to determine the efficacy and safety of each device.

Chapter II: Neurovascular Modeling: Small-Batch Manufacturing of Silicone Vascular Replicas

Abstract

The objective of this work is to develop an efficient methodology for manufacturing realistic cerebrovascular replicas. Brain MRA data from 20 patients were acquired. The centerline of the vasculature was calculated and geometric parameters measured to quantitatively describe the ICA siphon. A representative model was created based on the quantitative measurements. Using this virtual model, a mold with core-shell structure was designed and converted into a physical object by fused deposit manufacturing. Vascular replicas were created by injection molding of different silicones. Mechanical properties, including the stiffness and luminal coefficient of friction, were measured.

The AC, length and curvature of the ICA siphon were 4.15±0.09 mm, 22.60± 0.79 mm and 0.34±0.02 mm-1 (average ± standard error of the mean), respectively. From these image datasets, a median virtual model was created and this virtual model was transformed into a physical replica by an efficient batch manufacturing process. The coefficient of friction of the luminal surface of the replica was reduced by up to 55% using liquid silicone rubber coatings. Depending on the material used to make the replica, the modulus ranged from 0.67 to 1.15 MPa compared to 0.42 MPa for a cerebral artery from human autopsy studies. A population-representative, smooth, and true-to-scale

silicone arterial replicas with uniform thickness were successfully built for in-vitro neurointerventional device testing using a batch manufacturing process.

Introduction

Recent advances in minimally invasive neuroendovascular interventions such as aneurysm coiling, clot retrieval, balloon angioplasty and stenting have been applied in the treatment of cerebrovascular diseases[103, 119, 120]. For the successful development of new devices designed for the intracranial circulation, in vitro evaluation in realistic vascular replicas is an important part of the design phase[121-124]. Of particular importance is the ICA siphon, which offers challenging tortuosity for endovascular access. Several different manufacturing processes for fabrication of vascular replicas have been described previously. Physical 3D vasculature models have been obtained either by injecting methylmethacrylate into human cadavers to get vascular lumen casts[125-132] or by rapid prototyping based on imaging data[129, 130, 132]. Different methods, including repeated painting[125, 131], dip-spin processing[126], and lost-wax technique[128] have been applied to the casts to form the elastomeric replicas. The procedures mentioned above successfully fabricated a variety of vascular replicas; however, some limitations of these manufacturing processes cannot be ignored. First, the high friction resistance on the surface of silicone impeded the deliverability and deployment of endovascular devices in the silicone replicas[133]. Secondly, achieving desired wall thickness by repeated painting or dip-spin steps was time-consuming and not precise. Importantly, each model was essentially made by hand, and therefore with limited reproducibility and large time expenditure.

The goal of the earlier studies was to make patient-specific silicone models instead of a model capable of representing the geometry of a population of patients. To prepare the latter model, vessel characterization is essential. The morphology of intracranial arteries varies not only from location to location, and patient to patient but also as a result of a number of diseases[134, 135]. Therefore, vessel characterization provides the necessary data upon which to base a population averaged vascular replica. Various methods are available for vessel characterization in 2D or 3D space[136-138], and among them, tortuosity evaluation is widely discussed. To date, tortuosity lacks a universal definition[137], but is generally used to summarize curvature information along the centerline of a blood vessel[139]. Curvature at a point of the space centerline represents the rate of change of the tangent with respect to the arc length and can be calculated by using standard formulae from the Frenet-Serret theory of differential geometry[140, 141]. By collecting a set of curvature data, the total and average curvature of a vessel segment can be obtained.

During neuroendovascular therapy, access of neurovascular devices to the anterior intracranial circulation requires navigation through a relatively tortuous ICA siphon, where the anatomy can make access difficult[142]. In this study, the median AC, length, and diameter of the ICA siphon from 20 patients were used to build a true-to-scale, batch-manufactured, transparent silicone replica of a population representative model. Furthermore, the inner wall of silicone replica was modified by the LSR topcoat to provide lubricity for the delivery of endovascular devices.

Materials and Methods

Patient Selection and MR Imaging

Twenty anonymized brain magnetic resonance angiography (MRA) data sets were acquired from a retrospective review between December 30, 2007 and January 23, 2008 of patients (10 men and 10 women with a mean age 60.4 and 42.1 years old, respectively) having no pathological findings. MR imaging was performed using a 1.5T system (GE Signa Excite, Waukesha, WI) and a receiving 8-channel head coil. Brain 3D time of flight MRA (TOF MRA) data were acquired (TR, 33.3 ms; TE 6.9 ms; FA, 20º; FOV, 200 x 200mm; matrix 512 x 512; section thickness, 1.4mm with 0.7mm gap).

Vessel Segmentation and Centerline Generation

MRA images were imported slice-by-slice into Mimics (Materialise, Leuven, Belgium) and stacked to formulate a 3D model (Figure 2-1). The target vasculature was extracted from the neighboring tissue by thresholding. To generate a segmentation mask, minimum and maximum threshold values were set and segmentation was further restricted by cropping the mask. The selected pixels (highlighted in yellow in Figure 2-1) in each slice were connected, resulting in a clean mask for the use of 3D model construction. The 3D segmentation object was fixed to assure that there were no shells, holes, noise or bad edges, and smoothed before skeletonizing. The resulting centerline was composed of control points equally spaced at a constant 0.4 mm interval.

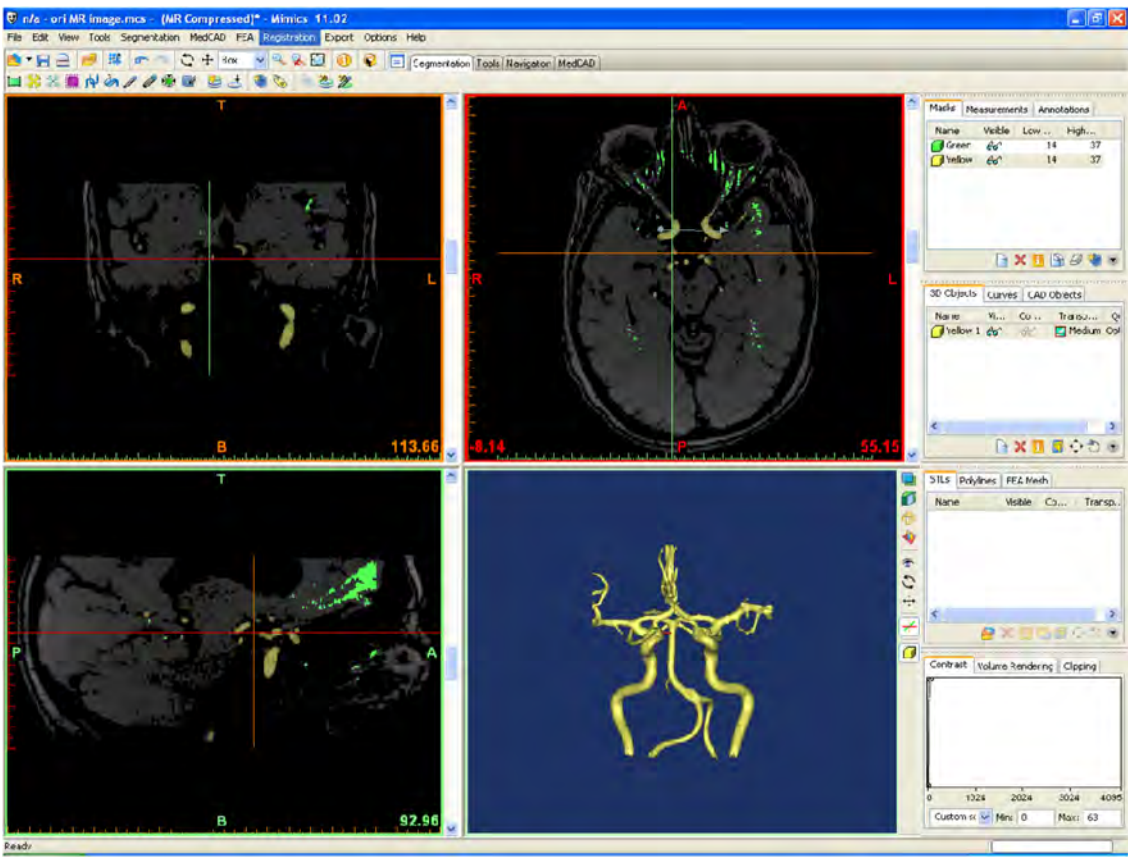

Figure 2-1 Mimics displayed the image data in several ways: (upper left) the coronal view, (upper right) the axial view, (bottom left) the sagittal view, and (bottom right) the 3D view.

Vessel Characterization and Model Selection

The path length of extracted centerline and the diameter of the best fit circle to the vessel cross-section at each control point were recorded and averaged. The results were presented as average ± standard deviation.

The AC of left and right ICA siphons of 20 patients was calculated. The vessel centerline r(s) = [x(s), y(s), z(s)] was first parameterized by arc length, and then fitted

with a 10^{th}-order polynomial for smoothing. To evaluate the goodness of fit, the degree of polynomial varying from 2 to 22 was applied to the original data set, respectively, and the root mean square error (RMSE) was calculated[143].

The smoothed centerline was re-sampled to give control points at constant 0.05 mm intervals for curvature evaluation. The curvature (k) at each control point and the AC were given by[140, 141]:

$$\kappa = \frac{|r'(s) \times r''(s)|}{|r'(s)|^3} \quad \text{Eq (1)} \qquad AC = \frac{\sum_{i=1}^{n} |\kappa_i|}{n} \quad \text{Eq (2)}$$

where r'(s) and r''(s) denoted the first and second derivatives of the centerline, and n indicated the total number of points.

The nonparametric Wilcoxon signed rank test was performed (GraphPad Prism 5, La Jolla CA) to compare the median of each vessel feature against a hypothetical median, which was every single geometric parameter for the left and right ICA siphons in each patient . In this test, p value greater than 0.05 concluded that there was no statistically significant difference between the median of a group of samples and the hypothesized median.

Generation of the Vascular Replica

A mold with a core-shell structure was created for silicone injection (Magics, Materialise, Leuven, Belgium). The inner core, representing the geometry of the

vasculature was encapsulated by the outer shell which was created based on the geometry of the core. The distance between the core and shell was the thickness of the silicone replica, which can be precisely controlled. In this study, the wall thickness was 1 mm.

The virtual design was transformed into a physical object (Prodigy Plus, Stratasys, Eden Prairie MN) using fused deposit manufacturing to build the model in a layer-by-layer manner, with a layer thickness of 0.178 mm (Figure 2-2). The extrusion head in the build envelop was heated to melt both the mold and support materials and was moved in both horizontal and vertical directions by a numerically controlled mechanism. The production capacity per batch was determined by the size of the target vasculature. For instance, 6 ICA-MCA core-shell models with a dimension of 47×41×81 mm3 each can be built in one batch, and completed in 30 hours. The dual build heads in the heated build envelop extruded the model (co-polymer of acrylonitrile, butadiene, and styrene) and support materials along the designated tool path. Both materials fused together to form a solid model. The soluble support material was removed in the sodium hydroxide solution at 70 ºC, which required approximately 24 hours.

Figure 2-2 Cross-sectional view of the vascular model during the build process

Xylene and 2-propanol were infused into the mold alternately to smooth the core and the inner wall of the shell. It was found that repeating the alternate rinse procedure for 5 times, each time for 1 minute, achieved an adequate smoothing result. The rinsed mold was dried in the ventilation system before silicone infusion.

Sylgard 184 silicone kit (Dow Corning, Midland MI) and an injection molding grade silicone, LIM 6030 pail kit (Momentive, New Milford CT), were infused into the core-shell mold. Sylgard 184 replica was found to be optically clear, and had higher Shore A hardness. Compared to Sylgard 184, LIM 6030 had higher elongation at break, tensile strength, and viscosity. The amount of thinner SF 96-5 (GES Waterford Plant, Waterford, NY) added to the LIM 6030 mixture accounted for 7% of total mixture weight. The silicone solution was mixed and degassed at room temperature under 76 cmHg vacuum. Higher injection pressure, at least 1200 mmHg, was required for the delivery of the viscous LIM 6030 as compared to 55 mmHg to infuse the Sylgard 184 into the mold.

The silicones were cured at 60 oC for 12 hours. The whole mold was immersed in xylene for mold dissolution overnight.

LSR Topcoat Modification

LSR topcoat (Momentive Performance Materials, Albany NY), a two-component translucent matte coating with a Brookfield viscosity of 1600 centipoise, was infused into smoothed, open-ended, straight silicone tubes (11 cm in length, and 4 mm in diameter) using a peristaltic pump, and then cured at 110oC in a ventilated oven for 30 min. This procedure was repeated from 0 to 3 times. The effect of multiple coatings on the COF was evaluated by using a customized friction rig (TA-265A, Texture Technologies Corp, Hamilton, MA) which was designed according to ASTM D1894. The schematic illustration of the friction rig was shown in Figure 2-3 (a), and a cone-ring structure was design to mount the silicone material (Figure 2-3 (b and c)).

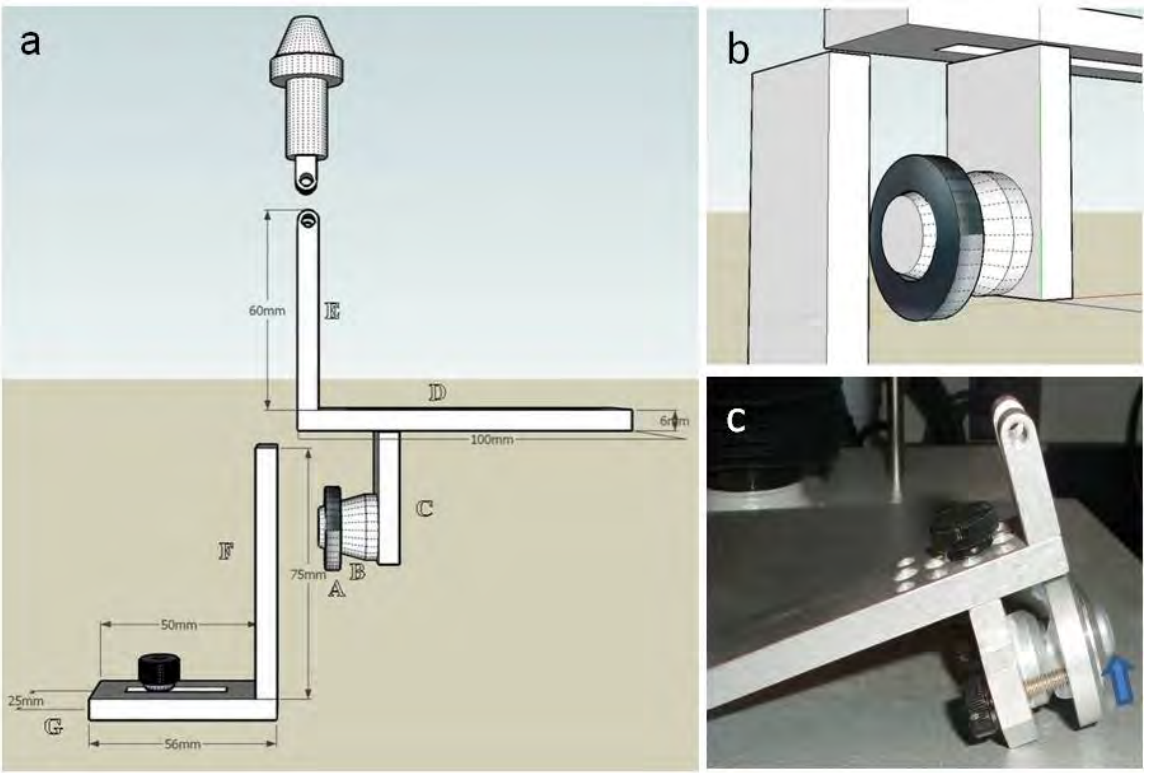

Figure 2-3 (a) The schematic illustration of the friction rig (b) The ring and cone were used to hold silicone tube material. The tube material was placed against the cone and the slid over it until a snug fit was achieved (c) A vessel sample (blue arrow) was mounted.

During the friction test, the inner lumen of the replica slid 20 mm over a flat surface at a sliding speed of 5 mm/sec for 25 times. A 200g weight was placed on the far end of D to create a higher normal force between the target surfaces. All tribological tests were conducted under ambient condition with a constant temperature of 21 ^{o}C. Five specimens were tested for each silicone material, and the average force was obtained to determine the static and dynamic COF of silicone material before and after LSR coating. The static COF was obtained from the averaged maximum force initiating motion between test material and surface, whereas, the dynamic COF was from the average force

measured for the duration of sliding. The free body diagram of the friction rig system was presented in Figure 2-4.

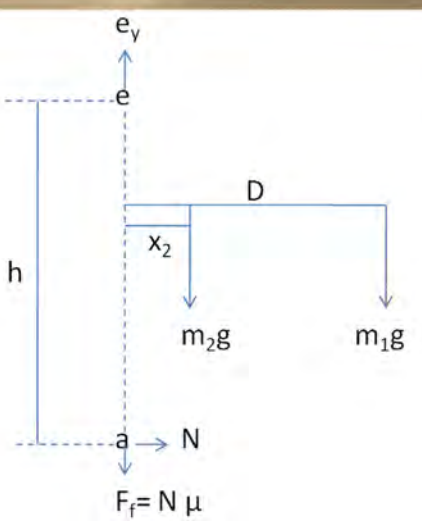

m_1 is mass added to cantilever (a 200g weight)
m_2 is mass of system
Assume $m_1 >> m_2$
Known: e_y (measured force), m_1, m_2, D, x_2, h
Unknown: N (normal force), F_f (friction force), μ (COF)
Find: μ

$$\sum F_y = 0$$

$e_y - m_2g - m_1g - F_f = 0$
$F_f = e_y - m_2g - m_1g$
$N\mu = e_y - g(m_2+m_1)$

$$\sum m = 0$$

Take moments about e and assume $x_2\, m_2g << D\, m_1g$
$hN - D\, m_1g = 0$
$N = D\, m_1g/h$

$$\mu = \frac{h[e_y - g(m_2+m_1)]}{D\, m_1g}$$

Figure 2-4 The friction rig system and its corresponding free body diagram.

The Student's t-test was performed to determine the statistical difference in friction before and after surface modification.

Tensile Test for Silicone Stripes

The stress-stretch relationship (S-S relationship) was obtained by using an Instron machine (model 5542) equipped with 0.5 kN load cell, having 651 mm vertical test space. The 5 mm wide, 50 mm long Sylgard 184 and LIM 6030 silicone strips with average thickness of 0.5± 0.06 and 0.5± 0.02 mm, respectively, were prepared for the tensile test. All the specimens (three specimens for each group) were subjected to the test at a cross-speed rate of 30 mm/min, and the S-S relationship of the silicone stripes were compared with that of the human MCA from autopsy which was performed quasi-statically at a strain rate of about 0.05 s^{-1} [144].

Results

The anatomy of the three cerebral vessels from patient 1 (PA1), patient 2 (PA2) and patient 3 (PA3) were shown in Figure 2-5 (a) through (c) having siphons with an AC ranging from 0.23 to 0.64 mm-1. PA1, PA2 and PA3 were selected to illustrate mild, moderate and severe curvature, respectively, of the ICA siphon in our patient population.

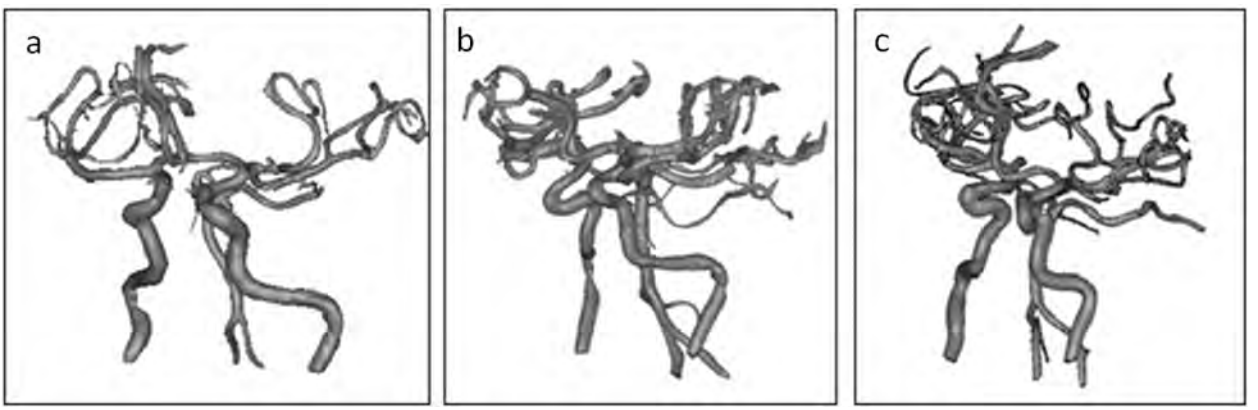

Figure 2-5 Virtual cerebrovascular models showed ICA siphons with low (a), medium (b), and high (c) curvature.

In the vessel characterization, the best-fit polynomial to smooth the original centerline data was determined by minimizing the error between of the polynomial curve and original centerline. Figure 2-6 showed that the total error decreases significantly up to the tenth-order polynomial fit, followed by a more gradual decline. The smoothed centerline was re-sampled before curvature calculation.

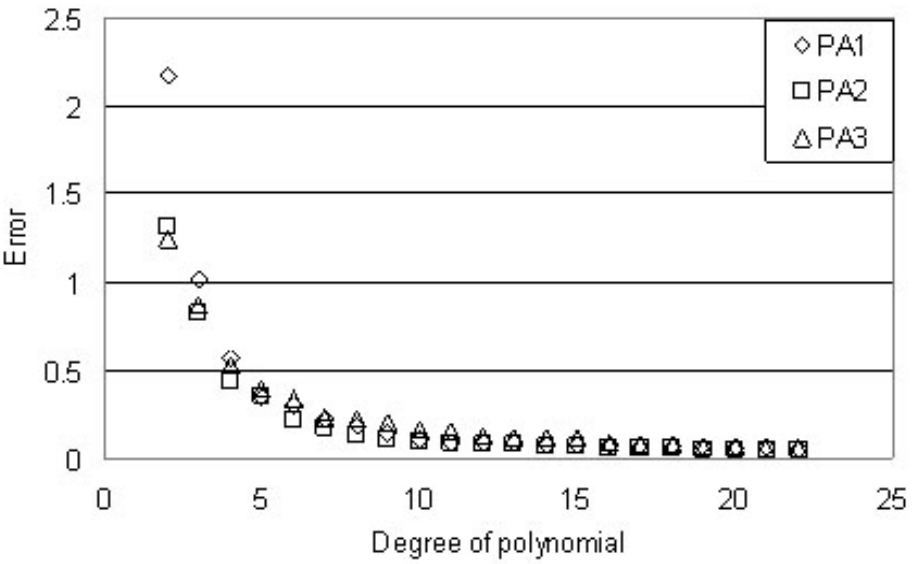

Figure 2-6 The total error decreased significantly up to the tenth-order polynomial fit, followed by a more gradual decline.

It was observed that the AC tended to increase with the decrease of the distance between control points, and became stable when the distance was less than 0.1 mm. This change was significant in the measurement of ICA siphon with severe tortuosity, whose AC increased from 0.45 to 0.65 mm-1 when the distance decreased from 0.4 to 0.01 mm. In this study, the polynomial curve was re-sampled to have points at constant 0.05 mm intervals for curvature calculation. By using the 10th-order polynomial to smooth the original centerline and giving control points with constant 0.05 mm intervals, the AC, arc length and diameter from 20 patients were 0.34±0.12 mm-1, 21.86±4.24 mm and 4.17±0.64 mm for the left ICA siphon, respectively. For the right siphon, the AC, arc length and diameter were 0.34±0.13 mm-1, 23.31±5.72 mm, and 4.12±0.44 mm,

respectively. In patient 18 (PA18), the p values resulted from the Wilcoxon signed rank test for comparisons in AC, length, and diameter were all greater than 0.05, indicating each measured parameter of PA18 had no significant difference to the corresponding median. The p-values were 0.24, 0.37, and 0.96 for the comparisons in AC, arc length and diameter, respectively, of the left ICA siphon, and 0.72, 0.29, and 0.49, respectively, for those of the right ICA siphon. This finding was only observed in PA18, and led us to select PA18 as a representative model of the chosen patient population in this study. The results of vessel characterization were shown in Figure 2-7.

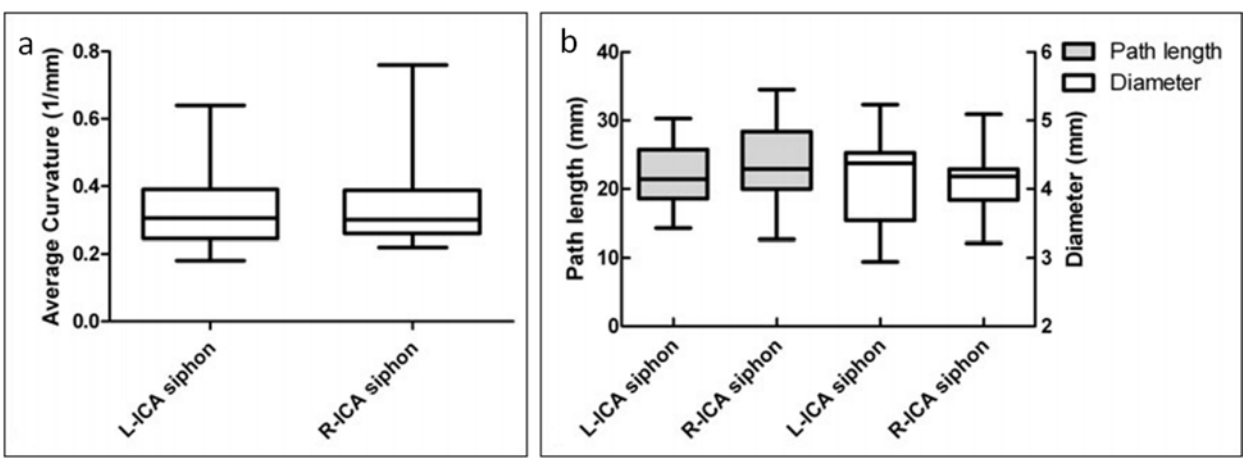

Figure 2-7 (a) AC and (b) length and diameter of the left and right ICA siphons from 20 patients.

A computer mold consisting of a core-shell structure for silicone injection was shown in Figure 2-8 (a). Silicone was infused into a mold (Fig 2-8 (b)), which contained the vasculature of circle of Willis (CoW) from PA2 as the core (Fig 2-8 (c)). Removal of the side braches and dissociation of artifactually fused vessels from the image reconstruction was done in Mimics. Figure 2-8 (d) and (e) showed silicone replicas of the

CoW from PA2 and the representative right ICA from PA18, respectively. Using this batch manufacturing process, 6 vascular replicas were made from the virtual model in 92 hours at a material cost of $250. The capital equipment and software used in this study were quite expensive; however, these tools were available at most universities and medical device companies.

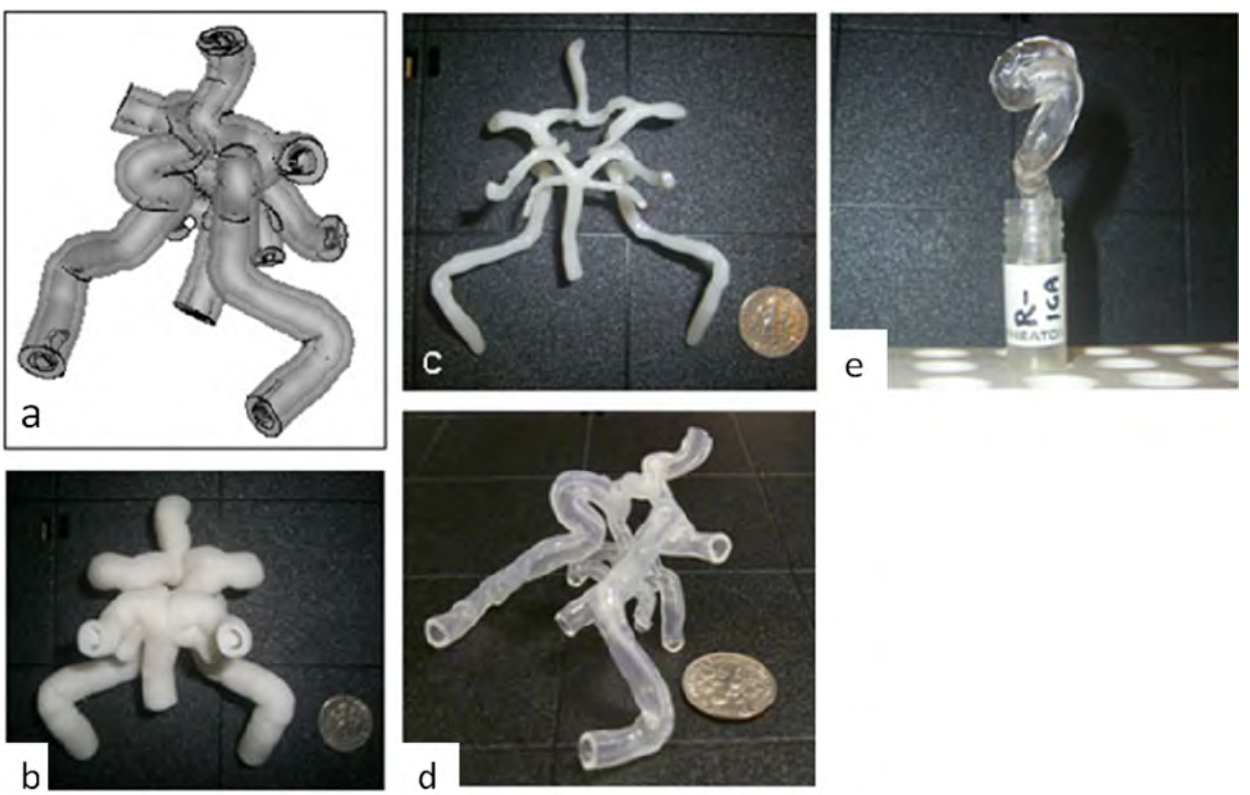

Figure 2-8 The virtual core-shell structure (a) was designed for the preparation of the physical ABS model (b) which contained the CoW (c) as the core. After silicone was cured, the ABS model (b) was dissolved in xylene, resulting in a transparent CoW silicone replica (d). By using the same manufacturing process, a representative right ICA siphon was built from PA18 (e).

The static and dynamic COF of Sylgard 184 and LIM 6030 with various number of LSR coatings were given in Table 2-1. The best values were obtained with a single

coating for Sylgard 184: COF reduces by 55%, with a minimum static COF of 0.334± 0.169, and dynamic COF of 0.312±0.174. For LIM 6030, a 47% reduction in COF was achieved with 3 layers of LSR topcoat, resulting in a static COF of 0.719±0.121, and dynamic COF of 0.683±0.120.

Table 2-1 Static and dynamic friction coefficients of Sylgard 184 and LIM 6030 samples for different number of coatings

Silicone Type / Coating Number	Sylgard 184		LIM 6030	
	Static COF	Dynamic COF	Static COF	Dynamic COF
0	0.738±0.093	0.707±0.089	1.346±0.113	1.298±0.113
1	0.334±0.169 (p=0.0016)	0.312±0.174 (p=0.0019)	1.052±0.216 (p=0.0273)	1.026±0.222 (p=0.0435)
2	0.366±0.114 (p=0.0005)	0.312±0.108 (p=0.0002)	0.815±0.114 (p<0.0001)	0.765±0.098 (p<0.0001)
3	0.471±0.091 (p=0.0018)	0.416±0.090 (p=0.0009)	0.719±0.121 (p<0.0001)	0.683±0.120 (p<0.0001)

The friction coefficient was presented as mean ± standard deviation. The Student's t-test was performed to compare the mean friction coefficient of coated and uncoated groups. The two-tailed p-value <0.05 indicated a significantly statistical difference.

The S-S relationship of LIM 6030 and Sylgard 184 were shown and compared with that of the human MCA from autopsy obtained from the quasi-static test conducted by Monson [144] in Figure 2-9. It was found that as human blood vessel, silicone rubber exhibited a nonlinear S-S relationship. Moreover, at low stretch, the slope of the S-S curve of LIM6030 was 0.67 MPa, similar to that of the MCA from autopsy (0.41 MPa).

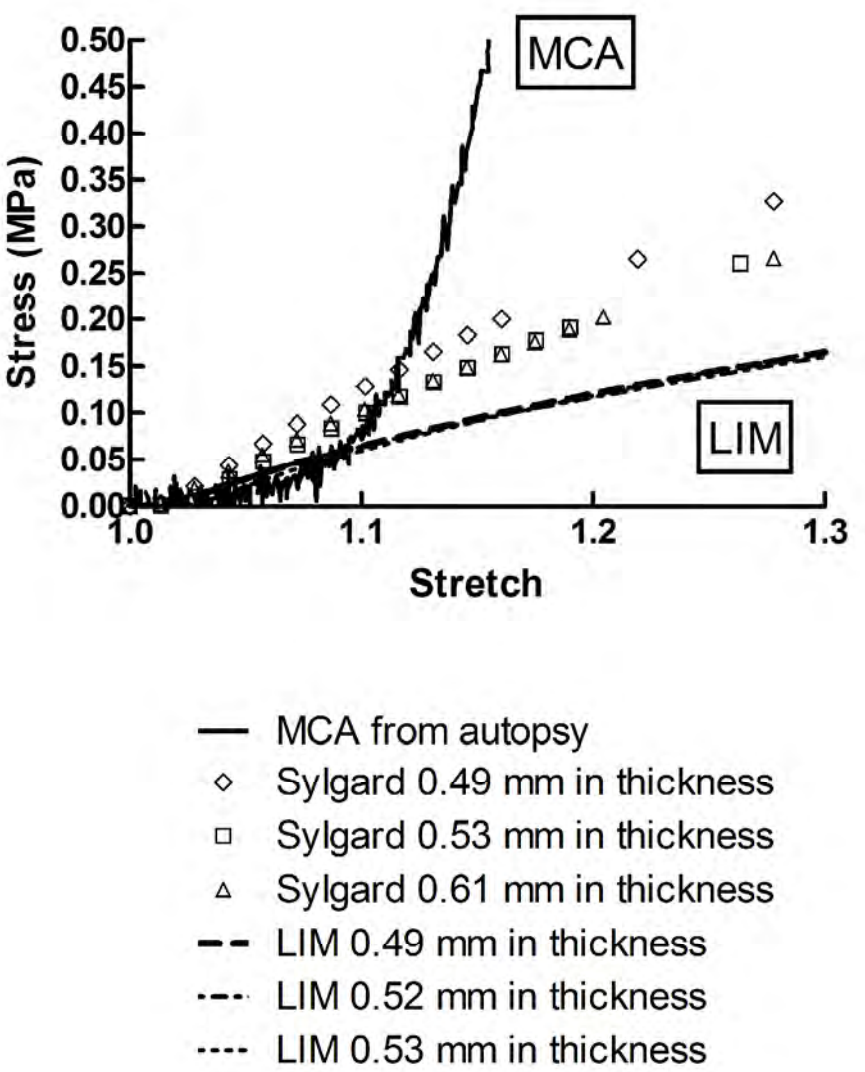

Figure 2-9 The S-S curves of Sylgard 184, LIM 6030, and human MCA from autopsy were compared. At low stretch, the elastic property of LIM6030 was closer to that of MCA from autopsy.

Discussion

A great deal of effort has been made on creating polymeric vascular models for surgical simulation, interventional practice, and hemodynamic research in vitro. Quantitating anatomic features of the arterial structures for disease or lesion prediction and diagnosis has also been widely investigated. To our knowledge, no studies have yet to apply the vessel characterization results to the replica manufacturing process. In this work, the disclosed manufacturing process of replicas was developed based on a model extracted from a characterized population of imaging datasets. This could be an even more powerful technique in the future as image databases grow, allowing an investigator to search for anatomy specific to a precise patient population for whom a given endovascular device is intended.

The image editing flexibility during the post-processing not only refines the vascular mesh, but also expands the applications of the silicone replicas. For instance, small vessel branches such as ophthalmic arteries can be removed resulting in a clean vasculature which contains only the interested structure like the CoW or ICA before centerline construction. To smooth the centerline, the RMSE describes how well the fitted curve matches the original data set. During the smoothing process, a high polynomial order does not guarantee better fitting results and can lead to oscillations between the data points. The tenth order polynomial had a RMSE of 0.1 for PA1 and PA2, and 0.16 for PA3 and was chosen as a smoothed centerline. To take minor changes along the vessel centerline into consideration, the curvature of every 0.05 mm segment was

measured and averaged. The median of each vascular feature was used to select a representative model in this study. The nonparameteric Wilcoxon signed rank test was eligible to be applied to this small case series (20 patients), and had fewer assumptions about the population distribution.

Arterial lumen replicas can be obtained from human cadavers[127, 131]. Postmortem alterations, including the shrinkage of arterial trees, produced dimensional errors of the in-vitro model. Using MRA data to acquire the geometry of the target vessels in our proposed manufacturing method avoided this problem and provided flexibility during the post-processing. It was mentioned in Ghazali's study[145] that the noninvasive, non-contrast enhanced 3D TOF MRA was highly accurate in depicting the arterial segments of the circle of Willis except the posterior communicating arteries, and the same observation also applied to this study. The poor depiction of posterior communicating arteries could be attributed to the saturation effect of slow flow and the flow parallel to the acquired section plane in addition to the normal anatomical variations in which these vessels were not present.

Other methods of replica construction have been used, such as that described by Knox et al.[128] where they created a reusable master mold of lumen replica based on the computed tomography scan data from a live patient to reproduce wax lumen models. The major difficulty of this technique was the fabrication of the master mold which required an experienced mold maker, was a time-consuming and expensive process, and the resulting mold was not easily modifiable to change the replica anatomy. Compared to

Knox's method, the construction of our core-shell structure was straightforward and efficient. On average, a virtual core-shell mold can be completed in 20 minutes after receiving the scan data, enabling reproducible manufacturing of replicas of any selected configuration.

In Sugiu's study[131] , 4 to 6 thin layers of silicone liquid were manually painted onto the wax lumen cast to simulate the vessel wall, however, the thickness and uniformity of the coating were not stated. Seong et al. [130] fabricated rabbit aneurysm replicas by using dip-spin method. The lumen cast polished by sand papers was dipped into the silicone mixture, and then mounted on a spinning shaft to obtain a layer of uniform silicone coating. The repeated coating procedure was time consuming and not reproducible. The described methodology, involving batch construction of an infusion mold and batch dissolution of the mold leaving behind an elastomeric vascular replica, served to improve these limitations. The core-shell mold kept the consistency of the replica dimensions, and saved time via the batch manufacturing. Due to the structural constraint, hand polishing was not applicable to our core-shell mold. To smooth the lumen surface, the mold was rinsed with xylene and 2-propanol alternately. This procedure allowed xylene to gradually dissolve model material and effectively prevented the core-shell structure from collapse.

Besides the soft replica described above, the rigid block model provided another option for in vitro use. Wetzel et al. used the 3D printer with the resolution of the build layer of 0.076 mm to form the wax copies of the vascular trees based on rotational

angiography data. The wax model was embedded in clear silicone which was then cured to form a solid block. The holes drilled in the silicone block drained the melted wax. After evacuation of the wax, a transparent rigid model containing the vascular lumen inside was prepared. The major concern of this lost-wax technique was the fragility of the wax which resulted in the breakage of the vessel branches smaller than 1 mm. By using the method reported here, silicone vascular replicas with branches smaller than 0.5 mm were made.

A common concern for selecting silicone as a material for vascular replica fabrication was its high friction. Surprisingly few attempts have been made to minimize the resistance between silicone replicas and medical devices. So far, an alternative material used to prepare vascular replica in the application of neurovascular modeling was poly-vinyl alcohol (PVA)[133]. The high water content of PVA hydrogel gave the vascular replica a naturally lubricated surface; however, the life of PVA replicas was limited, depending on the rate of water evaporation. Aside from using PVA in substitution for silicone, Parylene coating successfully reduced the COF of elastomers by forming a thin layer of Parylene film which closely conformed to the substrate[146]. The restriction of this coating method was the requirement of the coating system for vapor deposition during the process which may increase the cost and restrain the popularity of this technique. As compared to the aforesaid methods, LSR topcoat offered an easy and efficient option for smoothing inner wall of silicone vascular model. The low viscosity allowed LSR topcoat to easily flow through the long and tortuous model; furthermore, it only took 10-30 minutes to cure one layer of coating.

Rubber, like silicone, is generally amorphous, with few strong interactions between molecules. When the tensile force is applied, the tangled molecules are pulled to become stretched. In order to maintain the constant strain rate, additional force is needed on the stretched, oriented molecules. When a vessel is subjected to a tensile force, the elastin and collagen fibers significantly contribute to the low and high stiffness in the S-S curve[147]. The results from the tensile test in this study showed that the S-S relationship of LIM 6030 was similar to that of human MCA from autopsy at low stretch. To make this conclusion, it was necessary to clarify and discuss the potential differences between in vivo and in vitro test condition. The blood vessel wall is an anisotropic composite material in general, and receives multi-directional stress in the physiological environment. All specimens described herein were subjected to uniaxial tensile strength, and stretched longitudinally until breakage. Therefore, the results may not be able to represent the mechanical response in vivo. Furthermore, the contribution from the surrounding tissue to the mechanical response of the vessels to the load was not taken into consideration in the in-vitro and ex-vivo study. Lastly, factors such as age, sex and disease history of donor, type of vessel and strain rate may cause large variation in the S-S behavior for biological materials. It is noteworthy that the cerebral arteries are significantly stiffer and less stretchable before failure as compared to systemic arteries[148].

The described technique provides an efficient method for representative replica construction. However, there are technical difficulties which might be encountered while preparing the silicone models. Bubble formation during silicone injection may cause defects of the silicone replicas. High pressure required to infuse silicone liquid with high

viscosity into the mold may cause core structure motion, resulting in variation in wall thickness. Finally, more imaging data will need to be reviewed to create a more realistic environment for medical device testing, endovascular training and in vitro hemodynamic studies.

Conclusion

A small batch manufacturing process was introduced in this study to generate smooth, transparent, population based, anatomically accurate silicone cerebrovascular replicas. Importantly, this batch process allowed for reproducible replica generation. The manufacturing process for each silicone replica required 15.5 hours.

Acknowledgement

This work was supported by the National Institute of Biomedical Imaging and Bioengineering grant 1R21EB007767. The contents are solely the responsibility of the authors and do not necessarily represent the official views of the National Institutes of Health. The authors are also grateful to Dr. Monson for providing data on MCA stretch-stress relationship for comparison.

Chapter III: Ex-Vivo Modeling of Cerebral Emboli-Mimicking Clots

Abstract

Mechanical behavior of the embolus is one of the key factors that determine the efficacy of thrombectomy devices. The goal of this study is to characterize the mechanical properties and composition of thromboemboli from clinical cases as compared to commonly used EAs.

Clinical thromboemboli were obtained from patients with AIS by using aspiration devices and from carotid atherosclerotic plaques harvested during endarterectomy. On the bench, EAs commonly described in the literature were created from various blood donor species (human, porcine and bovine) with and without the addition of thrombin and barium sulfate. Stiffness and elasticity of the specimens were monitored with dynamic mechanical analyzer (DMA). Scanning electron microscopy (SEM) and histological analyses were performed to investigate the ultrastructure and composition of the specimens.

Of the clinical specimens, calcified thromboemboli showed the highest stiffness followed by those containing cholesterol crystals. The softest clot material was obtained from AIS patients and was found to be mainly composed of fibrin and erythrocytes. Of the EAs created in the lab, bovine EAs presented the highest stiffness. Addition of thrombin resulted in increases in stiffness and elasticity of human and porcine EAs. The presence of barium sulfate significantly reduced the elasticity of EAs. The stiffness and elasticity of the cerebral emboli analyzed in this study showed no significant differences

with those of the recalcified porcine EAs and thrombin-induced (5 NIHU/ml blood) human EAs. Stiffness of the carotid endarterectomies (CEA) specimens was similar with that of the bovine EAs and thrombin induced porcine EAs.

Introduction

With growing experience of penumbral imaging for patient selection and newer more effective mechanical recanalization devices, alternative endovascular therapy for AIS has become a viable treatment option[149]. There are presently two devices available in the United States for thrombectomy in acute ischemic stroke and many other technologies under evaluation. These devices produce recanalization, defined using the thrombolysis in myocardial infarction (TIMI) score applied to catheter angiography studies[98, 100], from 50% to 82% of cases. Currently, it is poorly understood what variables predict successful recanalization. Characterization of the embolus may be helpful in device selection and development.

In preclinical characterization of thrombectomy device technology, efficacy and safety are measured in large animal or in vitro vascular occlusion models[150-153] with endpoints such as number of thrombectomy attempts, the amount of EA removed from the occlusion site, and the risk of distal embolic shower[150, 151, 154-156]. All of these parameters are significantly affected by the mechanical properties of the EAs, an often overlooked component of the testing system. In the literature, many protocols to manufacture EAs exist and common variables include the donor species, concentration of thrombin and radiopaque additive such as barium sulfate[118, 151, 155-158]. Species differences in blood chemical composition, hematological values[159-162], thrombin effects on coagulation profile[163], functional structure of coagulation proteins[164, 165,166, 167], blood coagulation mechanism[168] and pH and ionic strength of the clotting environment[169,170-

[173]influence the structure (diameter, length and branch point density of the fibrin fibers[174]) and mechanical properties of the clotting materials in-vitro[160, 172, 175-177]. The mechanical properties of EAs formed in-vitro are normally investigated by using rheometry[178-180], thrombelastography[181, 182], and atomic force microscopy/fluorescence microscopy[183].

The aforesaid findings lead to the hypothesis that commonly employed EAs have different mechanical properties, and currently we do not know how they relate to human sources of thromboemboli that cause stroke. Human sources of thromboemboli are normally classified into three different types: white, red thrombus, and disseminated fibrin deposit[184]. The composition of all three varies in the relative amounts of fibrin, platelets and erythrocytes. The platelet and fibrin-rich white thrombus usually forms at injured vessel wall, particularly in areas where blood flow is fast, whereas the fibrin and erythrocyte-rich red thrombus may form in the venous system where the blood flow is retarded. Fibrin clots, containing some white and red blood cells but no platelets, can be found in small cerebral arteries of approximately one third of the patients with recent embolic infarcts[165]. The highly variable nature of these thrombi creates a challenge to the study of revascularization devices and drugs. Two recent studies analyzed the composition of emboli retrieved from the stroke patients. Marder et al. first systematically analyzed thrombi retrieved from ICA and MCA of patients with AIS, and discovered that 75 % of thromboemboli had random fibrin and platelet deposits interspersed with nucleated cells and confined erythrocyte-rich regions[185]. Another histological analysis was performed on thrombi extracted from 5 patients with AIS by using the MERCI retriever[186] and the results showed that most thrombi had a variable

composition of fibrin and red blood cells. Moreover, different degrees of calcification were seen in 2 thrombi. The abovementioned studies substantiated the structural and compositional variations between the in-vivo emboli and in-vitro EAs; however, no attempts have been made to characterize the mechanical properties of EAs and relate them to thromboemboli from patients.

The goal of this study is to explore the impact of the aforesaid variables on the mechanical properties of the EAs commonly used in the lab; namely, 1. Stiffness -- ability to deform the EA and 2. Elasticity -- ability of the EA to return to its original shape after deformation. Thereafter, mechanical properties of the EAs are compared with those of the thromboemboli retrieved from patients.

Materials and Methods

Preparation of Embolus Analogues

Our literature review showed that human, porcine and bovine blood donors are commonly used for EA preparation. EAs were generated by spontaneous coagulation (no thrombin added)[156] or created by thrombin-induced clotting[151]. The anticoagulant citrate dextrose solution (ACD)-containing blood was either recalcified by adding calcium[150, 155] or clotted with addition of thrombin (2.5 NIHU/ml blood) and barium sulfate (1g/10 ml blood)[158]. Barium sulfate is commonly added to the clot matrix to make the EA visible under X-ray[187-189]. In this study, the effects of thrombin (0, 2.5, and 5 NIHU/ml blood) and barium sulfate (0 and 1g/10 ml blood) on the stiffness and elasticity of the bovine, porcine and human EAs were studied.

Without the presence of thrombin, spontaneous coagulation was initiated by mixing bovine, porcine or human whole blood/ACD mixture (10:1) and calcium chloride (97 mmol/L) at a 5:1 ratio. Based on the species divergence of structure and function in fibrinogen[177] and specificity of the thrombin-fibrinogen interaction[176], bovine thrombin (Sigma T-7513) was used to initiate fibrin formation in bovine and porcine EAs; whereas, human thrombin (Sigma T-6884) was employed in human blood samples. Thrombin-induced clotting was conducted by simultaneously injecting whole blood/ACD mixture (10:1) and calcium chloride (97 mmol/L)/thrombin solution (1NIHU thrombin/4 μl solution) into silicone tubing (I.D. 6.35 mm) to give blood mixtures with final thrombin concentration of 5 and 2.5 NIHU/ml blood. Before injection, silicone tubing was rinsed with 70% alcohol followed by 0.9% saline. The radio-opaque EA was created by adding 1g barium sulfate into the 10 ml blood mixture which had a thrombin concentration of 2.5 NIHU/ml blood[158]. All EAs were aged in saline at room temperature for one day prior to characterization.

Collection of Thrombi from Patients

All human specimens were collected with approval from our Institutional Review Board. Nine emboli were obtained by aspiration from the ICA or MCA of 4 stroke patients (Figure 3-1 (a) to (c)).

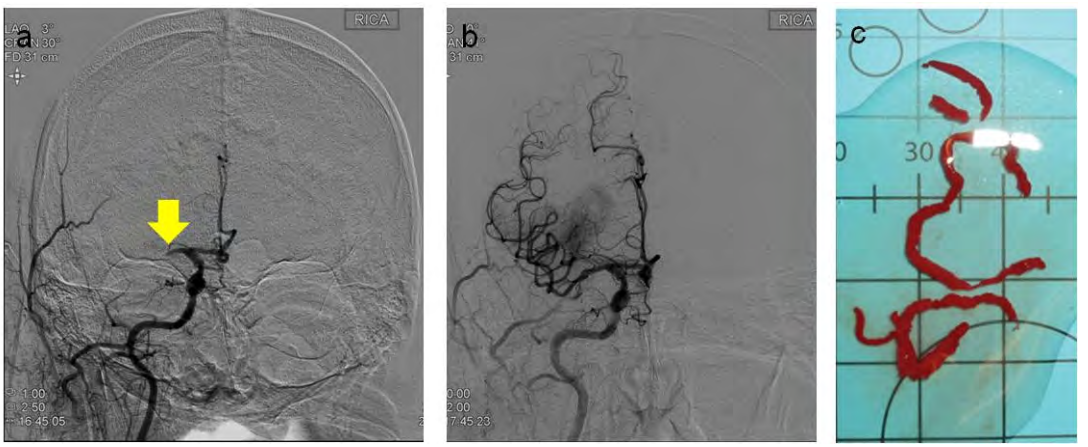

Figure 3-1 Patient presented with an AIS due to MCA occlusion (a, arrow). The embolus was aspirated from the MCA with the Penumbra system and successful recanalization was achieved (b). Examples of material extracted from stroke patients by aspiration (c).

Due to the fact that debris from atherosclerotic plaques and atrial fibrillation are well-documented as important sources of emboli to cause AIS[190,191], 26 atherosclerotic plaques removed during CEA and 1 atrial appendage were collected. Materials which were loosely attached to the lumen of the plaques and red thrombi which were removed from under the fibrous cap were considered as the potential sources of cerebral emboli. The materials were harvested from the plaques for analysis. After careful examination under the microscope, a total of 13 potential sources of emboli were extracted from 7 asymptomatic and 1 symptomatic plaques (8 patients). No thromboemboli were recovered from the atrial appendage. Clinical data of 12 patients and details of emboli are provided in Table 3-1, where the tested emboli were numbered by the procedure type (C: carotid endarterectomy, A: aspiration in acute ischemic stroke) followed by an integer denoting the order in which the embolus was obtained. In order to avoid confusion, the term "thromboemboli" henceforth refers to emboli obtained from this patient population.

Mechanical Characterization

DMA (Q800, TA Instruments, New Castle, DE) which had a force resolution of 0.00001 N, and a strain resolution of 1 nanometer was used to explore the stiffness and elasticity of the emboli and EAs. All the mechanical examinations were conducted using a submersion compression clamp within saline at 37^{o}C. The EAs were cut to have a height of 2 mm, and a caliper having a resolution of 0.1 mm was used to measure the diameter of the EA. The emboli retrieved from patients had an irregular shape and were carefully trimmed using micro-scissors and double-edged razor blades under the light microscope to have a height between 1 and 2 mm. To prevent test material (emboli or EAs) from slipping, 220-grit sandpaper was adhered to the compression disk.

In the controlled force mode, the test materials were first subjected to a preload force of 0.0001N, followed by a compression force ramp from 0.0001 N to 15 N at a rate of 0.5 N/min. The deformation of the test material caused by the compression stress was used to produce an engineering S-S curve. Onset point, the intersection of the initial and final tangent lines, was recorded to determined the strain at which a change in the slope of the S-S curve occurred. Stress was defined as force over surface area, and strain was referred to deformation in height over original height. To quantitatively describe the deformation of the test material under the compression force which simulated the large strain induced by the thrombectomy devices during treatment, stress variation over a range of strain (the slope of the S-S curve) was calculated. The secant modulus ($E_{\text{intitial strain-end strain}}$) is the slope of a line formed by connecting the point on the S-S curve from

defined initial to end strains. As such, $E_{\text{intitial strain-end strain}}$ is an indication of the stiffness of the material. The area under the S-S curve, which represents the energy required to deform the material, was also calculated.

In the stress-relaxation mode, the test materials were subjected to an initial strain of 60 % for 5 min, followed by a recovery period of 15 min. The strain recovery (%), a measure of material elasticity, was acquired.

Histological Assessment

Emboli and EAs were fixed in a 10 % buffered formalin solution for 48 hours. Specimens were then embedded in paraffin wax and cut into 5μm sections. Sections were dewaxed and hydrated to distilled water in preparation for a modified version of the Martius Scarlet Blue (MSB) method for staining fibrin, collagen and erythrocytes[192]. Alternating sections were stained with Hematoxylin and Eosin (H&E).

SEM

Emboli and EAs were fixed with 2.5% glutaraldehyde, and dehydrated in series of ethanol concentrations up to 100 %. To observe the interior of the emboli and EAs, samples were frozen in liquid nitrogen and fractured. Samples were critical-point-dried, mounted, and sputter-coated with iridium for SEM observation. Energy dispersive X-ray spectroscopy (EDS) was performed on two samples.

Statistical Analysis

Data were presented as mean ± standard error. Unpaired t-test was performed to compare the means of the non-calcified plaque materials and cerebral emboli retrieved from the AIS patients. One-way analysis of variance followed by Dunnett's or Tukey's post test was used to determine significance between patients' emboli (control) and EAs or between the EAs, respectively. Statistical significance was set at $p<0.05$. Statistical analysis was performed using GraphPad Prism (GraphPad Software Inc., San Diego, CA).

Results

The histology findings revealed that the EAs were mainly composed of homogeneously dispersed erythrocytes with several interspersed fibrin bands (Figure 3-2 (a)); moreover, a layer of dense fibrin mesh was formed on the outer surface of the EA that was against the silicone tubing (Figure 3-2(b)). The average onset point of these erythrocyte-rich EAs analyzed under DMA controlled force mode (n=65) was 89.11±0.55 %. In this study, two secant moduli, $E_{0\text{-}75\%}$ and $E_{75\text{-}95\%}$, were calculated to describe stiffness of EA.

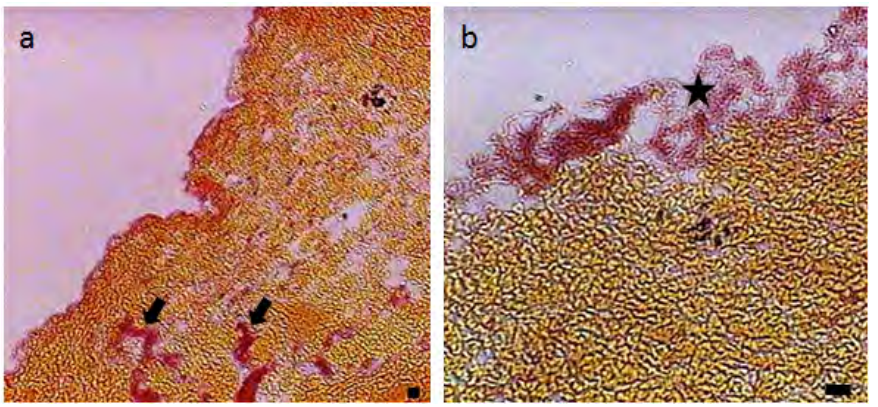

Figure 3-2 (a) The EA was mainly composed of erythrocytes (shown in yellow) with fibrin clumps dispersed in it (arrows, bar=10 microns). (b) A layer of fibrin was formed on the surface of the EA against the silicone tubing (asterisk, bar=10 microns).

Overall, bovine EAs showed the highest stiffness followed by porcine and human EAs (Figure 3-3 (a-b) and (e-f)). Without addition of thrombin, $E_{0\text{-}75\%}$ and $E_{75\text{-}95\%}$ of bovine EAs were statistically higher than those of porcine and human EAs ($p< 0.05$). However, there was no significant difference in stiffness between EAs made from porcine and human. Increases in stiffness and elasticity of human and porcine EAs were found when thrombin was present at a concentration of 5 NIHU/ ml blood ($p<0.05$). In the absence of thrombin and barium sulfate, the bovine EAs had strain recovery of 30.28 ±2.48 %, whereas strain recovery in human blood derived EAs was unmeasurable due to their fragile nature. Elasticity of the thrombin-induced porcine EAs was higher than that of the thrombin-induced human EAs ($p<0.05$) (Figure 3-3 (c)). As compared to the counterparts of the bovine and human EAs, thrombin-induced porcine EAs retracted the most (Figure 3-3 (d)). A significant decrease in elasticity ($p<0.05$) were found in all EAs containing barium sulfate (Figure 3-3 (g), Figure 3-4 (a) and (b)). With the presence of

barium sulfate, the area between initial to 95 % strain under the S-S curve tended to increase (Figure 3-3 (h)).

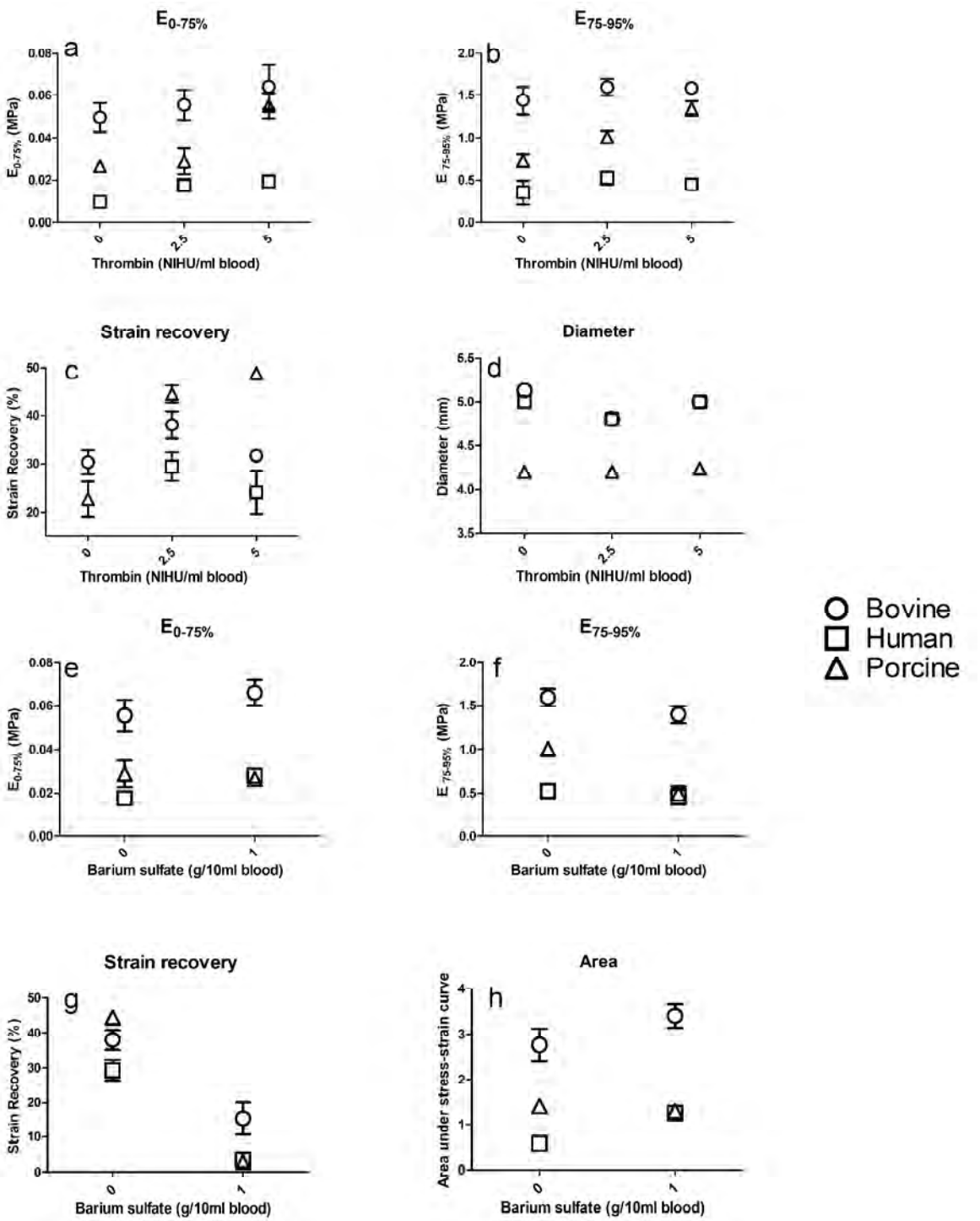

Figure 3-3 Impacts of thrombin and barium sulfate on the stiffness ($E_{0\text{-}75\%}$ and $E_{75\text{-}95\%}$), strain recovery and diameter of the EAs were shown in (a) to (g). An increase in area under the stress-strain curve was observed with the presence of barium sulfate (h).

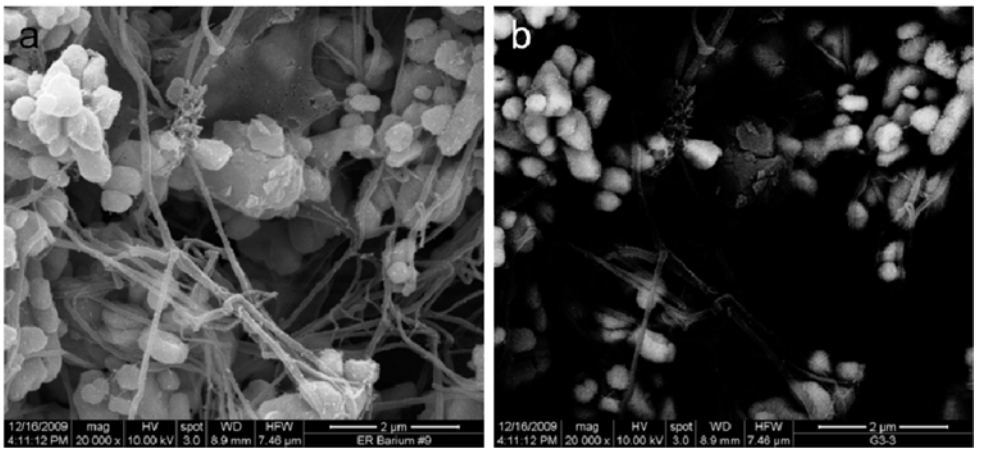

Figure 3-4 (a) A secondary electron image of the bovine EA with barium sulfate (x 20,000) (b) a mixed secondary and backscattered electron image of barium sulfate agglomerates (x 20,000).

From September 2009 to May 2010, 26 atherosclerotic plaques, 1 atrial appendage and cerebral emboli (from 4 AIS patients) were collected from 31 patients. With careful examination under microscope, 13 thrombi were harvested from 8 plaques collected at CEA and no emboli were found in the atrial appendage. Along with 9 cerebral emboli from the AIS patients, a total of 22 specimens from 12 patients (mean age, 70 years) with an average thickness of 1.43±0.11 mm and surface area of 6.22 ±0.97 mm^2 were characterized (Table 3-1).

Table 3-1 Demographic data of 12 patients and characteristics of 22 emboli.

Pa ient	Sex	Age	Pretreatment Diagnosis	Procedure	Specimen			
					No.†	Site	Source	Appearance & Composition
1	M	79	asymptoma ic left ICA stenosis	CEA	C1	ICA	excessive hrombus removed from he plaque	red, ery hrocyte-rich
					C2	ICA		off-white, partially calcified and fibrin-rich
2	F	77	asymptoma ic left ICA stenosis	CEA	C3	ICA		pink, platelet and fibrin-rich
					C4	ICA		pink, platelet and fibrin-rich
3	M	68	asymptoma ic ICA stenosis	CEA	C5	ICA		red, platelet and fibrin-rich
					C6	ICA		off-white, fibrin-rich wi h cholesterol crystals
4	M	64	high grade stenosis of he right ICA origin with intraluminal hrombus of he entire right ICA, M1, and proximal M2 divisions of he right MCA	aspiration	A1	MCA	artery-artery embolus associated wi h ipsilateral carotid disease	red, fibrin, erythrocyte, platelet and leukocyte-rich
5	M	65	right ICA origin >90% segmental stenosis with intraluminal thrombi at the proximal end and distal end of the lesion. Occlusion of he right MCA	aspiration	A2	ICA	cardiocembolic	red, fibrin, erythrocyte, platelet and leukocyte-rich
6	M	79	asymptoma ic right ICA stenosis	CEA	C7	ICA		yellow-white, calcium phosphates
7	M	74	asymptoma ic right ICA stenosis	CEA	C8	ICA	hrombi loosely attached to luminal surface	dark red, lipid, packed fibrin, fibronec in and cells
					C9	ICA		
8	M	72	asymptoma ic left ICA stenosis	CEA	C10	ICA		red, fibrin, erythrocyte and platelet-rich
					C11	ICA		red, fibrin, erythrocyte and platelet-rich
9	F	78	MCA occlusion	aspiration	A3	MCA	cardiocembolic	red, fibrin, erythrocyte, platelet and leukocyte-rich
10	M	54	MCA occlusion	aspiration	A4-A9	MCA	cardiocembolic	red, fibrin, erythrocyte, platelet and leukocyte-rich
11	M	53	symptoma ic ICA stenosis	CEA	C12	ICA	hrombi (1cm in leng h) loosely attached to fatty streak	red, fibrin, ery hrocyte and leukocyte-rich
12	M	81	asymptoma ic ICA stenosis	CEA	C13	ICA	hrombi loosely attached to luminal surface	dark red, lipid-rich

† The sample number (No.) is determined by the procedure type (C: caro id endarterectomy; A: aspiration in acute ischemic stroke) followed by an integer denoting he order in which it was obtained.

Emboli obtained from the patients can be classified into three categories; (1) calcified emboli (Figure 3-5 (a)) (2) aged emboli (Figure 3-5 (b)) and (3) red emboli (Figure 3-5 (c)), according to their composition and mechanical properties.

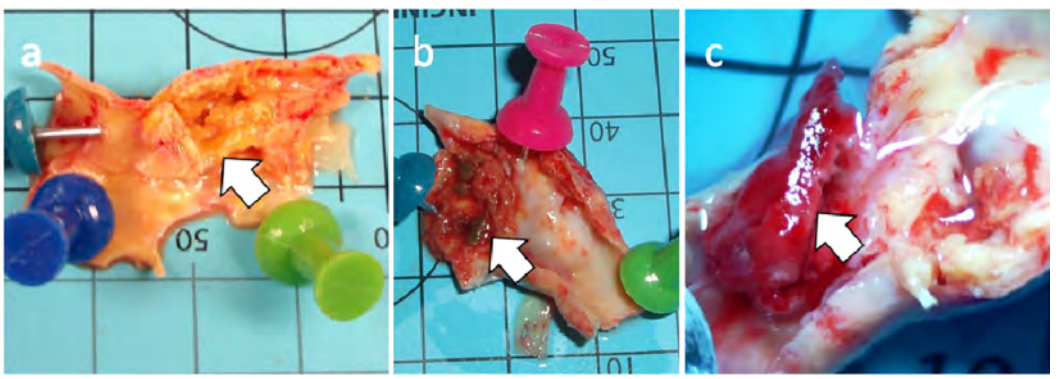

Figure 3-5 Thrombi containing calcified materials (a), cholesterol-rich materials (b) and fibrin and erythrocyte materials (c) were found in the atherosclerotic plaques.

The calcified emboli (C2 and C7, Table 3-1) had large amounts of Ca/P apatite (Figure 3-6 (a)). In Figure 3-6 (b) and (c), the SEM and histology results showed that the aged emboli had highly compacted structure, and consisted of old fibrin, adhesive proteins, connective tissue and other cells such as erythrocytes and platelets. The features of red emboli are presented in Figure 3-6 (d) to (f). Aggregation of erythrocytes (yellow in Figure 3-6 (d)) was trapped in the fibrin network. Leukocytes were dispersed throughout the embolus (Figure 3-6 (e)). At higher magnification, the histology findings further indicated that the cellular elements found in the cerebral emboli retrieved from the AIS patients were arranged in a specific layer-by-layer pattern (Figure 3-6 (f)).

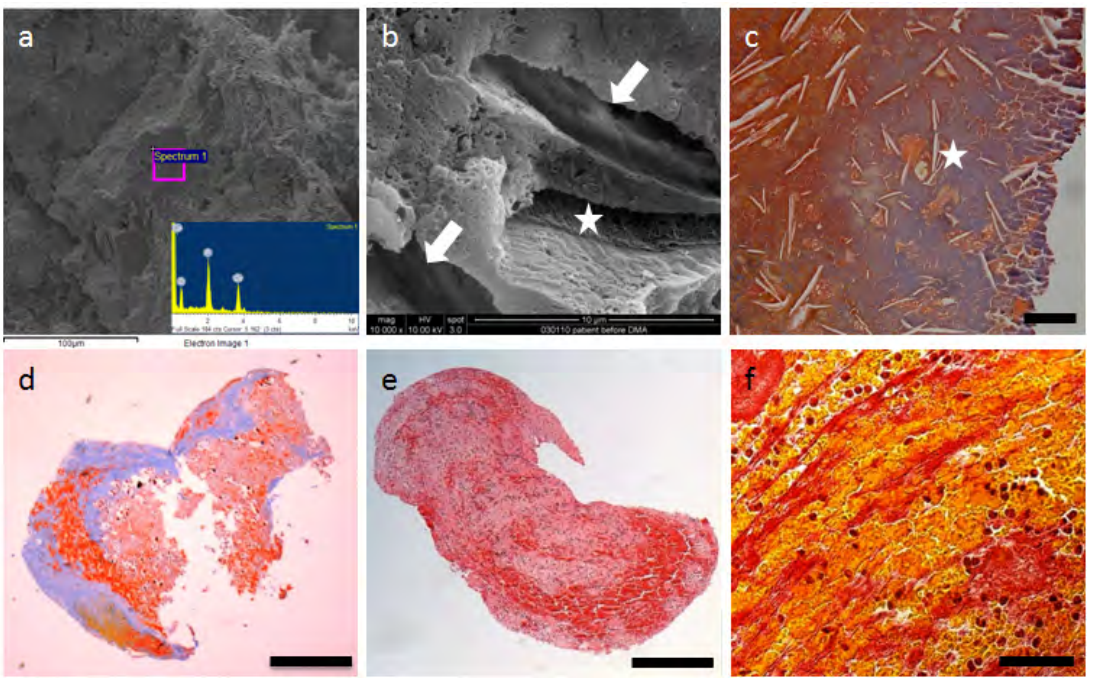

Figure 3-6 Morphological features and composition of a variety of emboli from patients. (a) A calcified embolus. Ca/P apatite was detected by the EDS scan (inset) (b) An aged embolus had a compact structure with fissures which were occupied by the cholesterol crystals (arrows) and fibrin at the edge of the specimen (asterisk). The SEM findings were related to the MSB result (x20, bar=100 microns) shown in (c). (d) MSB results showed that a red embolus was mainly composed of fibrin and erythrocytes (old fibrin in blue, erythrocytes in yellow and erythrocyte/fibrin mixture in red) (x2, bar=1mm). (e) Photomicrograph of a red embolus retrieved from the stroke patient (H&E x10, bar= 200 microns) revealed that the leucocytes were distributed throughout the embolus. (f) At x10, it was found that erythrocytes and fibrin strands were arranged in a layer-by-layer manner in the red embolus (MSB, bar= 200 microns).

The high stiffness of the calcified emboli was identified in Figure 3-7. The S-S curves of the calcified emboli (black curves) showed early onset point (42.90±8.03 %) and smaller strain under a 15 N force (the end of the test), and demonstrated that higher stress was required to cause 45 % strain (e.g., C7 in Figure 3-7) on calcified emboli as compared to other emboli. To achieve a fair comparison, $E_{0\text{-}45\%}$ was used to make comparisons between calcified and non-calcified materials; on the other hand, for comparisons made between non-calcified emboli with high strain, $E_{0\text{-}75\%}$ and $E_{75\text{-}95\%}$ were

applied. Late onset point (85.39±0.85 %) and large strain under a 15 N force were seen on the aged emboli (purple curves) collected during CEA, which were loosely attached to the vessel lumen and had a dark reddish-brown color. The stiffness of the aged emboli ($E_{0\text{-}45\%}$= 0.17±0.039 MPa) fell between that of the calcified emboli ($E_{0\text{-}45\%}$= 0.63±0.38 MPa) and red emboli ($E_{0\text{-}45\%}$= 0.026±0.0026 MPa). The red emboli had the latest onset point (91.29±0.82 %) and largest strain upon loading with 15 N.

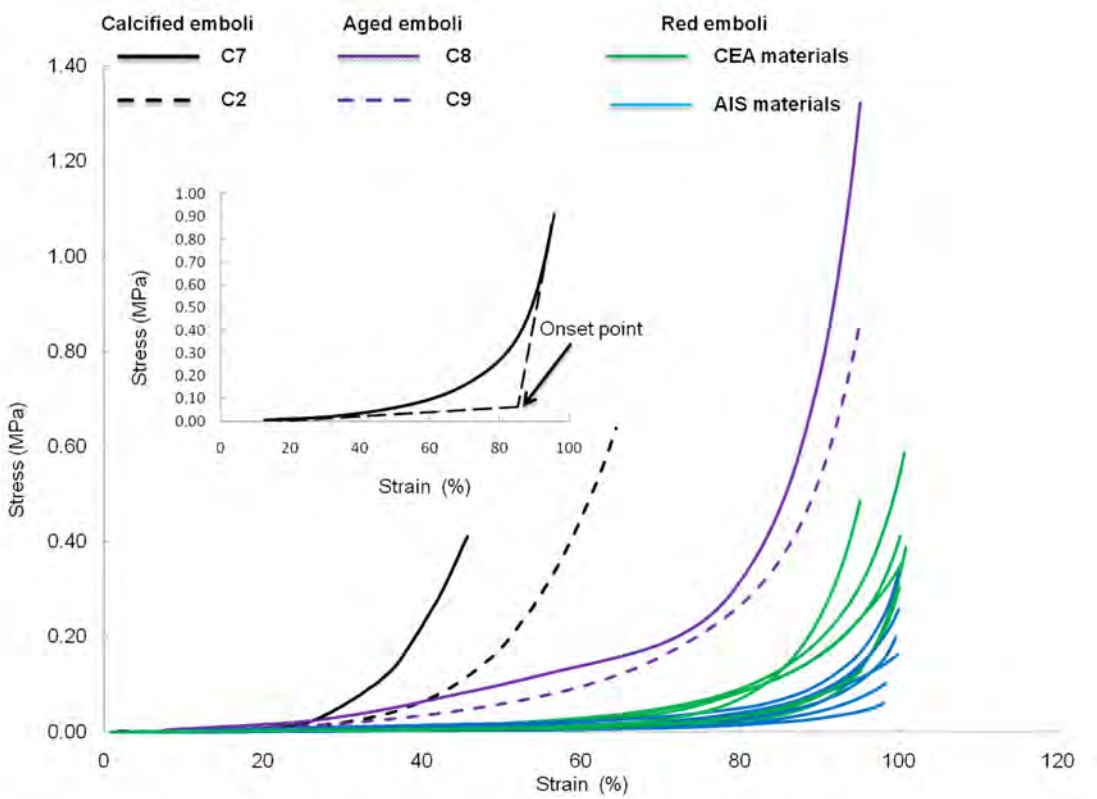

Figure 3-7 The engineering S-S curves show that at the end of the test, a 15 N force causes a 45.7 % strain to a highly calcified embolus (black solid line) and a 64.4 % strain to a partially calcified embolus (black dashed line). It is noted that the same compression force can result in a higher strain (> 80%) on the other emboli.

The average $E_{0\text{-}75\%}$ and $E_{75\text{-}95\%}$ of the emboli retrieved from the AIS patients were 0.04±0.01 MPa and 0.43±0.06 MPa, respectively, whereas those of the potential sources of non-calcified emboli obtained from the CEA plaques were 0.11±0.037 MPa and 1.60±0.50 MPa, respectively. It should be noted that large variations in $E_{0\text{-}75\%}$ and $E_{75\text{-}95\%}$ were seen in the CEA emboli due to the high variability in the composition as previously described (Figure 3-8). Stress relaxation tests revealed an average strain recovery of 32.86±2.33 %.

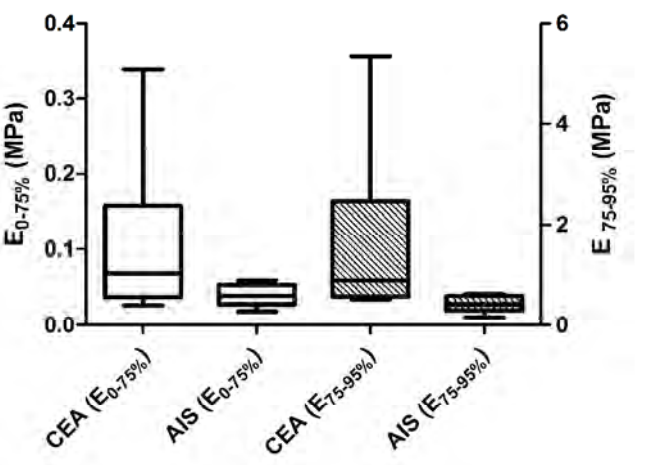

Figure 3-8 Comparisons of potential sources of emboli (CEA) and emboli those caused AIS in terms of $E_{0\text{-}75\%}$ and $E_{75\text{-}95\%}$. Large variations were observed in the CEA groups.

A series of comparisons between different types of EAs and emboli obtained showed recalcified porcine EAs , thrombin-induced (5 NIHU/ml blood) human EAs are similar to cerebral emboli retrieved from the AIS patients in terms of stiffness and elasticity ($p>0.05$) (Figure 3-9 (a) to (c)). The potential sources of the emboli collected at

CEA, bovine EAs and thrombin induced porcine EAs had no significant differences in stiffness (Figure 3-9 (d) and (e)).

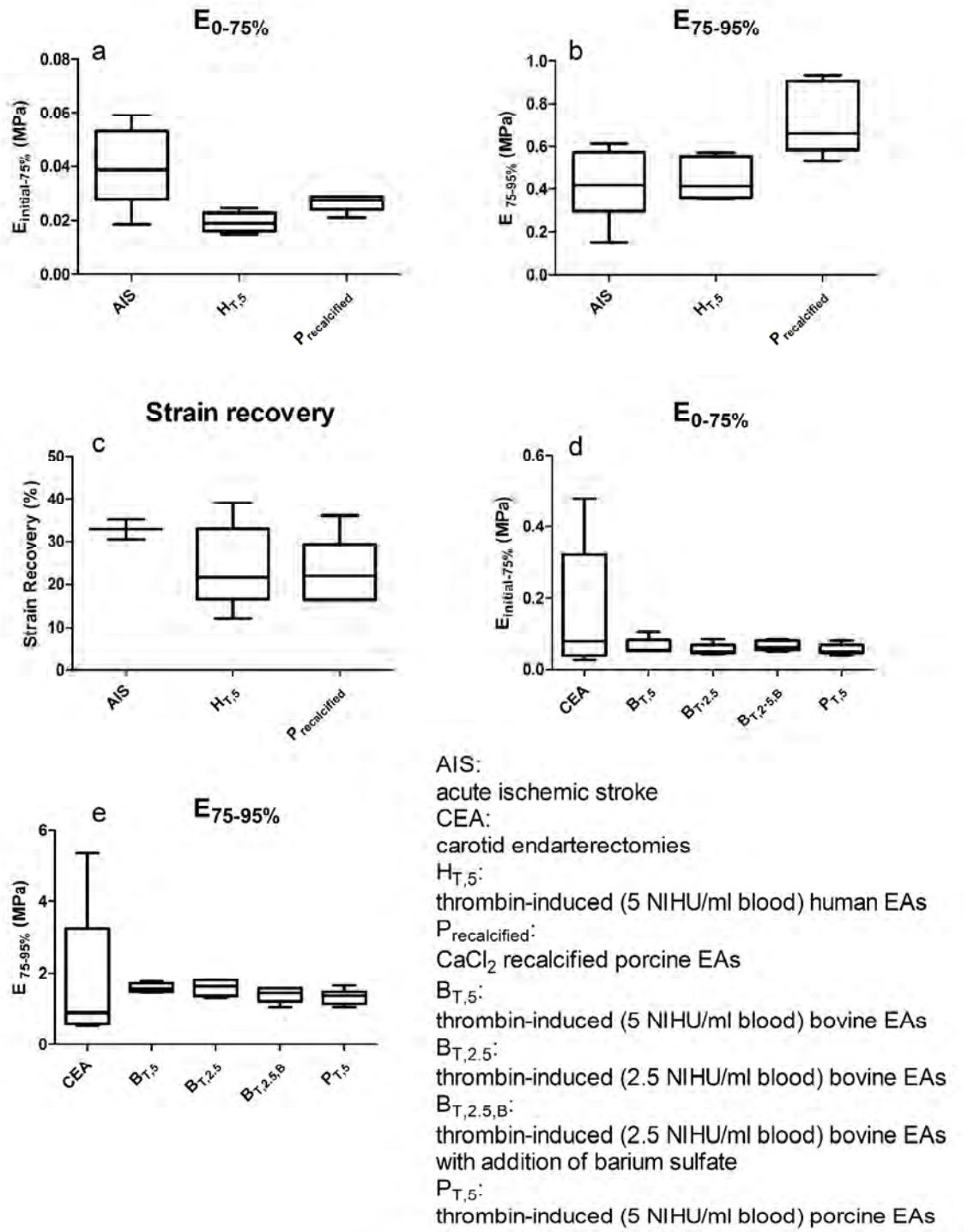

Figure3-9 A series of comparisons in terms of stiffness and elasticity between different types of EAs and emboli obtained from AIS ((a) to (c)) and during CEA ((d) and (e)).

Discussion

Embolus characteristics in terms of mechanical properties, composition and structure are important in the endovascular treatment of AIS. In prior research, EA stiffness was considered as a variable to create embolic occlusion in canine models for evaluation of recanalization via stent implantation[193]. In a more recent investigation, manual elongation tests were performed using forceps to stretch EAs[153]. In this present work, stiffness and elasticity of the EAs and emboli were quantitatively measured and compared to the clinical thromboemboli they are intended to represent. DMA compression test is ideal for characterization of soft viscoelastic materials, such as emboli and their analogues. As the name indicates, the mechanical responses of the viscoelastic materials are a mixture of viscous and elastic behavior. A complete strain recovery of an elastic material, like a spring, can be observed after removing the applied stress. On the contrary, viscous deformation is nonrecoverable (permanent). In the thrombectomy treatments, strain recovery (as an indication of elasticity) and stiffness of the emboli are important material characteristics to predict the safety and efficacy of the devices and procedure.

EAs prepared by using blood from different species produced different stiffness and elasticity, and these variations can be explained from the following considerations. Fibrin is the product formed after fibrinogen polymerization, and the major constituent of emboli and EAs. Fibrin fiber diameter and branchpoint densities increase as the fibrinogen concentration increases from 0.3 to 0.6 g/dl [175], and the stiffness of the EAs is

proportional to the starting fibrinogen concentration. The results of the mechanical characterizations in this study are consistent with the abovementioned findings. The average fibrinogen concentration in bovine plasma is between 0.5-0.7 g/dl, which is higher than that in pig (0.1-0.5 g/dl) and human (0.2-0.4 g/dl) plasma. Consequently, the bovine EAs showed higher $E_{0\text{-}75\%}$ and $E_{75\text{-}95\%}$ as compared to the porcine and human EAs. Significant increases ($p<0.05$) in stiffness and strain recovery of porcine EAs induced by adding 5NIHU/ml thrombin (Figure 3-3) were attributed to the reactive blood coagulation mechanism of the porcine blood as well as the presence of large amount of platelets in porcine plasma (250-500 $10^3/mm^3$ for porcine versus 150-450 $10^3/mm$ for human). Thrombin-activated platelets are known to be essential contributors to the EA elasticity and retraction[180].

Aggregation of barium sulfate was observed under SEM (Figure 3-4), indicating its low solubility in blood. Use of thrombin is suggested in the preparation of barium sulfate impregnated EAs to enable rapid formation of the fibrin matrix that traps the particles of barium sulfate enabling a more homogenous distribution. Influences of barium sulfate aggregations on the fibrin network structure such as pore size, density and branch points were not studied in this work; however, the inelastic nature of the barium sulfate led to a significant decrease in the strain recovery of EAs. As compared to the recalcified EAs, it was found that the S-S curves of the barium sulfate-containing EAs showed a gradual change in slope, and had a higher elongation. Additionally, the area between initial to 95 % strain under the S-S curve of the barium sulfate-containing EAs tended to increase, indicating that these materials became tougher (higher energy to

break). In the work by Gralla et al, barium sulfate containing EAs were used to evaluate the efficacy of the Catch device (Balt, Montmorency, France) in the occluded extracranial vessels of swine[158]. The authors describe 20 unsuccessful recanalization attempts performed with the Catch device where the applied force from the aspiration system initially elongated the EA, but was not sufficient to retrieve or fragment the EAs. The results from our present study show that barium sulfate doped porcine EAs are "elastic and tough" as compared to the emboli observed clinically, which may be in part responsible for the failure of the Catch device in these experiments.

The elasticity of the calcified emboli was not available in this study. The force required to cause 60 % strain on the calcified emboli exceeded the limitation of our equipment due to the high stiffness of the calcified emboli. The aged emboli had highly compact structure and the dark reddish-brown color. When these samples were prepared for DMA sample preparation, a lack of elasticity was observed, which could be associated with the protein degradation of these aged materials. This experience was concordant with the previous findings that the aged thrombi provided little resistant to mechanical thrombectomy[194]. As with recalcified porcine EAs and thrombin-induced human EAs, the red emboli showed higher elasticity with an average strain recovery of 32.86±2.33 %.

Our study was limited by a unidirectional compression test to explore the material properties anisotropic specimens. However, the small size of the thrombi makes it difficult to measure the hardness and elasticity in different directions. It is important to

note: (1) the modulus presented in this study is only for comparison due to the use of the sandpaper, and (2) unlike polymer and other synthetic materials, the stiffness of the biological tissue may depend on strain. Despite these limitations, we were able to fully characterize common EAs used in the laboratory and compare them with the thromboemboli they are intended to represent. Precise characterization of EAs is an important element to proper preclinical evaluation of thrombectomy devices.

Summary

Differences in structure and composition were observed between EAs and human thromboemboli. Recalcified porcine EAs and thrombin-induced (5 NIHU/ml blood) human EAs were similar with cerebral emboli retrieved from patients with AIS in terms of stiffness and elasticity. There was no significant variation between the stiffness of the material collected at CEA and bovine or thrombin induced procine EAs. Addition of barium sulfate for radioopacity in the EAs dramatically reduces the elasticity. Fully characterized EAs with known mechanical properties are now available for preclinical evaluation of thrombectomy devices.

Acknowledgement

This work was supported by the National Institute of Biomedical Imaging and Bioengineering grant 1R21EB007767. The contents are solely the responsibility of the authors and do not necessarily represent the official views of the National Institutes of Health.

Chapter IV: A Novel Model System of Cerebrovascular Occlusion for Preclinical Assessment of Mechanical Endovascular Treatment of Acute Ischemic Stroke

Abstract

The purpose of this study was to design an in vitro model system of cerebrovascular occlusion that allows realistic testing of mechanical thrombectomy devices.

The proposed model system was composed of a human vascular replica, an embolus analogue, and physiological hemodynamic conditions. The MERCI L5 Retriever, Penumbra system 054, Enterprise stent, and ultrasound waveguide device were evaluated in terms of the efficacy and safety. The primary efficacy endpoint was the amount of blood flow restored, and the secondary endpoint was the ability to achieve recanalization. The primary safety endpoint was an analysis of clot fragments and their size distribution.

The Penumbra system achieved the highest recanalization rate (80%) followed by the MERCI L5 Retriever (67%), Enterprise stent (17%) and ultrasound waveguide device (0%). Temporary flow restoration (29.28% ±6.42%) was recorded when the stent was self-expanded during the procedure. No EA fragments had dimension greater than 1000μm, and mean size of the small and large particles were between 32 to 40 μm and 219 to 273 μm, respectively, depending on the device used. The recanalization rate of the thrombectomy device was related to the ability of the device to capture the EA during removal of the device and the geometry of the vascular replica. The risk of the embolic

shower was influenced by the mechanical properties of the EA and the mechanism of action for the thrombectomy device.

Introduction

A model system of cerebrovascular occlusion is essential for evaluation of the mechanical thrombectomy devices. The models built for device testing in the previous studies were mostly composed of a straight-tubing system[154, 155, 195, 196] filled with water[197] or saline[151, 195], and occlusion sites created by using different kinds of EAs. Prior work focused on the consistency of the EA models[156], or laid emphasis on the geometry of the vascular replica[150], while other investigators stressed the hemodynamic simulation[154]. What seems to be lacking; however, is a reproducible and physiologically realistic model system that enlists all the aforesaid elements.

Mechanical removal of thromboembolic materials from cerebral arteries by using FDA-approved devices, the MERCI and Penumbra systems, has been widely-investigated in extracranial vascular occlusion animal models and in the clinical arena. The results showed that ,without adjunctive therapies, the recanalization rate (57.3% for MERCI L5 Retriever[98]) and clinical outcome (29% mRS $\leq$ 2 after 90 days with the Penumbra treatment[100]) of these devices still could be improved. Testing these devices in an experimental model not only provides information on EA-device interaction during the procedure but also helps device selection in different clinical scenarios.

Unlike balloon expandable stents, the flexible self-expanding nitinol stents are easier to be navigated in the tortuous cerebrovasculature, and deployed at lower radial

force[108, 198, 199]. The favorable outcome presented in the first FDA-approved prospective trial of primary intracranial stenting for acute stroke[109] suggested the potential utility of the self-expanding stent in the treatment of AIS. Ultrasonically driven waveguide has been shown to break thrombus into micro particles by cavitation and is currently FDA approved for thrombus ablation applications in the peripheral vasculature[155]. The application of waveguide ultrasound technique has tended to expand to the ablation of the thrombotic materials in cerebral arteries where the vessel geometry is more complex and tortuous. The success of this design may provide another option for physicians to treat patients with acute ischemic stroke.

The goal of this study is to build a reproducible occlusion model system incorporating human ICA/MCA vascular replica, blood- mimicking solution, physiological hemodynamic conditions, and a clinically relevant embolus analogue for evaluation of the aforesaid 4 endovascular devices.

Materials and Methods

Construction of Silicone Replica

The silicone ICA/MCA replica with a representative ICA siphon in terms of curvature, diameter, and length was selected from 20 patients and built by using a small-batch manufacturing process, as described in Chapter 2[200]. The AC, diameter, and length of the ICA siphon were 0.36 mm^{-1}, 4.21 mm, and 20.62 mm, respectively. The MRA dataset provided the geometry of the vasculature, and the image post-processing was performed in Mimics (Materialise, Leuven, Belgium). The virtual model was modified to

include only the ICA, M1 and M2 divisions. The two M2 divisions were artificially designed to rejoin distally having a fenestrated appearance to produce a single output that simplifies the flow rig. This simplified model was restricted to the critical vascular anatomy relevant to thrombectomy testing in an MCA occlusion by removal of branches such as the ophthalmic and anterior cerebral arteries. A core-shell mold was created in Magics (Materialise, Leuven, Belgium) based on the geometry of the vasculature reconstructed in Mimics for silicone (Sylgard 184, Dow Corning, Midland MI) infusion. A transparent and flexible silicone replica was obtained by dissolving the core-shell mold in xylene after curing. To reduce the friction between the device and the silicone replica, the inner wall of the resulting replica was lubricated by coating a layer of LSR topcoat (Momentive Performance Materials, Albany NY).

Flow Loop Design

The ICA/MCA replica was set in an acrylic box (20 cm × 13 cm × 10 cm), and the orientation of the replica was adjusted and maintained by rotating and sliding the connecting tubes (inner diameter = 4.8 mm) that served as the inlet and outlets to the vascular replica. The acrylic box containing the silicone replica was connected to a flow loop which contained a programmable piston pump (Shelley Medical Imaging Technologies, Ontario, Toronto, Canada*),* blood-mimicking fluid (60/40 water/glycerin) reservoir, and starling resistor chambers. A filter funnel employing a filter with a pore size of 54 microns was attached to the blood-mimicking fluid reservoir in an effort to reduce particle introduction into the system. A physiologically realistic pressure

waveform was generated by the pump to produce fluid velocities similar to those observed in the human carotid arteries. The Starling resistor adjusted the resistance so that the pressure was controlled. The data acquisition system (Dewetron Inc, Charlestown, RI) was equipped with an analog-to-digital converter, and incorporated the synchronized video captured by a digital camcorder. Analog channels were displayed in raw voltage, and the math channels were be used to calculate items such as corrected flow and pressure.

The schematic illustration of the flow loop is presented in Figure 4-1. The flow of the filtered blood-mimicking fluid pumped out from the reservoir simulated the CCA flow. The mock CCA divided to mimic the external and internal carotid arteries, and the latter was connected to the silicone ICA/MCA replica. Collateral flow derived from the ECA joined distal to the ICA/MCA model to maintain a realistic pressure gradient. The flow sensors (Transonic Systems Inc., Ithaca, NY) measured the CCA and MCA flow, and pressure transducers (Validyne Engineering, Northridge, CA) which have a good dynamic response, were used to record the proximal (P1 in Figure 4-1) and distal MCA (P2 in Figure 4-1) pressure. The blood-mimicking fluid travelled through the ECA was directed to a filtration system before re-entering the blood-mimicking fluid reservoir; on the other hand, fluid travelled through the ICA was collected in an empty container for particle analysis.

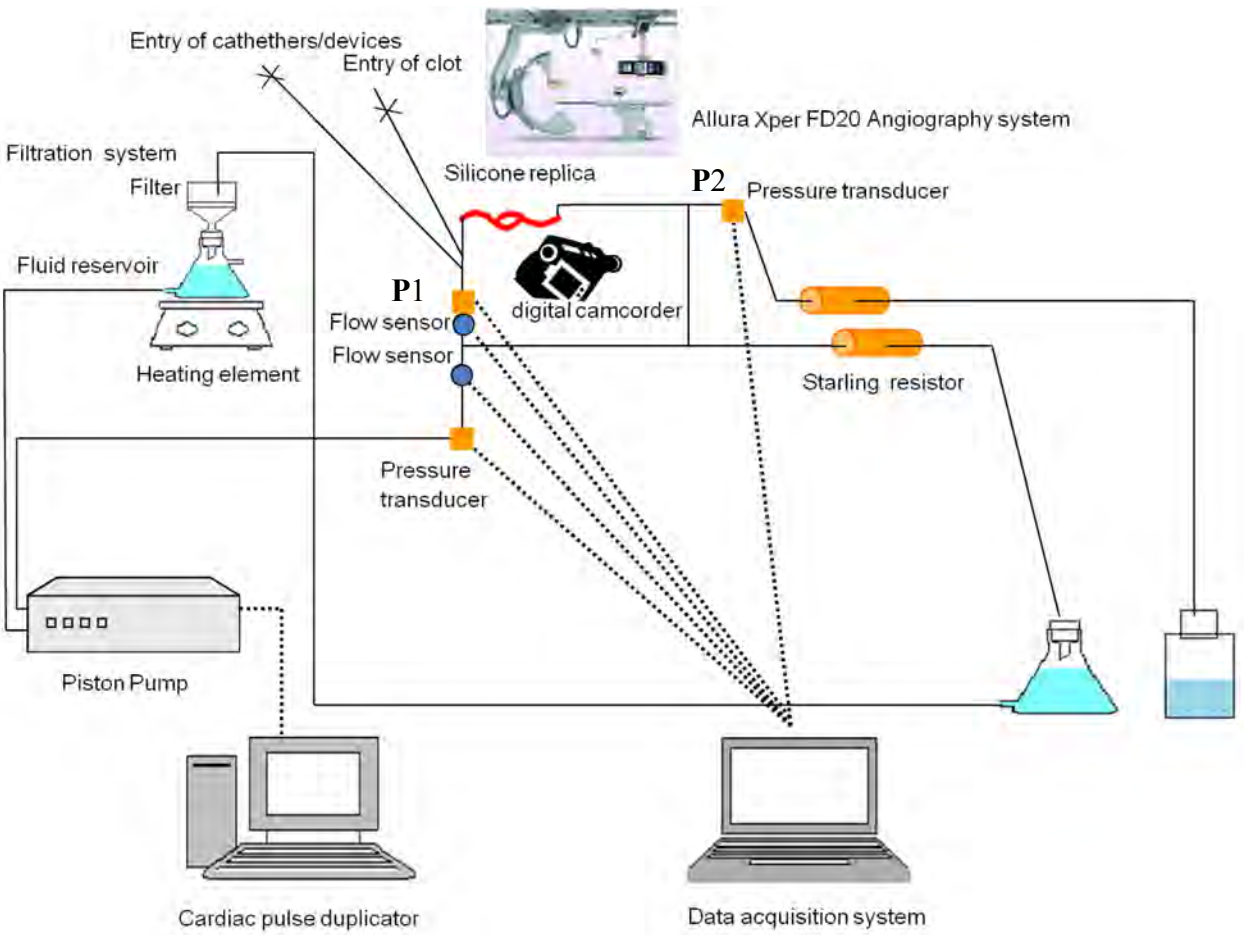

Figure 4-1 The schematic illustration of the flow loop. CCA was connected to the flow pump, and divided to form ICA and ECA. Collateral flow was diverted from the ECA region to distal MCA.

Preparation of Emboli and Creation of Occlusion

The radio-opaque bovine EA, mimicking the thrombi extracted from the atherosclerotic plaques, was prepared by thrombin-induced clotting for device testing as described in Chapter 3. Briefly, the EA was created by mixing thrombin/$CaCl_2$ solution and barium sulfate/ bovine blood mixture (1g barium sulfate/10 ml blood) at a thrombin concentration of 2.5 NIHU/ml blood. The concentrations of the thrombin and barium

sulfate used for EA preparation in this work were also commonly used in in-vitro modeling of EAs to create the vascular occlusion in animal models for thrombectomy device testing[153, 157].

Bovine EA was formed in silicone tubing with an inner diameter of 4.76 mm one day prior to the experiment, and it was cut by a scalpel to have a length of 1cm for creation of in-vitro occlusion. Weight of the bovine EA was measured by a scale with a resolution of 0.1 mg. EA was injected into the flow loop via a separate entry close to the silicone replica, and the pressure and flow changes caused by the occlusion were recorded.

Thrombectomy Devices and Procedures

All procedures were performed under x-ray guidance (Allura FD20, Philips Healthcare, Best the Netherlands).

The self-expandable stents, (Enterprise Vascular Reconstruction Device™ Codman Neurovascular, Raynham MA), with unconstrained stent length either of 28 or 37 mm and outer diameter of 4.5 mm were evaluated in this study (Figure 4-2). A 6Fr guide catheter was placed proximal to the occlusion in the ICA, and delivered the guidewire which was then softly advanced through the EA. A microcatheter (Prowler Plus, Codman Neurovascular) was navigated over the wire to the distal end of the occlusive EA. The guidewire was withdrawn followed by stent deployment for EA retrieval. The stent was deployed across the embolus and the expanded system was slowly withdrawn in an effort to retrieve the EA.

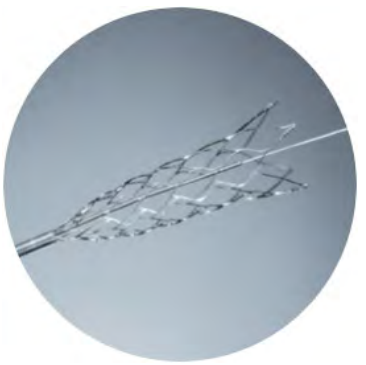

Figure 4-2 The Enterprise stent. The highly flexible stent is made of nitinol, and has a closed-cell design which makes the stent partially retractable and allows repositioning[201] (Courtesy of Codman Neurovascular Inc., Miami, FL).

To deliver the MERCI Retriever L5, a 9 Fr balloon guide catheter was inserted and positioned in the ICA. Navigation of the MERCI microcatheter 18L through the EA was performed over the wire with fluoroscopic navigation. The guidewire was exchanged for the MERCI Retriever L5, which was deployed beyond the occlusive EA. The corkscrew-shaped retriever engaged the EA, and was pulled back into the guide catheter with the microcatheter with proximal temporary balloon occlusion of the ICA. Vigorous aspiration to the balloon guide catheter was applied by using a syringe.

The Penumbra system consisting of a reperfusion catheter 054, separator 054, aspiration tubing and suction pump was set up for EA removal. An 8 Fr guide catheter was positioned in the proximal ICA and the reperfusion catheter was advanced through it to the proximal aspect of the bovine EA. The vacuum pump was operated and the separator 054 was inserted into the reperfusion catheter. The side port of the rotating hemostasis valve was connected to the aspiration tubing. During aspiration, the separator was advanced and retracted to assist with EA removal.

The ultrasonic endovascular system comprising an ultrasonic energy source, transducer and ultra thin wire developed by OmniSonics Medical Technologies (Wilmington, MA) was tested. A 6Fr guidecatheter was positioned in the ICA and through this a 0.028" Hypertransit microcatheter (Codman Neurovascular) was positioned across the occlusive embolus. The thrombectomy wire was delivered through the microcatheter which was then withdrawn to expose the active section of the wire. The ultrasonic transducer was coupled on the proximal end to the wire, which causes high-frequency vibration to the distal active section. The mechanical motion of the active section produced cavitation streaming that is necessary to fracture the fibrin matrix of the embolus. The system was activated at a frequency of 150 kHz and a voltage of 300 mV for 20 min.

Evaluation of Thrombectomy Treatments

A minimum of 5 experiments were carried out for each of 4 thrombectomy devices. To investigate the efficacy (ability to restore blood flow) of the tested devices the location where the device was deployed, percentage of the remaining clot by weight after the treatment, and percentage of flow restored were recorded. On the other hand, to assess the safety (embolic shower protection) of the thrombectomy devices, particle size analysis of the effluent following EA disruption was evaluated by using the Coulter Principle (Multisizer 4 Coulter counter, Beckman Coulter, Inc., Brea, CA). After catheter deployment, 400 mL blood-mimicking solution was collected as blank for particle analysis, and the results were subtracted from the following tests. A 2000 μm aperture

with a sensitivity range between 200 to 1600 μm and a 400 μm aperture which had a sensitivity range between 8 to 320 μm were used to measure the size and size distribution of the disrupted EAs. Large volume of blood-mimicking solution (400 mL) was required for each analysis with the use of 2000 μm aperture. The number of particle analysis tests was determined depending on the volume of solution collected during each experiment. At least 5 runs were performed with the 400 μm aperture due to the small amount of solution which was needed for each run. Average particle size (mean± standard error), particle number, and size distribution were recorded.

Results

Enterprise stent and MERCI Retriever were applied in 6 vessel occlusions each, and with Penumbra aspiration and ultrasonic endovascular system, 5 procedures were performed. A total of 22 experiments were conducted. Before occlusion, CCA and MCA flow were 367.4±1.37ml/min and 130.40± 1.71 ml/min (mean± standard error), respectively. Peak and minimal pressure of the MCA waveform were 116 and 81 mmHg, respectively, mimicking the systolic and diastolic blood pressure. The pressure gradient between the inlet and outlet of the vascular replica was 21.96 mmHg. After occlusion, MCA flow dropped to 0 ml/min, and an increase in pressure gradient between the proximal and distal MCA was observed (Figure 4-3).

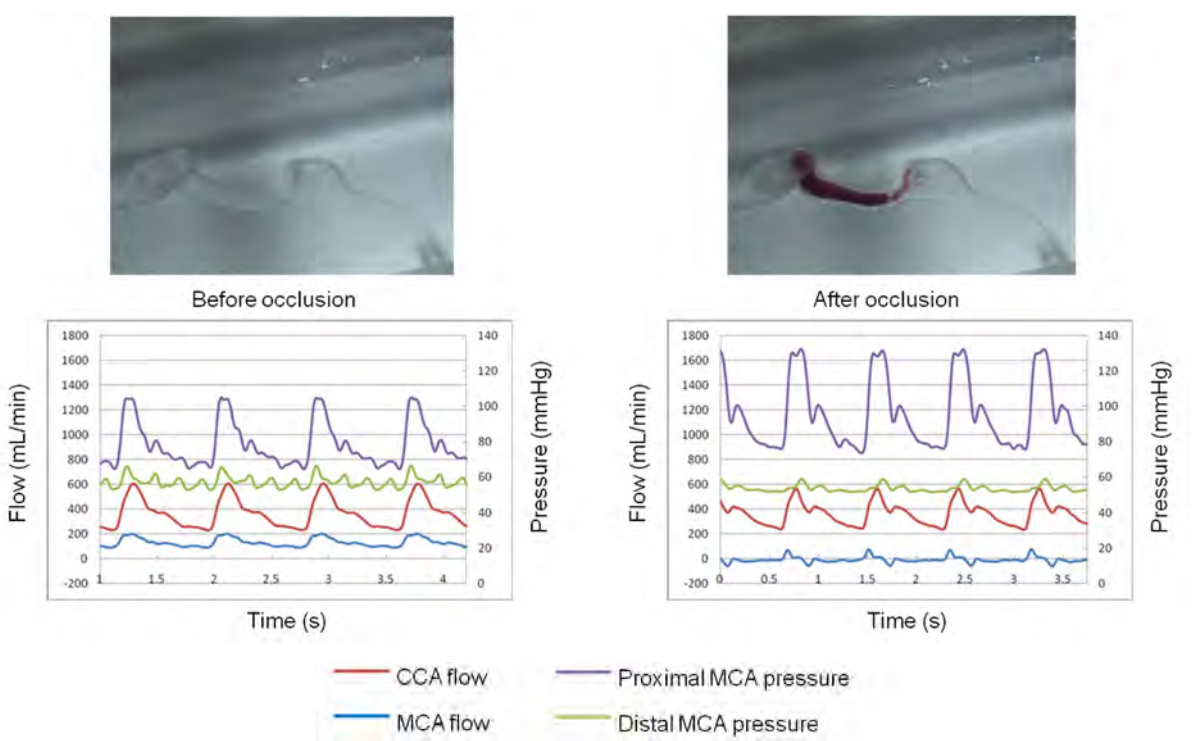

Figure 4-3 Variations of the hemodynamic variables before and after EA injection.

The average diameter of the ICA siphon was 4.21 mm, and the ICA had a maximum diameter of 5.7 mm (Figure 4-4 (a)). As a result of diameter differences between the bovine EA and vascular replica, it was found the vascular occlusion was formed at the MCA bifurcation (Figure 4-4 (b)). The nominal diameter of the MCA was 2.2 mm.

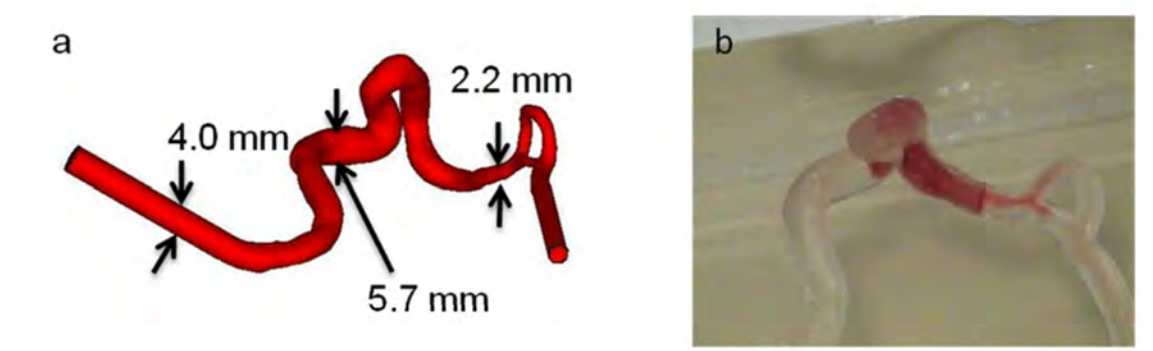

Figure 4-4 (a) The dimension and geometry of the ICA/MCA model (b) bovine EA with a diameter of 4.76 mm stopped before the MCA bifurcation.

Injection of EA and deployment of the device sometimes caused EA fragmentation and distal dislocation. Figure 4-5 (a) showed that fragmented EAs were seen in a test with the Enterprise stent. The stent was deployed distal to the EA, and compressed the EA during EA retrieval (Figure 4-5 (a)-(c)). No significant amount of visible EA particulates was generated due to the compression of the EA. Figure 4-5 (d)-(f) illustrated that the EA slipped through the stent when passing the ICA siphon, and resulted in an unsuccessful EA removal. This phenomenon was frequently observed in other 5 Enterprise stent tests. It should be noted that temporary flow restoration (29.28% ±6.42%) was measured when the stent was self-expanded during the procedure. In 6

experiments performed with the Enterprise stent, partial flow restoration (86.57%) was achieved in 1 experiment when part of the EA was removed by the device (Figure 4-6). The recanalization rate of the Enterprise stent in this study was 17%.

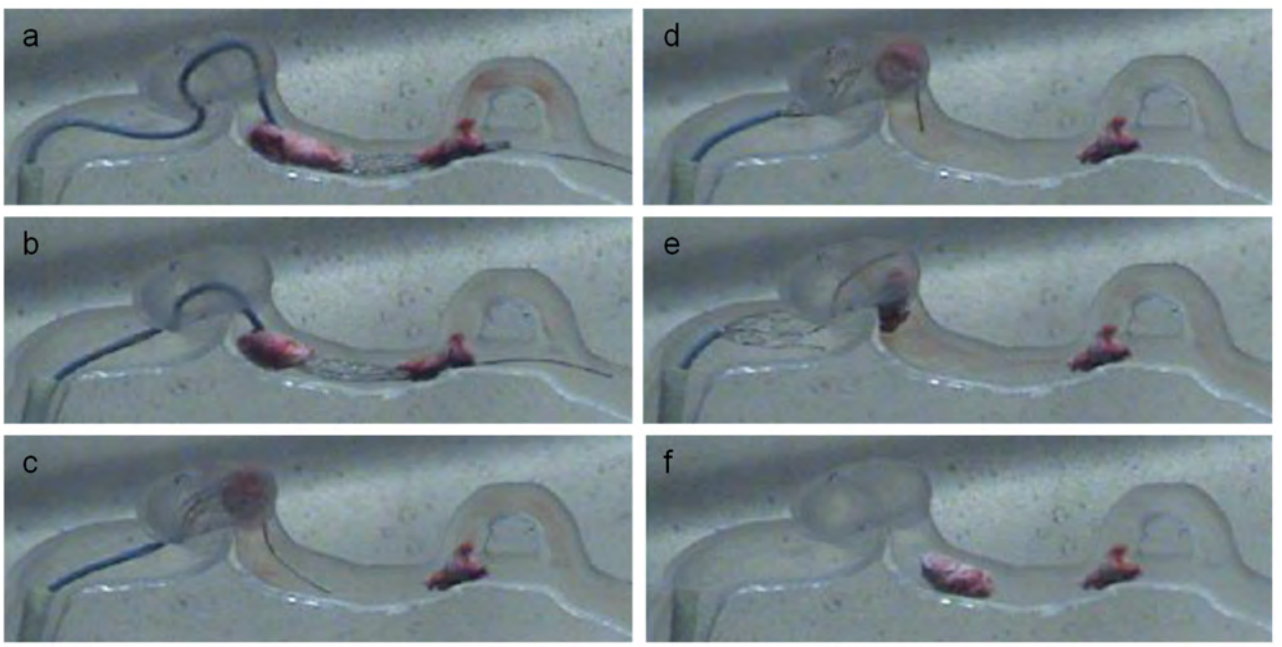

Figure 4-5 (a) to (c) Bovine EA was captured and compressed by the pulling maneuver. (d) to (f) The stent-EA contact was lost during the EA retrival. Only the stent was withdrawn into the guide catheter.

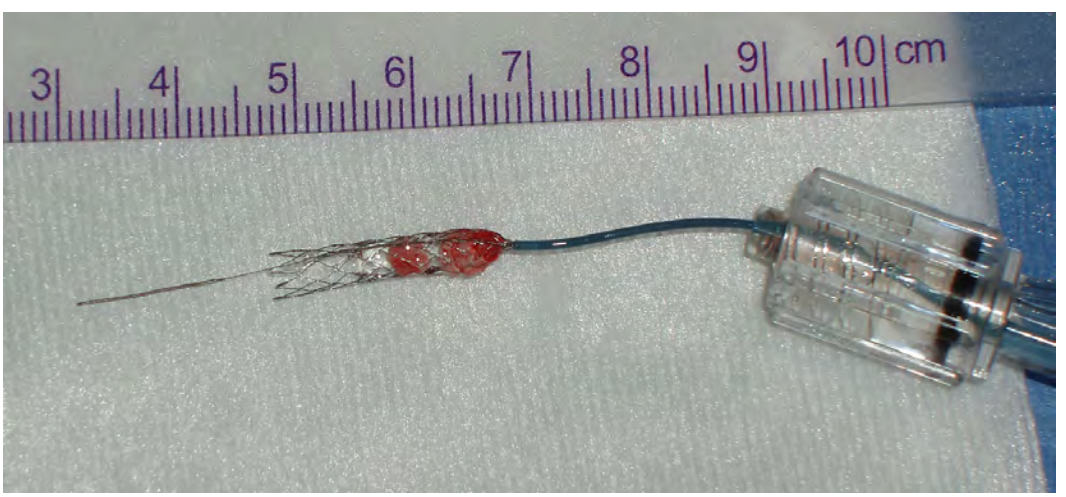

Figure 4-6 Bovine EA was successfully removed by the Enterprise stent.

With the assistance of aspiration, MERCI L5 Retriever achieved a 67% of recanalization rate (100% flow restoration was obtained). Like Enterprise stent, MERCI L5 Retriever was navigated to the distal end of the EA (Figure 4-7 (a)); moreover, EA was broken into few large pieces during the test (Figure 4-7 (b)). Successful EA mobilization by the MERCI L5 Retriever was demonstrated in (Figure 4-7 (c)-(f)). Bovine EA removed by the MERCI L5 Retriever was shown in Figure 4-8.

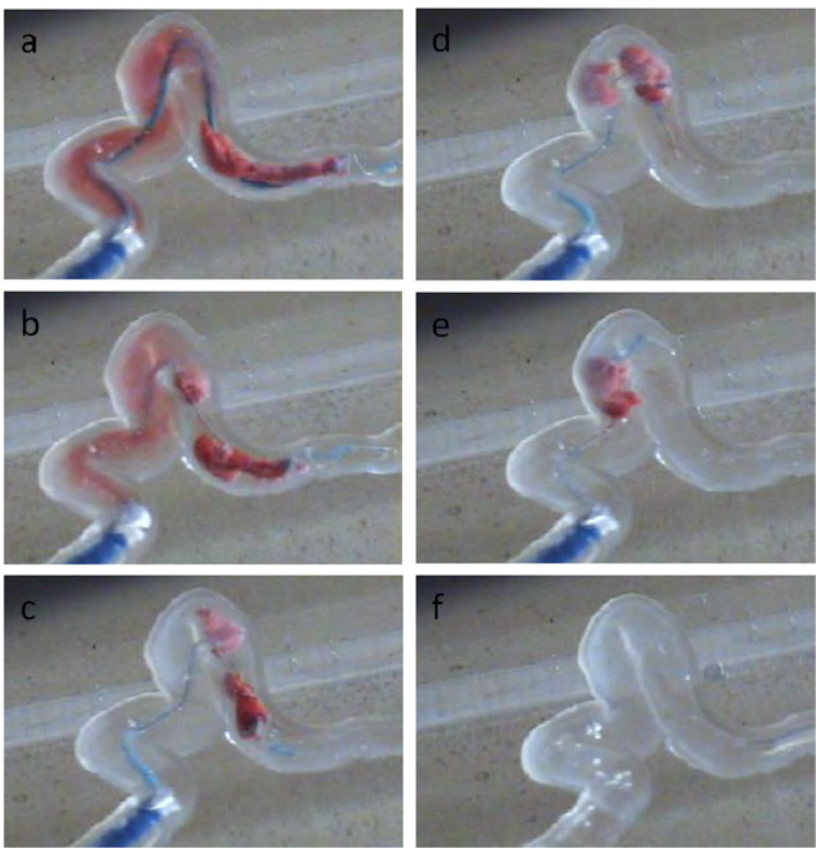

Figure 4-7 (a) and (b) MERCI L5 Retriever was deployed and ensnared the EA. (c) and (e) EA was slowly travelled through the ICA and aspirated into the guild catheter, resulting in a 100% flow restoration (f).

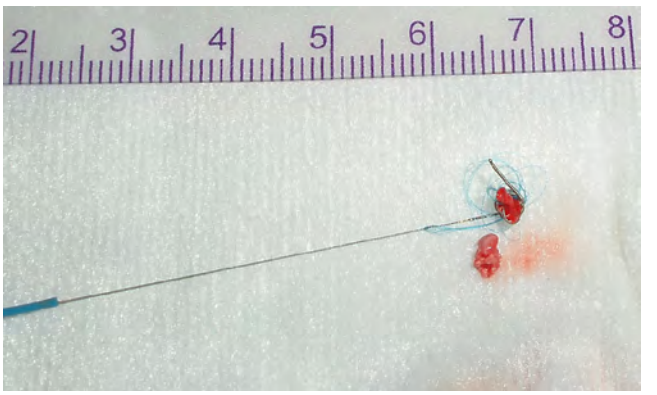

Figure 4-8 Bovine EA was removed by the MERCI L5 Retriever.

In the procedure with the use of Penumbra aspiration system, the reperfusion catheter reached the proximal end of EA, and the separator moved back and forth to disrupt the EA (Figure 4-9 (a)-(b)). The continuous aspiration-debulking process provided by the Penumbra system produced some visible EA particulates (Figure 4-9 (b)). After 2-3 passages of aspiration through the occluded area, 100% flow restoration was seen in 1 test, partial flow restoration (Figure 4-9 (c)) was measured in 3 tests, and no flow restoration was recorded in 1 test. Overall, the recanalization rate of Penumbra aspiration system was 80%.

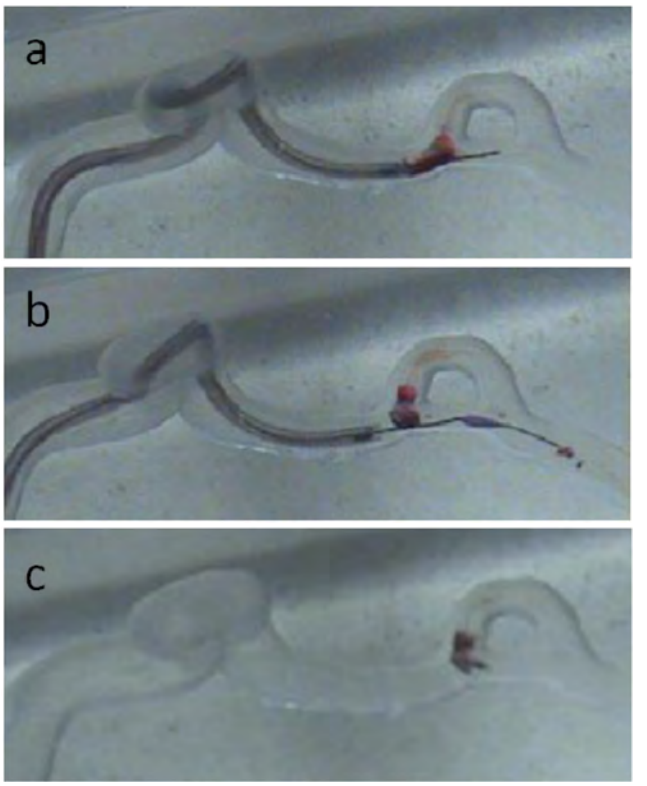

Figure 4-9 Partial revascularization of the MCA using the Penumbra aspiration system. (a)The reperfusion catheter was placed at the proximal end of the EA. (b) the separator ruptured the EA, and generated particles with an average size of 238.8 µm.

No flow restoration and pressure change were seen in all ultrasound waveguide treatments (Figure 4-10). The system was activated for 20 min in each occlusion. The wire was in good shape after each test, without any evidence of wire fracture. To ensure that the ultrasound waveguide system worked properly, the wire was embedded and activated in the EA formed in the straight tube. The EA disruption was seen in 20 seconds after the device activation.

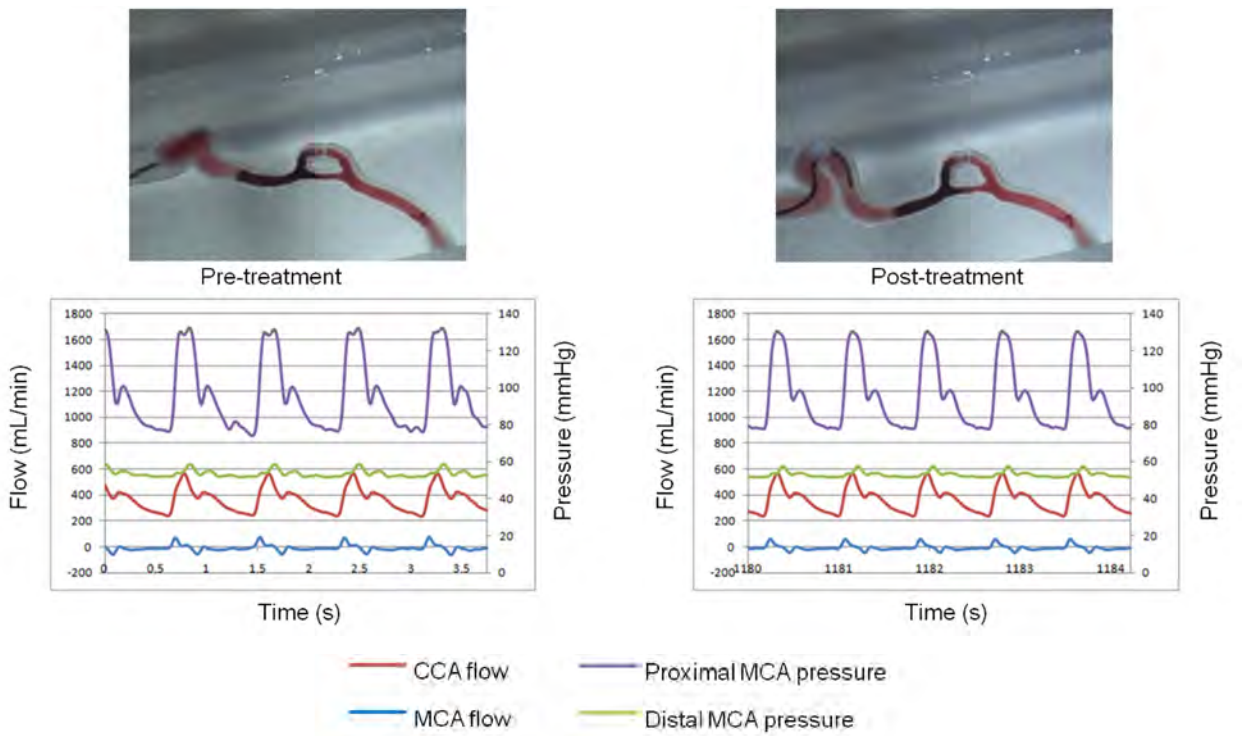

Figure 4-10 No flow was restored after a 20-min treatment by using the ultrasound waveguide wire.

The weight of the EA residues showed that the MERCI retriever and Penumbra aspiration device removed most of the EA (86% and 92%, respectively) as compared to the Enterprise stent (58%) and ultrasound waveguide (54%). Thousands of small particles with size smaller than 250 µm were analyzed in each device testing by using the 400µm aperture, and a large proportion of particulates had size fell between 13.5 to 50 µm (Figure 4-11(a)). Figure 4-11 (b) demonstrated that most large particles had size between 200 to 450 µm. By using the 2000µ aperture, it was found that the mean number and size of the particles in the blank was 2.65±1.04 and 131.3±27.54 µm, respectively (Figure 4-12 (a)). Figure 4-12 (b) showed that the Penumbra system generated more particles as compared to the Enterprise stent, MERCI retriever and ultrasound-based device

(MERCI:1.5±0.69; Penumbra:15.53±8.24; Enterprise:6.69±2.09; ultrasound:1.53±0.62). In addition, large variations in quantity of large particles were seen with the use of the Penumbra system. No significant difference in particle size was observed before and after the experiments Figure 4-12 (c). The mean particle size was 169.4±37.94, 248.4±47.44, 200.3±34.02 and 101.9±29.29 for the MERCI retriever, Penumbra system, Enterprise stent and ultrasound waveguide, respectively.

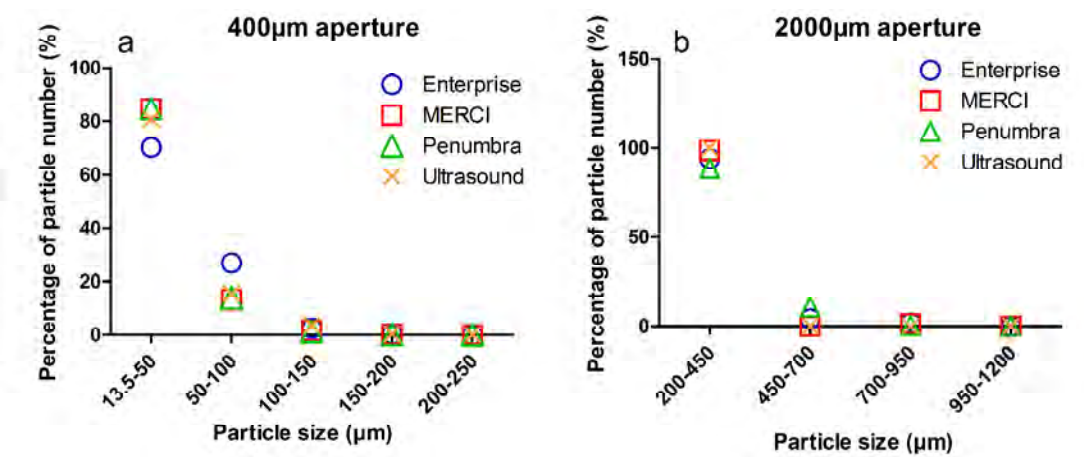

Figure 4-11 Size distribution of the particles generated by the thrombectomy devices.

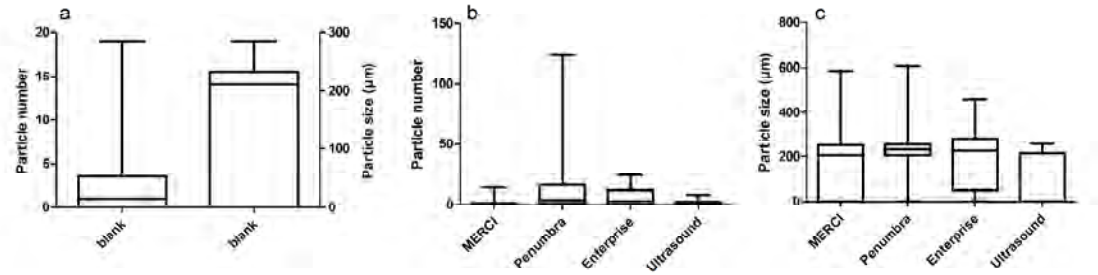

Figure 4-12 Number and size of the particles from the blank (a) and procedures conducted with Enterprise stent, MERCI retriever, Penumbra aspiration device and ultrasound waveguide (b-c). The measurements were performed with the use of the 2000 µm aperture.

Discussion

The in-vitro occlusion model system offers an alternative and convenient approach for pre-clinical evaluation of mechanical thrombectomy devices, and has advantages over the in-vivo animal model in terms of lower cost, high degree of reproducibility, quantitative analysis and no ethical considerations. In this study, a physiologically realistic model of cerebral occlusion was proposed and used to evaluate the efficacy and safety of 4 mechanical thrombectomy devices.

Factors such as anatomy of the human carotid arteries, similarities between embolus analogues and human sources of emboli, and hemodynamic variables were taken into consideration in the development of the occlusion model. The transparent vascular replica and the data acquisition system which incorporates the synchronized video captured by a digital camcorder provide real time EA-device interaction. In the previous work, to study the risk of emboli, the EA particulates were filtered by several meshes of different size and weighed by a scale[155, 195, 202]. Instead of sieving, the dimension of the

EA particulates was characterized by the Coulter principle. The disrupted EAs were stored in the blood-mimicking solution (water/glycerol mixture) which was the perfect solution for large apertures (400 and 2000μm) used in our application. During the analysis, the EA particulates were drawn through the aperture, resulting in an impedance change of the aperture. The change created a current fluctuation which was then converted into a voltage pulse. The volume of the EA particulates was proportional to the amplitude of the voltage pulse.

The Penumbra pivotal stroke trial completed in 2007 showed a racanalization (TIMI 2 or 3) rate of 81.6% [100], which was similar to our finding (80%). In addition, the observed recanalization rate of the MERCI L5 Retriever (67%), was also close to the number disclosed in clinical studies (57.3%)[98]. The Enterprise stent tested in this study had an unconstrained outer diameter of 4.5 mm which was smaller than the proximal diameter of the ICA replica. Thus the EA became disengaged from the stent during the retrieval process that explains the low recanalization rate of the Enterprise stent (17%). Further, this observation demonstrates the need for proximal aspiration through a balloon guidecatheter when using a stent system as a clot retriever. In a recent study, 90% recanalization was attained in patients using a similar stent-retriever device, the Solitaire system[111]. This device was deployed in AIS patients in whom the MERCI system failed to restore blood flow. It is likely that the high success rate reported and not reproduced in our model system may be attributed to two factors: 1. Our vascular replica had a focal ectatic dilation in the cavernous segment that exceeds the unconstrained diameter of the stent, and 2. Castaño et al. used a proximal temporary occlusion system (not approved

with the Solitaire thrombectomy system) that combined with aspiration may be the optimal adjunct technique for stent based thrombectomy technologies. EA fragmentation caused by the ultrasound waveguide wire was seen in the occlusion formed in straight tubing. However, no flow restoration was seen when activating this device in the ICA/MCA occlusion model. The unsuccessful recanalization may be attributed to the tortuosity of the cerebrovasculature which could impede the ultrasonic wave propagation.

To investigate the efficacy of the thrombectomy devices, the EA weight was measured pre- and post-treatment. During the measurement, the EA weight was affected by the amount of water/glycerol on the EA surface. To minimize the error, the excess water/ glycerol was removed. Less remaining EA was found in the groups with higher recanalization rate (the Penumbra and MERCI), which made it reasonable to suggest that the more EA removed, the higher recanlization rate could be achieved.

The dimension of the largest particulates produced by the thrombectomy device was between 700-950 μm, which was smaller than that of the particulates found in the earlier in-vitro studies (>1000 μm)[155, 195]. This finding was due to the barium sulfate effect on the mechanical properties of the EA. Barium sulfate reduced the elasticity and increased the toughness of the EA. With the presence of barium sulfate, the EA was less prone to break. More details regarding the mechanical properties of the EAs were stated in the previous chapter. The results of the blank tests showed that thousands of particles had dimension smaller than 100 μm, and the quantities varied in each blank test. Based on this observation, it was postulated that the small particulates measured by the 400 μm

aperture may include not only EA fragments but the small particles from the working environment.

Conclusion

A physiologically realistic model system of MCA occlusion was created for evaluation of the MERCI L5 Retriever, Penumbra aspiration system 054, self-expanding Enterprise stent and ultrasound waveguide wire. The recanalization rate of the thrombectomy device was related to the ability of the device to capture the EA during removal of the device and the geometry of the cerebrovasculature. The risk of the embolic shower was influenced by the mechanism of action for the thrombectomy device.

Acknowledgement

This work was supported by the National Institute of Biomedical Imaging and Bioengineering grant 1R21EB007767. The contents are solely the responsibility of the authors and do not necessarily represent the official views of the National Institutes of Health.

Final Summary and Conclusions

Currently, there are no standardized or validated cerebrovascular occlusion model systems with which to systematically evaluate and characterize mechanical thrombectomy devices. Further, development of said model system could be extrapolated to improve neurointerventional training of endovascular treatment in acute ischemic stroke. This thesis rigorously addresses each component of a cerebrovascular occlusion model system.

The 2D TOF MRA datasets were processed and edited to construct 3D vascular models for vessel characterization in terms of AC, length and diameter. Based on the results from the vessel characterization, a population averaged vasculature was determined from 20 patients and used to create the core-shell mold for preparation of the transparent and true-to-scale silicone replica. A simplified vascular replica consisting of the ICA and MCA to the MCA bifurcation was used for vascular occlusion simulation.

Mechanical properties of various types of EAs commonly used in the lab were explored and compared to those of the thromboemboli retrieved from AIS patients and atherosclerotic plaques. In the preliminary tests of our model system, a radio-opaque bovine EA with stiffness similar to the thrombi retrieved from the atherosclerotic plaques was selected to form an occlusion in the aforesaid replica for thrombectomy device testing. A computer-controlled pump was incorporated to generate a physiologically realistic carotid waveform, and pumped blood-mimicking fluid through the replica.

The MERCI L5 Retriever, Penumbra aspiration 054 system, Enterprise stent, and ultrasound driven waveguide were evaluated by using the occlusion model system. The flow restoration, the ability to achieve recanalization, size and size distribution of the EA fragments were analyzed to assess the efficacy and safety of the testing devices. The MERCI L5 Retriever and the Penumbra aspiration 054 system showed a 67 % and 80 % recanalization rate, respectively, which were similar to the numbers reported in the previous clinical studies, 57.3 % and 81.6 %, respectively. The Enterprise stent reliably restored blood flow but was only successful at thrombectomy in one experiment. The Penumbra system generated the most large clot fragments.

In conclusion, an anatomically and physiologically representative model system of cerebrovascular occlusion was successfully built for evaluation of mechanical thrombectomy devices in-vitro. Future work will include testing of thrombectomy devices in more tortutous vascular replicas with various EA models. Our eventual goal is to catalog a device performance envelop based on the mechanical properties of the thromboemboli. Ultimately, advanced imaging algorithms may become available to discern the composition of the embolus that when combined with the aforesaid catalog could guide device selection. As more devices become available, this information would be used to make the thrombectomy procedure more efficacious and cost-effective. The research described herein provides the fundamental framework for attainment of this challenging yet important goal.

Bibliography

1. Greil O, Pflugbeil G, Weigand K, et al. Changes in carotid artery flow velocities after stent implantation: a fluid dynamics study with laser Doppler anemometry. *J Endovasc Ther* 2003;10:275-284

2. Ku DN, Giddens DP. Pulsatile flow in a model carotid bifurcation. *Arteriosclerosis* 1983;3:31-39

3. Bharadvaj BK, Mabon RF, Giddens DP. Steady flow in a model of the human carotid bifurcation. Part I--flow visualization. *J Biomech* 1982;15:349-362

4. Grand W, Hopkins LN. Vasculature of the brain and cranial base: variations in clinical anatomy. New York: Thieme; 1999:21-50

5. Cho L, Mukherjee D. Basic cerebral anatomy for the carotid interventionalist: the intracranial and extracranial vessels. *Catheter Cardiovasc Interv* 2006;68:104-111

6. Lee RM. Morphology of cerebral arteries. *Pharmacol Ther* 1995;66:149-173

7. Harnsberger HR, Macdonald AJ. Section7 Intracranial arteries. *Diagnostic and surgical imaging anatomy Brain, head & neck, spine* 1st ed. Salt Lake City: Amirsys; 2006:I278-331

8. Hendrikse J, Hartkamp MJ, Hillen B, et al. Collateral ability of the circle of Willis in patients with unilateral internal carotid artery occlusion: border zone infarcts and clinical symptoms. *Stroke* 2001;32:2768-2773

9. Krabbe-Hartkamp MJ, van der Grond J, de Leeuw FE, et al. Circle of Willis: morphologic variation on three-dimensional time-of-flight MR angiograms. *Radiology* 1998;207:103-111

10. Christoforidis GA, Mohammad Y, Kehagias D, et al. Angiographic assessment of pial collaterals as a prognostic indicator following intra-arterial thrombolysis for acute ischemic stroke. *AJNR Am J Neuroradiol* 2005;26:1789-1797

11. Boyajian RA, Schwend RB, Wolfe MM, et al. Measurement of anterior and posterior circulation flow contributions to cerebral blood flow. An ultrasound-derived volumetric flow analysis. *J Neuroimaging* 1995;5:1-3

12. Scheel P, Ruge C, Petruch UR, et al. Color duplex measurement of cerebral blood flow volume in healthy adults. *Stroke* 2000;31:147-150

13. Vavilala MS, Lee LA, Lam AM. Cerebral blood flow and vascular physiology. *Anesthesiol Clin North America* 2002;20:247-264

14. Astrup J, Symon L, Branston NM, et al. Cortical evoked potential and extracellular K+ and H+ at critical levels of brain ischemia. *Stroke* 1977;8:51-57

15. Saver JL. Time is brain--quantified. *Stroke* 2006;37:263-266

16. Tanaka H, Fujita N, Enoki T, et al. Relationship between variations in the circle of Willis and flow rates in internal carotid and basilar arteries determined by means of magnetic resonance imaging with semiautomated lumen segmentation: reference data from 125 healthy volunteers *AJNR Am J Neuroradiol* 2006;27:1770-1775

17. Murray CJ, Lopez AD. Mortality by cause for eight regions of the world: Global Burden of Disease Study. *Lancet* 1997;349:1269-1276

18. Wang G, Pratt M, Macera CA, et al. Physical activity, cardiovascular disease, and medical expenditures in U.S. adults. *Ann Behav Med* 2004;28:88-94

19. Lloyd-Jones D, Adams RJ, Brown TM, et al. Heart disease and stroke statistics--2010 update: a report from the American Heart Association. *Circulation*;121:e46-e215

20. Aho K, Harmsen P, Hatano S, et al. Cerebrovascular disease in the community: results of a WHO collaborative study. *Bull World Health Organ* 1980;58:113-130

21. Wyatt MG, Watkinson AF. *Endovascular Therapies: current evidence*. Shrewsbury, UK: Harley; 2006:103-145

22. Powers WJ. Cerebral hemodynamics in ischemic cerebrovascular disease. *Ann Neurol* 1991;29:231-240

23. Lee DH, Kang DW, Ahn JS, et al. Imaging of the ischemic penumbra in acute stroke. *Korean J Radiol* 2005;6:64-74

24. Moustafa RR, Baron JC. Pathophysiology of ischaemic stroke: insights from imaging, and implications for therapy and drug discovery. *Br J Pharmacol* 2008;153 Suppl 1:S44-54

25. Symon L. The relationship between CBF, evoked potentials and the clinical features in cerebral ischaemia. *Acta Neurol Scand Suppl* 1980;78:175-190

26. Kaufmann AM, Firlik AD, Fukui MB, et al. Ischemic core and penumbra in human stroke. *Stroke* 1999;30:93-99

27. Baron JC, von Kummer R, del Zoppo GJ. Treatment of acute ischemic stroke. Challenging the concept of a rigid and universal time window. *Stroke* 1995;26:2219-2221

28. Adams HP, Jr., Bendixen BH, Kappelle LJ, et al. Classification of subtype of acute ischemic stroke. Definitions for use in a multicenter clinical trial. TOAST. Trial of Org 10172 in Acute Stroke Treatment. *Stroke* 1993;24:35-41

29. Sacco RL, Foulkes MA, Mohr JP, et al. Determinants of early recurrence of cerebral infarction. The Stroke Data Bank. *Stroke* 1989;20:983-989

30. Sacco RL, Toni D, Mohr JP. Classification of ischemic stroke. In: Barnett HJM, Mohr JP, Stein BM, et al., eds. *Stroke : pathophysiology, diagnosis, and management* 3rd ed. Philadelphia: W.B. Saunders; 1998:341-354

31. Special report from the National Institute of Neurological Disorders and Stroke. Classification of cerebrovascular diseases III. *Stroke* 1990;21:637-676

32. Martin R, Bogousslavsky J. Embolic versus Nonembolic Causes of Ischemic Stroke. *Cerebrovasc Dis* 1995;5:70-74

33. Dressler DK. Death by clot: acute coronary syndromes, ischemic stroke, pulmonary embolism, and disseminated intravascular coagulation. *AACN Adv Crit Care* 2009;20:166-176

34. Sukavaneshvar S. Assessment and management of vascular implant thrombogenecity. In: Wakhloo AK, Gounis MJ, Lieber BB, et al., eds. *Thrombus and stroke*. New York: Informa Healthcare; 2008:57-77

35. Ferro JM. Cardioembolic stroke: an update. *Lancet Neurol* 2003;2:177-188

36. Murtagh B, Smalling RW. Cardioembolic stroke. *Curr Atheroscler Rep* 2006;8:310-316

37. Kelley RE, Minagar A. Cardioembolic stroke: an update. *South Med J* 2003;96:343-349

38. Easton JD, Sherman DG. Management of cerebral embolism of cardiac origin. *Stroke* 1980;11:433-442

39. Sandercock P, Bamford J, Dennis M, et al. Atrial fibrillation and stroke: prevalence in different types of stroke and influence on early and long term prognosis (Oxfordshire community stroke project). *BMJ* 1992;305:1460-1465

40. Wolf PA, Abbott RD, Kannel WB. Atrial fibrillation as an independent risk factor for stroke: the Framingham Study. *Stroke* 1991;22:983-988

41. Virok D, Kis Z, Karai L, et al. Chlamydia pneumoniae in atherosclerotic middle cerebral artery. *Stroke* 2001;32:1973-1976

42. Gralla J, Brekenfeld C, Arnold M, et al. Acute stroke: present and future of catheter-based interventions. *Herz* 2008;33:507-517

43. Furlan A, Higashida R, Wechsler L, et al. Intra-arterial prourokinase for acute ischemic stroke. The PROACT II study: a randomized controlled trial. Prolyse in Acute Cerebral Thromboembolism. *JAMA* 1999;282:2003-2011

44. Stead LG, Gilmore RM, Bellolio MF, et al. Percutaneous clot removal devices in acute ischemic stroke: a systematic review and meta-analysis. *Arch Neurol* 2008;65:1024-1030

45. Rhoton AL, Jr. The cerebrum. Anatomy. *Neurosurgery* 2007;61:37-118

46. Maulaz AB, Bezerra DC, Bogousslavsky J. Posterior cerebral artery infarction from middle cerebral artery infarction. *Arch Neurol* 2005;62:938-941

47. Sacco RL, Toni D, Brainin M, et al. Classification of ischemic stroke. In: Mohr JP, Choi DW, Grotta JC, et al., eds. *Stroke : pathophysiology, diagnosis, and management* 4th ed. New York: Churchill Livingstone; 2004:61-74

48. Babarro EG, Rego AR, Gonzalez-Juanatey JR. Cardioembolic stroke: call for a multidisciplinary approach. *Cerebrovasc Dis* 2009;27 Suppl 1:82-87

49. Schiller F. Concepts of stroke before and after Virchow. *Med Hist* 1970;14:115-131

50. Watson T, Shantsila E, Lip GY. Mechanisms of thrombogenesis in atrial fibrillation: Virchow's triad revisited. *Lancet* 2009;373:155-166

51. Lusis AJ. Atherosclerosis. *Nature* 2000;407:233-241

52. Roquer J, Segura T, Serena J, et al. Endothelial dysfunction, vascular disease and stroke: the ARTICO study. *Cerebrovasc Dis* 2009;27 Suppl 1:25-37

53. Vanhoutte PM, Shimokawa H, Tang EH, et al. Endothelial dysfunction and vascular disease. *Acta Physiol* 2009;196:193-222

54. Lowe GD. Virchow's triad revisited: abnormal flow. *Pathophysiol Haemost Thromb* 2003;33:455-457

55. Ando J, Yamamoto K. Vascular mechanobiology: endothelial cell responses to fluid shear stress. *Circ J* 2009;73:1983-1992

56. Blann AD, Lip GY. Virchow's triad revisited: the importance of soluble coagulation factors, the endothelium, and platelets. *Thromb Res* 2001;101:321-327

57. Marin F, Roldan V, Climent VE, et al. Plasma von Willebrand factor, soluble thrombomodulin, and fibrin D-dimer concentrations in acute onset non-rheumatic atrial fibrillation. *Heart* 2004;90:1162-1166

58. Mahe I, Drouet L, Chassany O, et al. D-dimer: a characteristic of the coagulation state of each patient with chronic atrial fibrillation. *Thromb Res* 2002;107:1-6

59. Kahn SR, Solymoss S, Flegel KM. Nonvalvular atrial fibrillation: evidence for a prothrombotic state. *CMAJ* 1997;157:673-681

60. Lip GY, Lip PL, Zarifis J, et al. Fibrin D-dimer and beta-thromboglobulin as markers of thrombogenesis and platelet activation in atrial fibrillation. Effects of introducing ultra-low-dose warfarin and aspirin. *Circulation* 1996;94:425-431

61. White H, Boden-Albala B, Wang C, et al. Ischemic stroke subtype incidence among whites, blacks, and hispanics: the Northern Manhattan Study. *Circulation* 2005;111:1327-1331

62. Qureshi AI, Feldmann E, Gomez CR, et al. Intracranial atherosclerotic disease: an update. *Ann Neurol* 2009;66:730-738

63. Wong KS, Huang YN, Gao S, et al. Intracranial stenosis in Chinese patients with acute stroke. *Neurology* 1998;50:812-813

64. Yuan C, Zhang SX, Polissar NL, et al. Identification of fibrous cap rupture with magnetic resonance imaging is highly associated with recent transient ischemic attack or stroke. *Circulation* 2002;105:181-185

65. Itabe H. Oxidative modification of LDL: its pathological role in atherosclerosis. *Clin Rev Allergy Immunol* 2009;37:4-11

66. Matsuura E, Kobayashi K, Tabuchi M, et al. Oxidative modification of low-density lipoprotein and immune regulation of atherosclerosis. *Prog Lipid Res* 2006;45:466-486

67. Bevilacqua MP, Stengelin S, Gimbrone MA, Jr., et al. Endothelial leukocyte adhesion molecule 1: an inducible receptor for neutrophils related to complement regulatory proteins and lectins. *Science* 1989;243:1160-1165

68. Quinn MT, Parthasarathy S, Fong LG, et al. Oxidatively modified low density lipoproteins: a potential role in recruitment and retention of monocyte/macrophages during atherogenesis. *Proc Natl Acad Sci* 1987;84:2995-2998

69. Willeit J, Kiechl S. Biology of arterial atheroma. *Cerebrovasc Dis* 2000;10 Suppl 5:1-8

70. Rogers WJ, Prichard JW, Hu YL, et al. Characterization of signal properties in atherosclerotic plaque components by intravascular MRI. *Arterioscler Thromb Vasc Biol* 2000;20:1824-1830

71. Glagov S, Weisenberg E, Zarins CK, et al. Compensatory enlargement of human atherosclerotic coronary arteries. *N Engl J Med* 1987;316:1371-1375

72. Willeit J, Kiechl S, Oberhollenzer F, et al. Distinct risk profiles of early and advanced atherosclerosis: prospective results from the Bruneck Study. *Arterioscler Thromb Vasc Biol* 2000;20:529-537

73. Amento EP, Ehsani N, Palmer H, et al. Cytokines and growth factors positively and negatively regulate interstitial collagen gene expression in human vascular smooth muscle cells. *Arterioscler Thromb* 1991;11:1223-1230

74. Rekhter MD. Collagen synthesis in atherosclerosis: too much and not enough. *Cardiovasc Res* 1999;41:376-384

75. Libby P. Molecular bases of the acute coronary syndromes. *Circulation* 1995;91:2844-2850

76. Halvorsen B, Otterdal K, Dahl TB, et al. Atherosclerotic plaque stability--what determines the fate of a plaque? *Prog Cardiovasc Dis* 2008;51:183-194

77. Witztum JL. The oxidation hypothesis of atherosclerosis. *Lancet* 1994;344:793-795

78. Zaman AG, Helft G, Worthley SG, et al. The role of plaque rupture and thrombosis in coronary artery disease. *Atherosclerosis* 2000;149:251-266

79. Fuster V. Human lesion studies. *Ann N Y Acad Sci* 1997;811:207-224

80. van der Wal AC, Becker AE, van der Loos CM, et al. Fibrous and lipid-rich atherosclerotic plaques are part of interchangeable morphologies related to inflammation: a concept. *Coron Artery Dis* 1994;5:463-469

81. Ross R. Atherosclerosis--an inflammatory disease. *N Engl J Med* 1999;340:115-126

82. Libby P. Coronary artery injury and the biology of atherosclerosis: inflammation, thrombosis, and stabilization. *Am J Cardiol* 2000;86:3J-8J

83. Ruggeri ZM. The role of von Willebrand factor in thrombus formation. *Thromb Res* 2007;120 Suppl 1:S5-9

84. Dee KC, Puleo DA, Bizios R. Blood-biomaterial interactions and coagulation. *An introduction to tissue-biomaterial interactions*. Hoboken, N.J.: Wiley-Liss; 2002:53-88

85. Hoffman M, Monroe DM. Coagulation 2006: a modern view of hemostasis. *Hematol Oncol Clin North Am* 2007;21:1-11

86. Anderson JM, Cook G, Costerton B, et al. Host reactions to biomaterials and their evaluation. In: Ratner BD, ed. *Biomaterials science: an introduction to materials in medicine* 2nd ed. Amsterdam ; Boston: Elsevier Academic Press; 2004:293-345

87. Furie B, Furie BC. Mechanisms of thrombus formation. *N Engl J Med* 2008;359:938-949

88. Gebbink MF, Claessen D, Bouma B, et al. Amyloids--a functional coat for microorganisms. *Nat Rev Microbiol* 2005;3:333-341

89. Alexandrov AV. Current and future recanalization strategies for acute ischemic stroke. *J Intern Med*;267:209-219

90. Mosesson MW, Siebenlist KR, Meh DA. The structure and biological features of fibrinogen and fibrin. *Ann N Y Acad Sci* 2001;936:11-30

91. Wolberg AS. Thrombin generation and fibrin clot structure. *Blood Rev* 2007;21:131-142

92. Tissue plasminogen activator for acute ischemic stroke. The National Institute of Neurological Disorders and Stroke rt-PA Stroke Study Group. *N Engl J Med* 1995;333:1581-1587

93. Molina CA, Saver JL. Extending reperfusion therapy for acute ischemic stroke: emerging pharmacological, mechanical, and imaging strategies. *Stroke* 2005;36:2311-2320

94. Kim D, Jahan R, Starkman S, et al. Endovascular mechanical clot retrieval in a broad ischemic stroke cohort. *AJNR Am J Neuroradiol* 2006;27:2048-2052

95. Bose A, Henkes H, Alfke K, et al. The Penumbra System: a mechanical device for the treatment of acute stroke due to thromboembolism. *AJNR Am J Neuroradiol* 2008;29:1409-1413

96. Mayor S. Devices and drugs for stroke: why do regulations differ? *Lancet Neurol* 2009;8:982-983

97. Layton KF, White JB, Cloft HJ, et al. Expanding the treatment window with mechanical thrombectomy in acute ischemic stroke. *Neuroradiology* 2006;48:402-404

98. Smith WS, Sung G, Saver J, et al. Mechanical thrombectomy for acute ischemic stroke: final results of the Multi MERCI trial. *Stroke* 2008;39:1205-1212

99. Josephson SA, Saver JL, Smith WS. Comparison of mechanical embolectomy and intraarterial thrombolysis in acute ischemic stroke within the MCA: MERCI and Multi MERCI compared to PROACT II. *Neurocrit Care* 2009;10:43-49

100. The Penumbra pivotal stroke trial: safety and effectiveness of a new generation of mechanical devices for clot removal in intracranial large vessel occlusive disease. *Stroke* 2009;40:2761-2768

101. Kerber CW, Barr JD, Berger RM, et al. Snare retrieval of intracranial thrombus in patients with acute stroke. *J Vasc Interv Radiol* 2002;13:1269-1274

102. Malek AM, Higashida RT, Phatouros CC, et al. Treatment of posterior circulation ischemia with extracranial percutaneous balloon angioplasty and stent placement. *Stroke* 1999;30:2073-2085

103. Higashida RT, Halbach VV, Tsai FY, et al. Interventional neurovascular techniques for cerebral revascularization in the treatment of stroke. *AJR Am J Roentgenol* 1994;163:793-800

104. Ringer AJ, Qureshi AI, Fessler RD, et al. Angioplasty of intracranial occlusion resistant to thrombolysis in acute ischemic stroke. *Neurosurgery* 2001;48:1282-1288

105. Henkes H, Miloslavski E, Lowens S, et al. Treatment of intracranial atherosclerotic stenoses with balloon dilatation and self-expanding stent deployment (WingSpan). *Neuroradiology* 2005;47:222-228

106. Mori T, Kazita K, Seike M, et al. Successful cerebral artery stent placement for total occlusion of the vertebrobasilar artery in a patient suffering from acute stroke. Case report. *J Neurosurg* 1999;90:955-958

107. Levy EI, Ecker RD, Horowitz MB, et al. Stent-assisted intracranial recanalization for acute stroke: early results. *Neurosurgery* 2006;58:458-463

108. Zaidat OO, Wolfe T, Hussain SI, et al. Interventional acute ischemic stroke therapy with intracranial self-expanding stent. *Stroke* 2008;39:2392-2395

109. Levy EI, Siddiqui AH, Crumlish A, et al. First Food and Drug Administration-approved prospective trial of primary intracranial stenting for acute stroke: SARIS (stent-assisted recanalization in acute ischemic stroke). *Stroke* 2009;40:3552-3556

110. Wakhloo AK, Gounis MJ. Retrievable closed cell intracranial stent for foreign body and clot removal. *Neurosurgery* 2008;62:ONS390-393

111. Castano C, Dorado L, Guerrero C, et al. Mechanical thrombectomy with the Solitaire AB device in large artery occlusions of the anterior circulation: a pilot study. *Stroke*;41:1836-1840

112. Halkin A, Rosenschein U. Catheter-delivered ultrasound therapy for native coronary arterial thrombosis and occluded saphenous vein grafts. *Echocardiography* 2001;18:225-231

113. Mikulik R, Dusek L, Hill MD, et al. Pattern of response of National Institutes of Health Stroke Scale components to early recanalization in the CLOTBUST trial. *Stroke*;41:466-470

114. Tomsick T, Broderick J, Carrozella J, et al. Revascularization results in the Interventional Management of Stroke II trial. *AJNR Am J Neuroradiol* 2008;29:582-587

115. Atar S, Rosenschein U. Perspectives on the role of ultrasonic devices in thrombolysis. *J Thromb Thrombolysis* 2004;17:107-114

116. Pfaffenberger S, Devcic-Kuhar B, Kastl SP, et al. Ultrasound thrombolysis. *Thromb Haemost* 2005;94:26-36

117. Hajri Z, Boukadoum M, Hamam H, et al. An investigation of the physical forces leading to thrombosis disruption by cavitation. *J Thromb Thrombolysis* 2005;20:27-32

118. Hong AS, Chae JS, Dubin SB, et al. Ultrasonic clot disruption: an in vitro study. *Am Heart J* 1990;120:418-422

119. Lanzino G, Kanaan Y, Perrini P, et al. Emerging concepts in the treatment of intracranial aneurysms: stents, coated coils, and liquid embolic agents. *Neurosurgery* 2005;57:449-459

120. Nesbit GM, Luh G, Tien R, et al. New and future endovascular treatment strategies for acute ischemic stroke. *J Vasc Interv Radiol* 2004;15:S103-110

121. Levin DC, Becker GJ, Dorros G, et al. Training standards for physicians performing peripheral angioplasty and other percutaneous peripheral vascular interventions. A statement for health professionals from the Special Writing Group of the Councils on Cardiovascular Radiology, Cardio-Thoracic and Vascular Surgery, and Clinical Cardiology, the American Heart Association. *Circulation* 1992;86:1348-1350

122. Ikeda S, Arai F, Fukuda T, et al. Three dimensional photoelastic stress analysis on patient-tailored anatomical model of cerebral artery. *Proceedings of the 2004 international symposium on micro-nano mechatronics and human science : International symposium on micro-nano mechatronics and human science, Nagoya , Japan* 2004:145 - 150

123. Suzuki Y, Fujitsuka M, Chaloupka JC. Simulation of endovascular neurointervention using silicone models: imaging and manipulation. *Neurol Med Chir (Tokyo)* 2005;45:567-572

124. Gruber A, Bavinszki G, Killer M, et al. In vitro training model for endovascular embolization of cerebral aneurysms. *Minim Invasive Neurosurg* 1997;40:121-123

125. Barath K, Cassot F, Rufenacht DA, et al. Anatomically shaped internal carotid artery aneurysm in vitro model for flow analysis to evaluate stent effect. *AJNR Am J Neuroradiol* 2004;25:1750-1759

126. Cortez MA, Quintana, R., Wicker, R.B. Multi-step dip-spin coating manufacturing system for silicone cardiovascular membrane fabrication with prescribed compliance. *Int J Adv Manuf Technol* 2006;34:667-679

127. Gailloud P, Pray JR, Muster M, et al. An in vitro anatomic model of the human cerebral arteries with saccular arterial aneurysms. *Surg Radiol Anat* 1997;19:119-121

128. Knox K, Kerber CW, Singel SA, et al. Rapid prototyping to create vascular replicas from CT scan data: making tools to teach, rehearse, and choose treatment strategies. *Catheter Cardiovasc Interv* 2005;65:47-53

129. Markl M, Schumacher R, Kuffer J, et al. Rapid vessel prototyping: vascular modeling using 3t magnetic resonance angiography and rapid prototyping technology. *MAGMA* 2005;18:288-292

130. Seong J, Sadasivan C, Onizuka M, et al. Morphology of elastase-induced cerebral aneurysm model in rabbit and rapid prototyping of elastomeric transparent replicas. *Biorheology* 2005;42:345-361

131. Sugiu K, Martin JB, Jean B, et al. Artificial cerebral aneurysm model for medical testing, training, and research. *Neurol Med Chir (Tokyo)* 2003;43:69-72

132. Wetzel SG, Ohta M, Handa A, et al. From patient to model: stereolithographic modeling of the cerebral vasculature based on rotational angiography. *AJNR Am J Neuroradiol* 2005;26:1425-1427

133. Ohta M, Handa A, Iwata H, et al. Poly-vinyl alcohol hydrogel vascular models for in vitro aneurysm simulations: the key to low friction surfaces. *Technol Health Care* 2004;12:225-233

134. Bullitt E, Muller KE, Jung I, et al. Analyzing attributes of vessel populations. *Med Image Anal* 2005;9:39-49

135. Waaijer A, van Leeuwen MS, van der Worp HB, et al. Anatomic variations in the circle of Willis in patients with symptomatic carotid artery stenosis assessed with multidetector row CT angiography. *Cerebrovasc Dis* 2007;23:267-274

136. Bullitt E, Gerig G, Pizer SM, et al. Measuring tortuosity of the intracerebral vasculature from MRA images. *IEEE Trans Med Imaging* 2003;22:1163-1171

137. Dougherty G, Varro J. A quantitative index for the measurement of the tortuosity of blood vessels. *Med Eng Phys* 2000;22:567-574

138. Malamateniou C, Counsell SJ, Allsop JM, et al. The effect of preterm birth on neonatal cerebral vasculature studied with magnetic resonance angiography at 3 Tesla. *Neuroimage* 2006;32:1050-1059

139. Wood NB, Zhao SZ, Zambanini A, et al. Curvature and tortuosity of the superficial femoral artery: a possible risk factor for peripheral arterial disease. *J Appl Physiol* 2006;101:1412-1418

140. O'Flynn PM, O'Sullivan G, Pandit AS. Methods for three-dimensional geometric characterization of the arterial vasculature. *Ann Biomed Eng* 2007;35:1368-1381

141. Vrtovec T, Likar B, Pernus F. Quantitative analysis of spinal curvature in 3D: application to CT images of normal spine. *Phys Med Biol* 2008;53:1895-1908

142. du Mesnil de Rochemont R, Yan B, Zanella FE, et al. Conformability of balloon-expandable stents to the carotid siphon: an in vitro study. *AJNR Am J Neuroradiol* 2006;27:324-326

143. Spiess AN, Feig C, Ritz C. Highly accurate sigmoidal fitting of real-time PCR data by introducing a parameter for asymmetry. *BMC Bioinformatics* 2008;9:221

144. Monson KL, Goldsmith W, Barbaro NM, et al. Significance of source and size in the mechanical response of human cerebral blood vessels. *J Biomech* 2005;38:737-744

145. Ghazali R, Shuaib I. Comparison between 3D TOF magnetic resonance angiography and intraarterial digital subtraction angiography in imaging the Circle of Willis. *MJMS* 2003;10:37-42

146. Goda T, Konno T, Takai M, et al. Photoinduced phospholipid polymer grafting on Parylene film: Advanced lubrication and antibiofouling properties. *Colloids and Surfaces B: Biointerfaces* 2007;54:67-73

147. Fung YC. Bioviscoelastic solids. *Biomechanics : mechanical properties of living tissues*. New York: Springer-Verlag; 1981:242-320

148. Monson KL, Goldsmith W, Barbaro NM, et al. Axial mechanical properties of fresh human cerebral blood vessels. *J Biomech Eng* 2003;125:288-294

149. Donnan GA, Baron JC, Ma H, et al. Penumbral selection of patients for trials of acute stroke therapy. *Lancet Neurol* 2009;8:261-269

150. Asakura F, Yilmaz H, Abdo G, et al. Preclinical testing of a new clot-retrieving wire device using polyvinyl alcohol hydrogel vascular models. *Neuroradiology* 2007;49:243-251

151. Liebig T, Reinartz J, Hannes R, et al. Comparative in vitro study of five mechanical embolectomy systems: effectiveness of clot removal and risk of distal embolization. *Neuroradiology* 2008;50:43-52

152. Brekenfeld C, Schroth G, El-Koussy M, et al. Mechanical thromboembolectomy for acute ischemic stroke: comparison of the catch thrombectomy device and the Merci Retriever in vivo. *Stroke* 2008;39:1213-1219

153. Kan I, Yuki I, Murayama Y, et al. A novel method of thrombus preparation for use in a swine model for evaluation of thrombectomy devices. *AJNR Am J Neuroradiol (Published on Jan 21, 2010)*

154. Muller-Hulsbeck S, Grimm J, Leidt J, et al. Comparison of in vitro effectiveness of mechanical thrombectomy devices. *J Vasc Interv Radiol* 2001;12:1185-1191

155. Salazar GM, Faintuch S, Gladstone SR, et al. In vitro analysis of downstream particulates with mechanical thrombectomy devices: comparison of 20-kHz sonothrombolytic and rotating dispersion wire systems. *J Vasc Interv Radiol* 2009;20:634-639

156. Krueger K, Deissler P, Coburger S, et al. How thrombus model impacts the in vitro study of interventional thrombectomy procedures. *Invest Radiol* 2004;39:641-648

157. Gralla J, Schroth G, Remonda L, et al. A dedicated animal model for mechanical thrombectomy in acute stroke. *AJNR Am J Neuroradiol* 2006;27:1357-1361

158. Gralla J, Schroth G, Remonda L, et al. Mechanical thrombectomy for acute ischemic stroke: thrombus-device interaction, efficiency, and complications in vivo. *Stroke* 2006;37:3019-3024

159. Jain NC. *Essentials of veterinary hematology*. Philadelphia: Lea & Febiger; 1993:21-23

160. Gersh KC, Nagaswami C, Weisel JW. Fibrin network structure and clot mechanical properties are altered by incorporation of erythrocytes. *Thromb Haemost* 2009;102:1169-1175

161. Puig-de-Morales-Marinkovic M, Turner KT, Butler JP, et al. Viscoelasticity of the human red blood cell. *Am J Physiol Cell Physiol* 2007;293:C597-605

162. Glover CJ, McIntire LV, Brown CH, 3rd, et al. Dynamic coagulation studies: influence of normal and abnormal platelets on clot structure formation. *Thromb Res* 1975;7:185-198

163. Siller-Matula JM, Plasenzotti R, Spiel A, et al. Interspecies differences in coagulation profile. *Thromb Haemost* 2008;100:397-404

164. Bijnens AP, Knockaert I, Cousin E, et al. Expression and characterization of recombinant porcine plasminogen activator inhibitor-1. *Thromb Haemost* 1997;77:350-356

165. Kirchhof K, Welzel T, Zoubaa S, et al. New method of embolus preparation for standardized embolic stroke in rabbits. *Stroke* 2002;33:2329-2333

166. Chow TW, McIntire LV, Peterson DM. Importance of plasma fibronectin in determining PFP and PRP clot mechanical properties. *Thromb Res* 1983;29:243-248

167. Erickson HP. Stretching fibronectin. *J Muscle Res Cell Motil* 2002;23:575-580

168. Mason RG, Read MS. Some species differences in fibrinolysis and blood coagulation. *J Biomed Mater Res* 1971;5:121-128

169. Weiner M, Weisberg LG. Clot firmness. *Blood* 1957;12:1125-1131

170. Gennisson JL, Lerouge S, Cloutier G. Assessment by transient elastography of the viscoelastic properties of blood during clotting. *Ultrasound Med Biol* 2006;32:1529-1537

171. Shulman S, Ferry J. The conversion of fibrinogen to fibrin.II. Influence of pH and ionic strength on clotting time and clot opacity. *J Phys Chem* 1950;54:66-79

172. Di Stasio E, Nagaswami C, Weisel JW, et al. Cl- regulates the structure of the fibrin clot. *Biophys J* 1998;75:1973-1979

173. Brass EP, Forman WB, Edwards RV, et al. Fibrin formation: effect of calcium ions. *Blood* 1978;52:654-658

174. Weisel JW. Biophysics. Enigmas of blood clot elasticity. *Science* 2008;320:456-457

175. Ryan EA, Mockros LF, Weisel JW, et al. Structural origins of fibrin clot rheology. *Biophys J* 1999;77:2813-2826

176. Stormorken H. Species differences of clotting factors in ox, dog, horse, and man; thrombin and fibrinogen. *Acta Physiol Scand* 1957;40:167-181

177. Gentry PA. Comparative aspects of blood coagulation. *Vet J* 2004;168:238-251

178. Kawamoto Y, Kaibara M. Viscoelasticity of fibrinogen solution and of blood during coagulation studied by a new damped oscillation rheometer. *Biorheology* 1988;25:289-295

179. Riha P, Wang X, Liao R, et al. Elasticity and fracture strain of whole blood clots. *Clin Hemorheol Microcirc* 1999;21:45-49

180. Tynngard N, Lindahl T, Ramstrom S, et al. Effects of different blood components on clot retraction analysed by measuring elasticity with a free oscillating rheometer. *Platelets* 2006;17:545-554

181. Luddington RJ. Thrombelastography/thromboelastometry. *Clin Lab Haematol* 2005;27:81-90

182. Kawasaki J, Katori N, Kodaka M, et al. Electron microscopic evaluations of clot morphology during thrombelastography. *Anesth Analg* 2004;99:1440-1444; table of contents

183. Liu W, Carlisle CR, Sparks EA, et al. The mechanical properties of single fibrin fibers. *J Thromb Haemost*;8:1030-1036

184. Rand ML, Murray RK. Hemostasis & Thrombosis. In: Murray RK, Granner DK, Mayes PA, et al., eds. *Harper's Illustrated Biochemitry*

26 ed: Lange Medical Books/McGraw-Hill; 2003:598-608

185. Marder VJ, Chute DJ, Starkman S, et al. Analysis of thrombi retrieved from cerebral arteries of patients with acute ischemic stroke. *Stroke* 2006;37:2086-2093

186. Almekhlafi MA, Hu WY, Hill MD, et al. Calcification and endothelialization of thrombi in acute stroke. *Ann Neurol* 2008;64:344-348

187. Gralla J, Burkhardt M, Schroth G, et al. Occlusion length is a crucial determinant of efficiency and complication rate in thrombectomy for acute ischemic stroke. *AJNR Am J Neuroradiol* 2008;29:247-252

188. Brekenfeld C, Tinguely P, Schroth G, et al. Percutaneous transluminal angioplasty and stent placement in acute vessel occlusion: evaluation of new methods for interventional stroke treatment. *AJNR Am J Neuroradiol* 2009;30:1165-1172

189. Mordasini P, Hiller M, Brekenfeld C, et al. In vivo evaluation of the Phenox CRC mechanical thrombectomy device in a swine model of acute vessel occlusion. *AJNR Am J Neuroradiol*;31:972-978

190. Wechsler LR. Ulceration and carotid artery disease. *Stroke* 1988;19:650-653

191. Wolf PA, Abbott RD, Kannel WB. Atrial fibrillation as an independent risk factor for stroke: the Framingham Study. *Stroke* 1991;22:983-988

192. Lendrum AC, Fraser DS, Slidders W, et al. Studies on the character and staining of fibrin. *J Clin Pathol* 1962;15:401-413

193. Levy EI, Sauvageau E, Hanel RA, et al. Self-expanding versus balloon-mounted stents for vessel recanalization following embolic occlusion in the canine model: technical feasibility study. *AJNR Am J Neuroradiol* 2006;27:2069-2072

194. Grimm J, Jahnke T, Muhle C, et al. Influence of thrombus age on the mechanical thrombectomy efficacy of the amplatz thrombectomy device in vitro. *Cardiovasc Intervent Radiol* 2003;26:265-268

195. Muller-Hulsbeck S, Bangard C, Schwarzenberg H, et al. In vitro effectiveness study of three hydrodynamic thrombectomy devices. *Radiology* 1999;211:433-439

196. Yasui K, Qian Z, Nazarian GK, et al. Recirculation-type Amplatz clot macerator: determination of particle size and distribution. *J Vasc Interv Radiol* 1993;4:275-278

197. Small WT, Wilson TS, Buckley PR, et al. Prototype fabrication and preliminary in vitro testing of a shape memory endovascular thrombectomy device. *IEEE Trans Biomed Eng* 2007;54:1657-1666

198. Levy EI, Mehta R, Gupta R, et al. Self-expanding stents for recanalization of acute cerebrovascular occlusions. *AJNR Am J Neuroradiol* 2007;28:816-822

199. Brekenfeld C, Schroth G, Mattle HP, et al. Stent placement in acute cerebral artery occlusion: use of a self-expandable intracranial stent for acute stroke treatment. *Stroke* 2009;40:847-852

200. Chueh JY, Wakhloo AK, Gounis MJ. Neurovascular modeling: small-batch manufacturing of silicone vascular replicas. *AJNR Am J Neuroradiol* 2009;30:1159-1164

201. Weber W, Bendszus M, Kis B, et al. A new self-expanding nitinol stent (Enterprise) for the treatment of wide-necked intracranial aneurysms: initial clinical and angiographic results in 31 aneurysms. *Neuroradiology* 2007;49:555-561

202. Muller-Hulsbeck S, Grimm J, Liess C, et al. Comparison and modification of two cerebral protection devices used for carotid angioplasty: in vitro experiment. *Radiology* 2002;225:289-294